A watercolor illustration of a field of stylized trees. The trees are drawn with black outlines, featuring a series of arching branches that resemble a canopy. The background is a soft watercolor wash of light green and pale blue, suggesting a sky and ground. The overall style is artistic and illustrative.

**Modeling the
coupled exchange
of water and CO₂
over croplands**

Marie Combe

Modeling the coupled exchange of water and CO₂ over croplands

Marie Combe

Thesis committee

Promotors

Prof. Dr W. Peters

Professor of Air Quality and Atmospheric Chemistry,
Meteorology and Air Quality Group, Wageningen University.
Professor of Atmospheric Composition Modeling,
University of Groningen.

Prof. Dr M.C. Krol

Professor of Air Quality and Atmospheric Chemistry,
Meteorology and Air Quality Group, Wageningen University.

Co-promotor

Prof. Dr J. Vilà-Guerau de Arellano

Professor of Atmospheric Boundary Layer,
Meteorology and Air Quality Group, Wageningen University.

Other members

Prof. Dr N.P.R. Anten, Wageningen University

Prof. Dr A. Verhoef, University of Reading

Dr S. Dekker, University Utrecht

Prof. Dr H. Dolman, VU University Amsterdam

This research was conducted under the auspices of the SENSE Graduate School.

Modeling the coupled exchange of water and CO₂ over croplands

Marie Combe

Thesis

submitted in fulfilment of the requirements for the
degree of doctor at Wageningen University
by the authority of the Rector Magnificus
Prof. Dr Arthur P.J. Mol,
in the presence of the Thesis Committee
appointed by the Academic Board,
to be defended in public
on Friday 2 December 2016
at 11 a.m. in the Aula
of the university.

Marie Combe

Modeling the coupled exchange of water and CO₂ over croplands

152 pages

PhD thesis, Wageningen University, Wageningen, NL (2016)

With references and a summary in English

ISBN 978-94-6257-925-5

DOI <http://dx.doi.org/10.18174/389747>

Contents

1	Introduction	9
1.1	The global carbon cycle	10
1.2	Cropland carbon cycling processes and their scales	12
1.3	Local coupling of water and CO ₂	14
1.4	Aim and approach of this thesis	17
1.4.1	Cropland surface models	17
1.4.2	Atmospheric models	19
1.4.3	Crop-atmosphere observations	19
1.5	Outline and overarching research questions	20
2	Two perspectives on the coupled carbon, water and energy exchange in the planetary boundary layer	23
2.1	Introduction	24
2.2	Methods	26
2.2.1	Observations	26
2.2.2	Models	28
2.2.3	Simulation setup	33
2.2.4	Sensitivity analysis	35
2.3	Results	35
2.3.1	Intercomparison of coupled models against observations	35
2.3.2	Sensitivity analysis of an upper-atmosphere forcing	40
2.4	Discussion	46
2.4.1	On the importance of upper-atmosphere processes	46
2.4.2	On the performance of our models	47
2.5	Conclusion	49

3	Plant water-stress parameterization determines the strength of land-atmosphere coupling	51
3.1	Introduction	52
3.2	Research strategy	54
3.2.1	Conceptual view of the land-atmosphere system	54
3.2.2	Description of the MXL-A-g _s model	56
3.2.3	Diagnostic variables	61
3.2.4	Sensitivity analysis	61
3.3	Results	63
3.3.1	Coupling points	63
3.3.2	Temporal evolution of a dry spell	65
3.3.3	Sensitivity to model errors	68
3.4	Discussion	70
3.5	Conclusion	73
4	Grain yield observations constrain cropland CO₂ fluxes over Europe: method and validation	75
4.1	Introduction	76
4.2	Model description	78
4.2.1	Crop photosynthesis and respiration	78
4.2.2	Crop water-stress response	80
4.2.3	Soil respiration and resulting net ecosystem exchange	81
4.3	Material and methods	82
4.3.1	Model input data and spatial implementation	82
4.3.2	Crop growth optimization	82
4.3.3	Model Validation	84
4.4	Results	85
4.4.1	Grain yield optimization	85
4.4.2	Daily CO ₂ exchange	86
4.4.3	Decadal CO ₂ exchange	88
4.4.4	Cropland CO ₂ exchange during droughts	89
4.5	Discussion	93
4.5.1	Performance and limits of the framework	93
4.5.2	Potential applications of WOFOST-opt	96
4.6	Conclusion	96

5 Discussion and outlook	99
5.1 On the water-stress response of crops	99
5.2 On the coupling of cropland and atmosphere	102
5.3 On the atmospheric CO ₂ budget over croplands	103
5.4 Scaling our findings up to the European continent	105
5.5 Outlook	107
6 Summary	109
Appendices	113
Appendix A: GECROS, A-g _s and MXL model settings	113
Appendix B: MXL-A-g _s model equations	116
Appendix C: Updated MXL-A-g _s model settings (Chapter 3)	119
Appendix D: FluxNet sites information	120
Appendix E: WOFOST-opt model statistics	121
References	123
Acknowledgments	143
About the author	145
List of journal publications	147
Graduate school certificate	149

1

Introduction

Carbon dioxide (CO₂) is the most important anthropogenic greenhouse gas responsible for global warming, and thus the attribution of past changes in the atmospheric CO₂ concentrations has been a key area of climate change research (Ciais et al., 2013; Myhre et al., 2013). It is now unequivocal that human fossil fuel burning has caused the rapid growth in atmospheric CO₂ since the industrial revolution (Myhre et al., 2013). Today, the global ocean and land sinks of carbon cannot keep up with these ever growing anthropogenic CO₂ emissions, as each of the two global sinks only absorb about a quarter of the total emissions (Le Quéré et al., 2015; Ciais et al., 2013). The inter-annual variability of this (im)balance is largely determined by the fluctuating capacity of the terrestrial biosphere to absorb and store CO₂, as the ocean sink varies much less (Le Quéré et al., 2015). This is why understanding the processes that govern the size and variability of the land sink is critical for projecting future atmospheric CO₂ growth and subsequent changes in climate.

The land-atmosphere interactions and feedback mechanisms that shape the terrestrial carbon cycle are multiple and complex, and they are changing under elevated CO₂ and climate change (Ciais et al., 2013). A positive fertilization effect of elevated CO₂ on the biosphere productivity has been recognized (Dekker et al., 2016; Franks et al., 2013; Keenan et al., 2013), but it is unclear how large an effect this will have on the land CO₂ sink as soil respiration should be stimulated by global warming (Karhu et al., 2014) and plants adapt their stomata to these new elevated CO₂ conditions (Buckley and Schymanski, 2014; Medlyn et al., 2011; Katul et al., 2010). In addition to the atmospheric CO₂ growth and elevated global temperature, extreme weather events such as heat waves, droughts and floods are predicted to become more frequent (Fischer and Knutti, 2014; Seneviratne et al., 2012). The capacity of terrestrial ecosystems to withstand those extremes and to be resilient is thus in question (e.g. Frank et al., 2015; Niu et al., 2014). In the end, the interactions of carbon uptake, water use and energy release at the surface will be key in determining future atmospheric CO₂ concentrations. While a strong focus has been put on the contribution of forests and grasslands to carbon cycling in a changing climate, less attention has been given to the impact of croplands.

Croplands occupy roughly one fifth of the land area over Europe, and one eighth over the globe (Ramankutty et al., 2002). Although croplands do not store a lot of carbon over decades (Lal, 2004) because most of their products are rapidly consumed, they do heavily impact atmospheric CO₂ concentrations from the daily to the seasonal time-scales. On these short time-scales, croplands have been shown to significantly affect the measured CO₂ concentrations both near agricultural fields (Tolk et al., 2009) and in remote areas of the globe (Gray et al., 2014). More specifically, one third of the increase in the seasonal cycle of atmospheric CO₂ has been attributed to croplands (Gray et al., 2014; Zeng et al., 2014) as the global cultivated area and crop productivity have been ever increasing during the green revolution to meet global demand for food and feed (Pingali, 2012). Conversion of land into croplands (Ramankutty et al., 2002), and efforts in crop engineering and breeding (e.g. Lawlor, 2013) continue to this date as the global population is expected to peak at 9 billions within the next 30 years (Roberts, 2011). Thus the breadth of cropland expansion and the improved crop productivity will greatly condition the future seasonal cycle of atmospheric CO₂ and future food production. And as cropland CO₂ uptake is coupled with transpiration fluxes, it will also drive soil moisture depletion, influence the development of droughts and heat waves (Wolf et al., 2016; Miralles et al., 2014), and the cloud formation and precipitation patterns (Koster et al., 2015; Koster, 2004). This is why cropland-atmosphere interactions are a key area of research not only in short-term studies of atmospheric CO₂, but also for crop sciences, hydrology and numerical weather prediction.

While observations inform us on the carbon cycle of croplands, models fill the gaps over the global land heterogeneity and help test our fundamental understanding of it. This is why in this thesis we question the representation of croplands-atmosphere exchanges of CO₂ used in atmospheric transport models, numerical weather prediction and Earth system models. We adopt a multi-disciplinary approach to learn about the crop-specific and atmospheric processes that impact the coupled exchange of CO₂ and water at the surface. Our analysis spans the local to continental scale within Europe, and the diurnal to yearly time-scales, and we support it with observations of the cropland and atmosphere. In the next section, we briefly consolidate our knowledge of the global carbon cycle before re-focussing on the core topic of this thesis: cropland-atmosphere exchanges of CO₂.

1.1 The global carbon cycle

The global carbon cycle refers to the biological, chemical and physical processes of carbon exchange within and between the four major carbon reservoirs of the Earth system: the ocean, the land, the lithosphere and the atmosphere. These processes span various timescales from seconds (e.g. plant photosynthesis) to millennia (e.g. sedimentary rock formation), and dif-

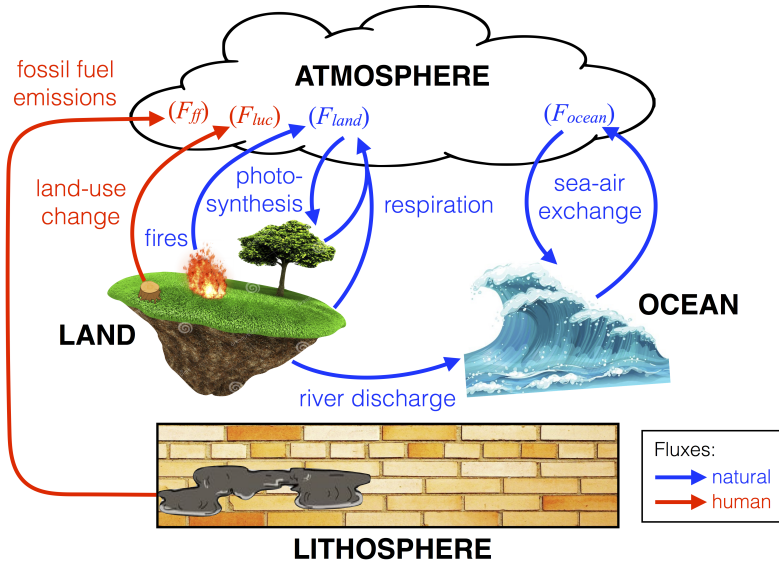


Figure 1.1 – Dominant carbon exchange processes at the time scales of seconds up to a decade. Here we only represent exchanges occurring at the interface of the global reservoirs, however internal cycling does occur within the land, ocean and atmosphere. Global croplands are part of the land reservoir.

ferent spatial scales from micrometers (e.g. cell respiration) to hundreds of kilometers (e.g. large-scale atmospheric and ocean circulation). This thesis puts emphasis on the carbon cycling processes that occur over seconds up to a decade, and from the local to the continental scale, processes that we summarize in Fig. 1.1. In this relatively short-term view of the carbon cycle, we thus exclude the influence of millennia-long processes such as weathering, vulcanism or sea-floor spreading.

A central goal of global carbon cycle studies is to estimate the cumulative effect of the processes represented in Fig. 1.1 on the atmosphere, in order to make future projections of CO_2 and climate change. For this purpose, atmospheric scientists compute a flux budget that expresses the growth in the global atmospheric CO_2 concentration (dC/dt , in PgC yr^{-1}). Since the industrial revolution, this budget is the result of four global CO_2 fluxes, also represented in parentheses in Fig. 1.1: the net land exchange (F_{land}), the net ocean exchange (F_{ocean}), the fossil fuel emissions (F_{ff}), and the land-use change emissions (F_{luc}):

$$\frac{dC}{dt} = \underbrace{F_{land} + F_{ocean}}_{\substack{\text{net negative fluxes} \\ \text{or "sinks"}}} + \underbrace{F_{ff} + F_{luc}}_{\substack{\text{net positive fluxes} \\ \text{or "sources"}}}. \quad (1.1)$$

Since the second world war, this budget has been largely driven by the exponential rise in F_{ff} , which has forced the land and ocean to respond to the enhanced atmospheric CO_2 concentrations, and to increase the size of F_{ocean} and F_{land} . This has resulted in the strong global carbon budget imbalance that we know today: in 2015, F_{land} and F_{ocean} have been estimated respectively at -3.0 and -2.6 PgC yr^{-1} , and F_{ff} and F_{luc} respectively at $+9.0$ and $+0.9 \text{ PgC yr}^{-1}$, resulting in a global growth of atmospheric CO_2 of $+4.4 \text{ PgC yr}^{-1}$ or $+2.1 \text{ ppmv yr}^{-1}$ (Le Quéré et al., 2015). But among the four global fluxes of CO_2 of Eq. 1.1, F_{land} has been shown to be the most variable from year to year (between a large sink of -4.1 PgC yr^{-1} and a small source of $+0.4 \text{ PgC yr}^{-1}$) and most uncertain (with a 1σ of 0.8 PgC yr^{-1} , see Le Quere 2015). To reduce the uncertainties on F_{land} , it is crucial to understand the dominant biochemical and physical processes that build up all land CO_2 fluxes. From here on, we deal strictly with the dominant processes occurring over croplands, as these have been less extensively studied than forests and grasslands by atmospheric scientists.

1.2 Cropland carbon cycling processes and their scales

Carbon cycling over croplands involves four exchange processes between the land and atmosphere, which are photosynthesis, respiration and fires (see F_{land} in Fig. 1.1), plus an additional off-site process: harvest consumption. We exclude here the on- and off-site fossil fuel emissions from fertilizer production, tractor use, harvest trade, and the land-use change emissions from conversion from and to croplands, as we consider these are part of F_{ff} and F_{luc} in Fig. 1.1. This cropland carbon cycle moreover involves a small removal of cropland soils into rivers and ultimately oceans. In addition, a series of internal carbon cycling processes takes place within the land and atmosphere overhead: processes of (a) lateral transfer of a carbon pool (e.g. harvest transport), and (b) transfers between pools (e.g. decay of soil organic matter). Finally, some external biological processes (e.g. crop phenology) exert a strong control on the rates of photosynthesis and respiration of crops. We present a list of all these cropland processes in Fig. 1.2 organized by their temporal and spatial scales. The cut-off signs on the x- and y-axes identify the scales we address in this thesis (from seconds to a year, and from the local to continental scales) and we will not discuss processes that are beyond this scope.

First at the local and instantaneous scale in Fig. 1.2, environmental conditions such as light, temperature, humidity, CO_2 concentration – conditions which are partly controlled by the atmospheric dynamics overhead and by the vegetation – determine the size of the photosynthesis and respiration fluxes. On the one hand, photosynthesis is the removal of CO_2 from the atmosphere by living plants, and on the other hand, respiration is the release of CO_2 from all living organisms to the atmosphere. Two types of respiration are usually dis-

1.2. CROPLAND CARBON CYCLING PROCESSES AND THEIR SCALES

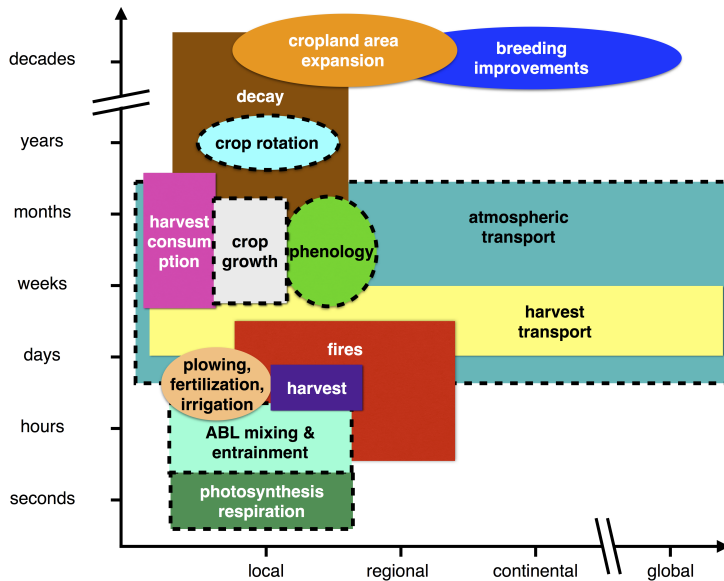


Figure 1.2 – Time and spatial scales of the carbon cycling processes at play above croplands. The cut-off sign on the x - and y -axes represents the limits of the scales we aim to address in this thesis. Carbon exchange and transport processes are strictly in rectangles, while other processes that affect the rates of photosynthesis and respiration are in ovals. Boxes with thick dashed borders indicate the processes under study in this thesis.

tinguished: autotrophic (i.e. the respiration from photosynthetic plants) and heterotrophic (i.e. the respiration from all other organisms, from soil biota to animals). Globally, total land photosynthesis, autotrophic and heterotrophic respiration are estimated to be roughly around -123 , $+60$ and $+60$ PgC yr^{-1} (Hashimoto et al., 2015; Beer et al., 2010), with a net residual of -3 PgC yr^{-1} as mentioned earlier. Since these fluxes are difficult to measure separately, the individual flux estimates have a substantial uncertainty. Moreover, as suggested by Fig. 1.2, these fluxes vary in space and time at smaller scales than the yearly and global scales. Hence our understanding of the local and short-term land-atmosphere interactions that build up these fluxes is very important.

Sudden perturbations from humans or fires can disturb the instantaneous state of the land-atmosphere. These perturbations essentially remove a part of the living terrestrial biosphere and transport it either directly back to the atmosphere in the case of fires, or to a transient pool of solid carbon in the case of a harvest, which will be redistributed and consumed by humans and cattle later on. Globally, fires have been estimated to release between 1.8 to 2.6 PgC yr^{-1} (2002-2011 estimates), and since this number is at present relatively well-constrained (Shi et al., 2015), we will not focus on this exchange process in this thesis. The removal of the

harvest and its dislocation are important, but will not be discussed in detail. Instead, we will focus on two other processes that regulate the rates and timing of carbon cycling over croplands: phenology and rotation. On the multi-annual scale, crop rotation (i.e. the year-to-year changes in crop species decided by the farmer) plays a role in determining the potential magnitude of photosynthesis and respiration, and thus in determining the accumulation of carbon into plant organs otherwise known as crop growth. On the seasonal scale, crop phenology (i.e. the timing of crop development and maturation) determines the length of the growing season, which is the crop's time-window of opportunity for carbon accumulation.

Finally, the only processes that span all spatial scales of Fig. 1.2 are the carbon transport processes within the land and atmospheric compartments. Firstly, atmospheric CO_2 transport encompasses the local and diurnal process of atmospheric boundary-layer development and entrainment (i.e. mixing and dilution of the local CO_2 concentration) but also the horizontal advection and large-scale movements of air masses, which redistribute CO_2 across the continental domain and allows further local mixing and surface exchange. Secondly, harvest consumption represents a local release of CO_2 that can be delayed up to a year if harvest products are stored. In this thesis, we will only address atmospheric transport, although harvest consumption is important for spatio-temporal patterns of CO_2 cropland-atmosphere exchange. These aspects could easily be considered in a follow-up study (see Chapter 5).

To summarize, in this thesis we address all carbon cycling processes highlighted with a dashed border in Figure 1.2, starting from the smaller spatiotemporal scales and then zooming out to the larger ones. In the first chapters, we thus focus on the diurnal processes of photosynthesis and respiration and ABL development, and especially the local implications of having a coupled exchange of water and CO_2 through the plant stomata. We lay the basis for this initial analysis in the next section.

1.3 Local coupling of water and CO_2

Figure 1.3 focusses on the local and diurnal scales of Fig. 1.2 and illustrates the interactions taking place between a fully coupled crop surface and atmosphere, which we analyze in Chapters 2 and 3. During daytime, plants absorb the energy of sunlight (i.e. the shortwave radiation) and use it to synthesize sugars from atmospheric CO_2 and soil moisture. To perform photosynthesis, plants absorb CO_2 from the atmosphere and release water vapor through a unique entry point, the stomata, which are microscopic openings in the leaf surface. This effectively couples the water and carbon exchanges of the plant during daytime. In addition to performing photosynthesis in the leaves, all plant cells respire and thereby release CO_2 to produce the necessary energy for cellular activity. This respiration process uses the sugars previously produced by photosynthesis and oxygen absorbed by the roots from the soil pores.

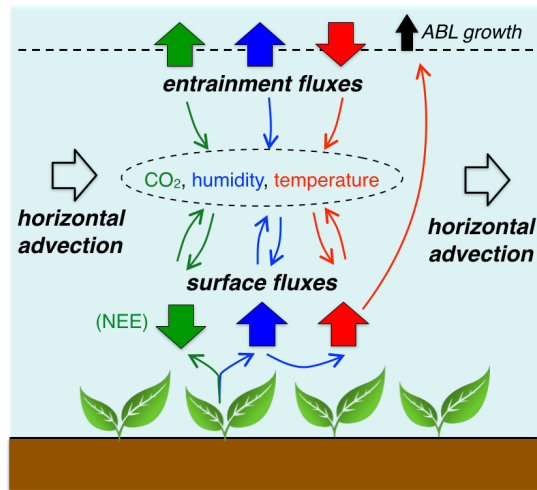


Figure 1.3 – Conceptual view of the coupled crop-atmosphere system. We illustrate the basic interactions of the carbon (green), water (blue), and heat (red) cycles that govern the atmospheric CO₂ budget of Eq. 1.2.

Contrarily to photosynthesis, this process is not regulated by the stomata. In terms of net exchange of CO₂ with the atmosphere (or net ecosystem exchange, NEE), photosynthesis is dominant over respiration for a grown unstressed crop. During nighttime, photosynthesis ceases in the absence of solar radiation, but respiration continues.

Because stomata are the main exchange point for CO₂ and water vapor between crops and the atmosphere, it is the size of the stomatal aperture that determines how much of the absorbed shortwave radiation can be used for CO₂ assimilation and transpiration by the plant, and subsequently how much of the surface energy is left to be emitted as sensible heat or transferred to the ground. The stomatal aperture is dynamically regulated by the plants as they experience more or less favorable environmental conditions in terms of light, temperature, CO₂ concentration, humidity and soil moisture. This regulation by the plants is particularly drastic under water-limited conditions, as plants close their stomata in order not to lose too much water. In the end, plants therefore dynamically control the surface energy balance (i.e. the partitioning of energy used for photosynthesis, evapotranspiration, and heat release, see the corresponding three surface fluxes arrows in Fig. 1.3) on the time scales of minutes. This, in turn, is crucial for the development of turbulent motions of the air right above them.

The atmospheric boundary layer (ABL) is the lowest layer of the atmosphere that is directly influenced by the cropland exchange of heat, water vapor, and CO₂. The upper limit of the ABL is a region characterized by a positive gradient of potential temperature, roughly located 1-2 km above the crop surface in the temperate latitudes of the globe. This tem-

perature gradient – or “inversion” – is quite important as it indicates a stable stratification (i.e. the warmer upper layer stays above) and acts as a permeable lid. During the day, the release of sensible heat by the crop surface triggers buoyant turbulent mixing of air in the ABL that causes it to grow by entrainment, i.e. by incorporating some free tropospheric air into the mixed ABL, effectively moving up the region of the temperature inversion. This entrainment process, which speed is indirectly controlled by the plants but also by the large-scale atmospheric conditions of the day (e.g. stability, subsidence), generates an exchange of water, CO₂, and heat between the ABL and the free troposphere above. These entrainment fluxes (see Fig. 1.3) occur at the time scale of minutes like the surface fluxes. They modify atmospheric conditions within the ABL and ultimately feed back onto the surface fluxes.

Atmospheric conditions evolve along the day as a result of the coupled surface and ABL-top fluxes of water, carbon and heat, and of the ABL growth. This evolution is moreover affected by horizontal movements of air masses – or “horizontal advection” – that introduces a third set of carbon, water and heat exchange at the lateral boundary of the air column (see Fig. 1.3). Horizontal advection is not a turbulent exchange process like entrainment or a biochemical exchange process like at the crop surface, but a physical process simply driven by large-scale atmospheric pressure differences. We can express the diurnal evolution of the CO₂ concentration in the mixed ABL (in ppm s⁻¹) as the budget of all aforementioned processes:

$$\frac{dc}{dt} = \underbrace{\frac{1}{h}}_{\text{dilution}} \times \left(\underbrace{\frac{\text{NEE}}{\bar{\rho}_{\text{air}} \times \frac{M_{\text{CO}_2}}{M_{\text{air}}}}}_{\substack{\text{Surface} \\ \text{biochemical flux of CO}_2}} - \underbrace{\overline{w'c'_e}}_{\substack{\text{Entrainment} \\ \text{turbulent flux of CO}_2}} \right) + \underbrace{adv_c}_{\substack{\text{Horizontal advection} \\ \text{flux of CO}_2}}. \quad (1.2)$$

with h in m, NEE in kg m⁻² s⁻¹, $\overline{w'c'_e}$ in ppm m s⁻¹, and adv_c in ppm s⁻¹. Note that we convert NEE to ppm m s⁻¹ by dividing it by the average density of air and by the ratio of molar masses of CO₂ (M_{CO_2}) and air (M_{air}). This diurnal budget of CO₂ is the basis of the analysis we perform in Chapters 2 and 3, where we investigate the local interactions of the carbon, water and heat cycles. It typically translates into a decrease of the CO₂ concentration during daytime, as long as the sunlight feeds the crop surface with sufficient energy for the biochemical and turbulent processes.

At night, an entirely different chain of processes takes over. Without sunlight, plants interrupt photosynthesis and their coupled transpiration but continue to respire. As they have no shortwave radiation to absorb and release as sensible heat, buoyant turbulence stops in the ABL but wind shear-generated turbulence may continue. The radiative cooling (i.e. cooling by emission of longwave radiation) of the surface and of the lower part of the atmosphere causes the air to stratify. This stratification deepens through the ABL if no clouds are present to trap the long wave radiation emitted by the surface and if wind shear turbulence is

weak. Due to the trade-off between stratification by radiative cooling and turbulence generated by wind shear, conditions in the nocturnal ABL can vary greatly from completely stable and stratified, to intermittently turbulent, relatively well-mixed, or even to a stably stratified surface layer coexisting with a mixed upper ABL. As a general rule, plant respiration will greatly increase CO_2 concentrations near the ground during the night, and while CO_2 transport throughout the nocturnal ABL is hard to predict, it is usually smaller than during daytime. As the nocturnal ABL, but also the transition from and to the daytime ABL are difficult to describe, we will limit ourselves to the analysis of the daytime ABL, especially the strongly mixed cases that typically occur during sunny cloudless days in summer. In the next section, we introduce the general aim of this thesis and the methods we have selected to tackle it.

1.4 Aim and approach of this thesis

In this thesis we question the current representation of CO_2 exchange above croplands in common land-surface models, and its impact on the modeled atmospheric CO_2 concentration. To achieve our goal, we use a bottom-up modeling approach of the processes considered in Fig. 1.2. We compare two modeling approaches to represent the surface CO_2 and water exchange over croplands: land-surface models and crop growth models. We combine these models – in a coupled or non-coupled fashion – to atmospheric models, and compare the results to observations of the crop-atmosphere system.

1.4.1 Cropland surface models

First, we have chosen to employ two land-surface models: A- g_s (Jacobs 1994, in Chapters 2 and 3) and SiBCASA (Schaefer et al. 2008, in Chapter 4). Like many modern land-surface models, A- g_s and SiBCASA compute the vegetation net ecosystem exchange by combining (a) a model for the biochemical reactions of leaf C_3 and C_4 photosynthesis (originating from Farquhar et al., 1980), (b) a CO_2 diffusion scheme with the calculation of a stomatal conductance to model the transport of CO_2 from outside to inside the leaf (started by Collatz et al., 1991; Ball et al., 1987), and (c) an upscaling algorithm to infer the canopy net CO_2 flux from the leaf flux. Notable differences exist between these two models, like the modified version of the Farquhar model they use, the formulation of the atmospheric humidity stress they adopt (using relative humidity in SiBCASA or vapor pressure deficit in A- g_s), and the upscaling scheme they have each designed. The common advantage of all diffusion-based land-surface models is that their stomatal conductance formulation facilitates modeling a full surface energy balance and coupling the surface and atmosphere, which is why they are used extensively in weather and climate models (e.g. A- g_s in Boussetta et al.,

2013), and coupled carbon-climate models (Arora et al., 2013). Similarly, we use $A-g_s$ in Chapters 2 and 3 to study a fully coupled crop-atmosphere system at the diurnal scale, and in the process we contribute to the ongoing debate about how soil moisture stress should be represented in land-surface models (Verhoef and Egea, 2014; De Kauwe et al., 2013; Egea et al., 2011). Furthermore at the larger scales, both $A-g_s$ and SiBCASA have been parameterized to represent various global biomes (e.g. broadleaf forests, grasslands, croplands), and this parameterization is known to oversimplify the representation of crop phenology and crop growth (Gervois et al., 2004) and to neglect the impact of crop management. This is why we take SiBCASA estimates of seasonal cropland NEE as our benchmark in Chapter 3, from which we can improve.

Second, we also employ two crop growth models: GECROS (Yin and van Laar 2005, in Chapter 1) and WOFOST (Supit et al. 1994, in Chapters 4 and 5). Both models are issued from a long line of empirical crop yield models initiated at Wageningen University by de Wit (1978), Goudriaan (1977), van Keulen (1975) and Penning De Vries et al. (1974). These models compute only crop photosynthesis and respiration, which is why we complement them with a well-established representation for soil respiration (Lloyd and Taylor, 1994) to obtain NEE. Similarly to the land-surface models described above, the crop models represent (a) leaf photosynthesis and (b) an algorithm to upscale to the canopy level, however they do not use a diffusion scheme. In addition, they comprise crop-specific processes of phenology and growth, plus irrigation and nitrogen fertilization options. We assume in this thesis that our crops are all rain-fed (i.e. not irrigated) and well-fertilized, thus we only include the effects of water stress. The most striking difference between the two crop growth models is how they implement soil moisture stress on canopy photosynthesis. While GECROS calculates the amount of available soil moisture and evaluates if that is enough to maintain the transpiration flux (so-called evaporative demand approach), WOFOST assesses soil moisture stress in regard to the wilting point and critical point of the soil, as is done by many land-surface models (so-called β approach). The second most striking difference is that GECROS offers a diagnostic equation for stomatal conductance, but not WOFOST. In Chapter 2, we thus attempt to couple GECROS with an atmospheric model. In the process we demonstrate that the evaporative demand approach for water stress does not allow for a realistic representation of the crop-atmosphere coupling. Moreover, both GECROS and WOFOST were designed purely to estimate crop yield and have never been verified against observations of NEE, nor have they ever been coupled to a surface energy balance and atmospheric model before (except the current unpublished efforts of Ingwersen et al. on NOAH-GECROS at the University of Hohenheim). This is why, after discarding GECROS and its water-stress parameterization in Chapter 2, we use WOFOST uncoupled to the atmosphere and evaluate its surface CO_2 exchange against observations across Europe in Chapter 4.

1.4.2 Atmospheric models

To obtain a fair balance between the representation of surface and atmospheric processes, we combine the cropland surface models described above to a diurnal atmospheric scheme, the MXL model (Vilá-Guerau de Arellano et al., 2009) in Chapters 2 and 3. MXL is a diurnal mixed-ABL scheme, which conceptualizes the most important processes of daytime convective ABL dynamics over a homogeneous land-surface (thus smaller than 1-5 km²). It solves the governing equations of wind, temperature, humidity and CO₂ evolution during daytime using a well-mixed ABL assumption (Tennekes, 1973; Lilly, 1968), which occurs typically over land during clear sky days. Entrainment fluxes are parameterized and turbulence does not need to be resolved, thus it is the least computationally-expensive atmospheric model. It can easily be coupled to a land-surface scheme, which is why we use it in Chapters 2 and 3 coupled with our cropland surface models, to study the full diurnal and local coupling of a cropland with the ABL. Specifically, we focus on the impact of this coupling on the CO₂ concentrations right above. In Chapter 4, we cease with the fully coupled land-atmosphere approach, and we represent the impact of the atmosphere on croplands by supplying re-analysis weather data from the ECMWF model (Dee et al., 2011).

1.4.3 Crop-atmosphere observations

To support our numerical results, we use eddy-covariance (EC) measurements of surface fluxes (NEE, sensible and latent heat) and of the atmospheric state (temperature, humidity, CO₂ concentration), as well as lidar measurements of ABL height. The EC technique has become the most important method to measure the net surface exchange of heat, water, and CO₂ over land (Baldocchi, 2003). EC flux measurements are usually done as a temporary setup over short (e.g. one season) to long periods of time (e.g. 10 years) and are typically performed at a two/three-meter height above surface. The EC flux set-up measures surface exchange of heat, water, and CO₂ by sampling fast fluctuations of concentrations and vertical velocities. The technique integrates fluxes over an area of the order of 10-500 m² with a minimal impact on the vegetation. There is currently an active network for EC measurements around the globe (see the FluxNet community, with a data portal at <http://fluxnet.fluxdata.org>) and thus standardized measurements have been performed at numerous locations across Europe – although less at cropland sites. EC measurements can thus help validate surface fluxes and the atmospheric state from our models. In Chapters 2 and 3, we complete the EC flux and concentration measurements of NEE, sensible heat flux, latent heat flux, CO₂, air temperature, and humidity, with measurements of soil moisture and boundary-layer height to infer the behavior of the fully coupled daytime crop-ABL system at one location in the Netherlands. In Chapters 4, we simply use the EC measurements of NEE to validate our representation of the seasonal cropland NEE over Europe.

1.5 Outline and overarching research questions

In this thesis, we pursue three research objectives, which structure our analysis (see Fig. 1.4). Our first objective is to investigate the full set of interactions that take place between croplands and the atmosphere at the diurnal scale, for the carbon and water cycles. This first objective is twofold. Firstly, we explore how these interactions shape the local ABL CO_2 concentration at the daily scale, considering not only atmospheric but also surface drivers of the budget presented in Eq 1.2 (see Chapter 2). Secondly, we investigate how such interactions are affected under water stress as stomatal regulation is the key point of control for the plants on (a) CO_2 fluxes and (b) ABL growth and entrainment of CO_2 (see Chapter 3). Our second research objective is to reproduce the processes that drive the net carbon exchange or NEE above croplands, from the diurnal to the seasonal scale. We focus on the seasonal impact of crop growth, crop phenology and crop rotation on the timing and magnitude of the instantaneous rates of CO_2 exchange above croplands (see Chapter 4). Finally, our third objective is to infer the impact of such seasonal cropland CO_2 exchange and of the atmospheric CO_2 transport on the concentrations measured over Europe.

Several overarching research questions emerge from these objectives. Our first and second are two faces of the same coin, as we investigate the governing processes of the cropland-atmosphere exchange of CO_2 , and their proper representation in models:

Research question 1: *What are the main surface and atmospheric processes that determine the ABL CO_2 budget from the hourly to the seasonal scales?*

Research question 2: *What are the advantages and drawbacks of crop growth models compared to terrestrial biosphere models when representing cropland NEE from the diurnal to the seasonal scales?*

We tackle these questions from Chapters 2 to 4 by modeling the processes of Fig. 1.2 from the smaller to the larger spatiotemporal scales, and verifying our representation(s) with a complete set of observations of the cropland fluxes and atmospheric conditions overhead.

The third overarching question of this thesis is related to the key control from the vegetation on the crop-atmosphere carbon cycle:

Research question 3: *How should we represent plant water-stress in (crop)land-surface models?*

We answer this question in Chapters 2 and 3, as we test different parameterizations for plant water stress.

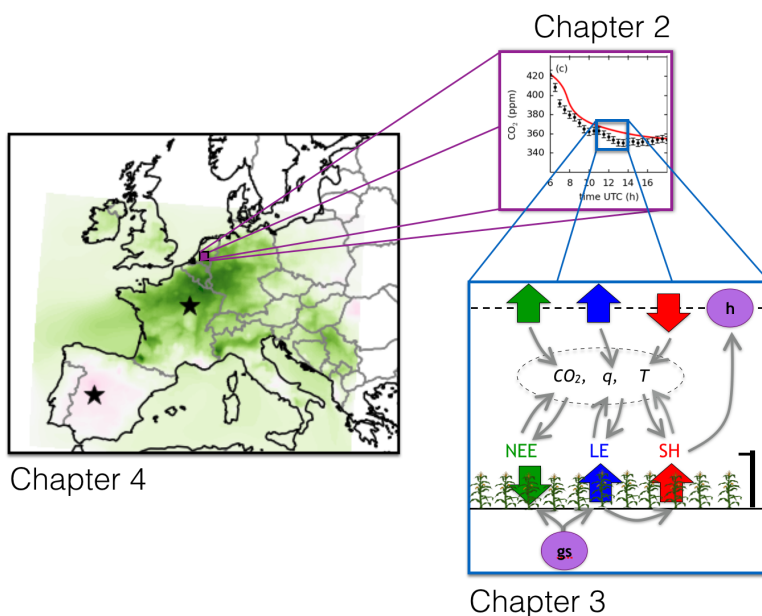


Figure 1.4 – Structure of the thesis. Chapters 2 & 3 focus on the daily to hourly CO₂ exchange above croplands at a point location in the Netherlands, then Chapter 4 deals with the daily to seasonal cropland emissions of CO₂.

Our fourth and final overarching question is specifically to understand the breadth of the improvement we can make by using a specialized representation of cropland CO₂ exchange to model cropland NEE and furthermore the atmospheric CO₂ concentration:

Research question 4: *What is the impact of an improved representation of cropland NEE on the modeled CO₂ mole fractions across Europe?*

We address this question in Chapters 4 and 5, as we first represent cropland CO₂ fluxes with a crop growth model that assimilates grain yield observations, and then we transport the CO₂ concentrations over Europe with an atmospheric transport model. We will come back to these overarching research questions in the thesis Summary, after going through the chapters outlined in Fig 1.4, and the general discussion.

2

Two perspectives on the coupled carbon, water and energy exchange in the planetary boundary layer

Understanding the interactions between the land surface and the atmosphere is key to modelling boundary-layer meteorology and cloud formation, as well as carbon cycling and crop yield. In this study we explore these interactions in the exchange of water, heat and CO₂ in a cropland–atmosphere system at the diurnal and local scale. To that end, we couple an atmospheric mixed-layer model (MXL) to two land-surface schemes developed from two different perspectives: while one land-surface scheme (A-g_s) simulates vegetation from an atmospheric point of view, the other (GECROS) simulates vegetation from a carbon-storage point of view. We calculate surface fluxes of heat, moisture and carbon, as well as the resulting atmospheric state and boundary-layer dynamics, over a maize field in the Netherlands, on a day for which we have a rich set of observations available. We show that the atmospheric-oriented model (MXL-A-g_s) outperforms the carbon storage-oriented model (MXL-GECROS) on this diurnal scale. We find this performance is partly due to the difference of scales at which the models were made to run. Most importantly, this performance strongly depends on the sensitivity of the modelled stomatal conductance to water stress, which is implemented differently in each model. This sensitivity also influences the magnitude of the surface fluxes of CO₂, water and heat (surface control) and subsequently impacts the boundary-layer growth and entrainment fluxes (upper atmosphere control), which alter the atmospheric state. These findings suggest that observed CO₂ mole fractions in the boundary layer can reflect strong influences of both the surface and upper-atmosphere conditions, and the interpretation of CO₂ mole fraction variations depends on the assumed land-surface coupling. We illustrate this with a sensitivity analysis where high subsidence and soil moisture depletion, typical for periods of drought, have competing and opposite effects on the boundary-layer height h . The resulting net decrease in h induces a change of 12 ppm in the late-afternoon CO₂ mole fraction. Also, the effect of such high subsidence and soil moisture depletion on the surface Bowen ratio are of the same magnitude. Thus, correctly including such two-way land-surface interactions on the diurnal scale can potentially improve our understanding and interpretation of observed variations in atmospheric CO₂, as well as improve crop yield forecasts by better describing the water loss and carbon gain.

This chapter is published as Combe, M., Vilà-Guerau de Arellano, J., Ouwersloot, H. G., Jacobs, C. M. J., and Peters, W.: Two perspectives on the coupled carbon, water and energy exchange in the planetary boundary layer, *Biogeosciences*, 12, 103-123, doi:10.5194/bg-12-103-2015, 2015.

2.1 Introduction

The land surface and atmosphere interact on many time scales, and understanding their exchange of energy, water, carbon and chemical tracers is key to many research fields, including climate modelling (Cox et al., 2013; Sitch et al., 2008), crop yield prediction (Lobell et al., 2011), hydrology (Teuling et al., 2010), atmospheric composition (Bonan, 2008) and meteorology (Vilà-Guerau de Arellano et al., 2012). When the interaction concerns a vegetated surface and the planetary boundary layer overhead, the cycles of carbon, water and energy are strongly coupled, notably at the surface. Responding to their environment, plants regulate the exchange of CO₂ and water vapour through the opening and closing of their stomata (Jarvis, 1976; Cowan, 1978; Ball, 1988), which in turn impacts the energy partitioning at the surface. This plant control over the carbon, water and energy exchange plays a key role, especially in climate change studies, which is why the current generation of climate models all include mechanisms to describe the stomatal response of vegetation to changing environmental conditions (Farquhar et al., 1982; Collatz et al., 1991; Leuning et al., 1995; Jacobs et al., 1996). The ongoing rise of temperature and CO₂ concentration are already shown to affect the coupled cycles of water and carbon as plants have become more efficient in water use over the past decades (Keenan et al., 2013; Brienen et al., 2011; Silva and Horwath, 2013). Quantitative understanding of these interactions between plants and the atmosphere is therefore needed.

The development of numerical models to describe land–atmosphere interactions is based on two perspectives. While vegetation models focus on carbon accumulation in land-surface types, such as forests and crops, and treat the atmosphere as a prescribed upper boundary condition, the atmospheric models focus on weather forecast and use land surface as a prescribed lower boundary condition. The former group includes (dynamic) vegetation models and crop yield models such as LPJ (Sitch et al., 2003), ORCHIDEE-STICS (Smith et al., 2010) and CERES-maize (Bert et al., 2007). The latter includes submodels of numerical weather prediction systems and atmospheric transport models such as in SiBcrop-RAMS (Corbin et al., 2010), RAMS-Leaf3-5PM (Tolk et al., 2009) and WRF-VPRM (Ahmadov et al., 2007). The next generation of vegetation and atmospheric models integrates both perspectives by allowing two-way interactions between the land and the atmosphere. In these models, carbon from the atmosphere is accumulated into vegetation, which in turn feeds back energy, water and CO₂ into the atmosphere overhead (e.g. the C⁴MIP models HadCM3LC, IPSL-CM4-LOOP, Bern-CC in Cox et al., 2013; Friedlingstein et al., 2006).

Recent studies have analysed the underlying mechanisms of land–atmosphere interactions and feedbacks using two-way couplings between the land surface and the planetary boundary layer (Santanello et al., 2013; McGrath-Spangler and Denning, 2010; van Heerwaarden et al., 2009). Among them, Vilà-Guerau de Arellano et al. (2012) have clearly demonstrated

the importance of how these interactions are described. They showed that future conditions of CO₂ level rise and warming would influence the boundary-layer cloudiness by affecting the plant stomatal aperture and vapour pressure deficit (VPD), thus changing both evapotranspiration and atmospheric humidity. Upper-atmosphere conditions, which are connected to large-scale synoptic weather patterns, were suggested to further affect the stomatal response through their control of the daytime boundary-layer growth and entrainment. Although the Vilà-Guerau de Arellano et al. study only focused on the diurnal and local scale with a relatively simple coupled model, the implications for two-way coupled models operating on much larger and longer scales were evident.

In this study, we continue this approach and analyse the coupling between the heat, moisture and carbon cycles for a maize field. We specifically focus on the diurnal scale, like Vilà-Guerau de Arellano et al. (2012), paying particular attention to the simulation of carbon fluxes and especially photosynthesis, which have a cumulative impact on crop growth and crop yield at the seasonal scale. We also explore the relative importance of upper-atmosphere conditions like subsidence, compared to the role of surface forcings like soil moisture, for the determination of CO₂ mole fractions. We choose to focus on crop–atmosphere interactions because croplands occupy a fifth of the European Union land surface (FAOSTAT 2011 land-use statistics), are important for food production and yet are often not well represented in land-surface models. In dynamic global vegetation models (DGVM) and soil–vegetation–atmosphere transfer models (SVAT models), they are conceptualised either as natural (e.g. Sitch et al., 2003) or managed grass (e.g. Krinner et al., 2005) and only distinguished by C₃ or C₄ plant photosynthesis. Differences between species of crops in development are often not simulated but rather are prescribed using seasonal leaf area index (LAI). Also, nitrogen stress or the effect of management options (fertilisation, irrigation, ploughing) are often not implemented at all, although they have been shown to have a large impact on crop carbon cycling (Ciais et al., 2010; Lehuger et al., 2010; Gervois et al., 2008). In contrast to DGVMs, process-based crop models could potentially better represent these crop characteristics (Challinor et al., 2009; Betts, 2005).

In order to investigate the differences between the generic and specialised representation of crop biology, we use a process-based crop yield forecast model, the genotype-by-environment interaction on crop growth simulator (GECROS; Yin and van Laar, 2005), and a more meteorological-oriented, surface–atmosphere exchange model, A-g_s (Ronda et al., 2001). We couple them to the same atmospheric mixed-layer model (MXL) and compare their ability to reproduce crop–atmosphere interactions. Both models simulate the daytime carbon, water and heat surface fluxes, with A-g_s more focussed on representing the individual surface energy balance terms. The additional levels of complexity embedded in GECROS are the separation of the effects of diffuse and direct radiation on photosynthesis, the internal calculation of crop LAI, the allocation and storage of carbon into crop organs (leading to

crop yield) and the interaction of the carbon and nitrogen cycles (nitrogen stress). We assess both models using a very comprehensive observational data set from a maize field in the Netherlands (Jans et al., 2010) that includes atmospheric variables (temperature, humidity, radiation), the surface fluxes of CO₂, water and (sensible and ground) heat, the soil temperature and humidity and the seasonal crop development (crop height, LAI, dry matter weight). We combine it with boundary-layer height data from a nearby meteorological station (Cabauw experimental site). It is important to stress that these observations were conducted at the same local scale as we simulate (field scale), which is smaller than typically simulated in climate models (i.e. 50 km resolution at minimum). In order to bridge these different scales (Eitzinger et al., 2008; Betts, 2005), we couple both our surface models, GECROS and A-g_s, to a model for the atmospheric boundary layer (ABL). This framework enables us to draw conclusions about the key boundary-layer–vegetation interactions, and we use it to answer two research questions:

1. What are the essential processes at the surface and upper atmosphere governing the coupled carbon, water and energy budgets in the daytime crop–atmosphere system?
2. Which modelling perspective can best reproduce these essential processes, and what does it teach us about the level of complexity needed in a daytime diurnal land-surface scheme?

We hypothesise that:

1. In addition to surface processes, entrainment and subsidence are essential processes which determine the carbon, water and energy budgets of the daytime crop–atmosphere system.
2. MXL-GECROS can best reproduce the daytime crop–atmosphere interactions because of the higher level of crop biology detail embedded in the model.

The next section presents a description of our surface and atmospheric models as well as of their coupling strategy. We then present our findings with the full daytime intercomparison of our two coupled models against observations and a sensitivity analysis of the two-way daytime crop–atmosphere interactions.

2.2 Methods

2.2.1 Observations

In order to verify the behaviour of the cropland–atmosphere system, we use a comprehensive set of surface exchange, atmosphere, soil and crop growth observations, which were performed in 2007 and 2008 in a maize field located in Wageningen, the Netherlands (see

Jans et al., 2010). This data set consists of half-hourly averages of the sensible and latent heat fluxes and CO₂ exchange, obtained with the eddy covariance (EC) technique. They are quality-controlled according to the protocols described in Aubinet et al. (2012). These EC observations are supported by various continuous micrometeorological measurements in the air and in the soil. In addition to the continuous measurements, this data set includes soil type, crop management data and intermittent observations of crop height, plant area index (PAI; i.e. a proxy for LAI) and the dry weight of crop organs over the growing season. To complete the atmospheric observations from Jans et al., we use the boundary-layer height from the wind profiler measurements of the closest meteorological station (Cabauw, the Netherlands) located approximately 50 km west from the maize site (Cabauw experimental site for atmospheric research, online database available at <http://www.cesar-database.nl>). In the absence of boundary-layer height data for Wageningen, this is the best estimation possible.

Because we want to focus on the diurnal scale to study the interactions and feedbacks of our maize–atmosphere system, we specifically pick 1 day of observations, 4 August 2007: a sunny, cloudless day with a convective atmospheric boundary layer above the maize field. We pick that specific date because our atmospheric boundary-layer model can only reproduce well-mixed boundary layers and we want to avoid sensitive periods of emergence and senescence times for the crop. On 4 August 2007 our maize crop is in the reproductive stage, at the peak of its growth (see PAI in Fig. 2.1).

On 4 August 2007, the continuous measurements show a daytime energy gap of 19% between the net absorbed radiation and the sum of the surface (latent, sensible and ground) heat fluxes. This energy gap is typical for a crop like maize, mainly due to heat storage (Meyers and Hollinger, 2004). The gap can also be partially generated by photosynthesis, which can proceed at unusually large rates for maize, large-scale heat transport processes and measurement accuracy (Foken et al., 2010; Foken, 2008). Since the two surface schemes we use assume the closure of the surface energy budget, we allocate the missing energy (or residual) into extra sensible and latent heat in the observations, using the Bowen ratio to determine the partitioning (see Eq. 2.1).

$$\text{Flux}_{\text{corrected}} = \text{Flux}_{\text{observed}} + \text{Residual} \times f, \quad (2.1)$$

$$\text{with } f = \begin{cases} \frac{\beta}{1+\beta} & \text{for SH} \\ \frac{1}{1+\beta} & \text{for LE} \end{cases}$$

This method ensures the observed Bowen ratio is conserved after correction. It has been previously used by Barbaro et al. (2014), Foken (2008), Twine et al. (2000) and Beljaars and Bosveld (1997). For reference, we show in Fig. 2.3 both the observed and corrected fluxes. Note that the corrected fluxes are used in the further model comparisons.

2.2.2 Models

In order to study the daytime cropland–atmosphere system, we couple two surface schemes, GECROS and A-g_s, to a convective atmospheric boundary-layer scheme, MXL, and analyse their behaviour compared to our observations on 4 August 2007.

MXL, a convective atmospheric boundary-layer scheme

Our atmospheric boundary-layer scheme is a box model, which describes accurately the development of the daytime atmospheric boundary layer when turbulence is strong (mixed-layer situation). The first studies to develop the concept of a mixed-layer model were done by Lilly (1968), Betts (1973), Carson (1973) and Tennekes (1973). The version used in this paper has been described by Vilá-Guerau de Arellano et al. (2009). The ABL is well mixed during this strongly convective daytime regime, and thus we infer that the instantaneous atmospheric variables assume a single value throughout the whole ABL. The top of the boundary layer is characterized by potential temperature, moisture and CO₂ inversions, simplified as sudden “jumps” or gradients, which sharply separate the ABL state from the free tropospheric profiles. The evolution of the ABL state and height over time is determined by boundary fluxes (surface, entrainment and advection) of heat, moisture and CO₂. Entrainment fluxes are calculated. The MXL model has been widely tested and is a robust model for sunny days with few to no boundary-layer clouds – all conditions met on 4 August 2007 over our maize field.

GECROS, a crop yield forecast model

GECROS is a land-surface model specialised in crop carbon storage (i.e. a crop yield forecast model). We use version 1.0, which was released by Yin and van Laar (2005). GECROS is from the two-big-leaf family of models initiated by De Pury and Farquhar (1997), which means the crop canopy is simplified into two leaves, each possessing one substomatal cavity. One leaf represents the entire sunlit leaf area of the canopy, the other represents the entire shaded leaf area; their proportions evolve with crop age and solar angle. The two big leaves work in parallel for daytime photosynthetic and transpiration processes. This enables different efficiencies of photosynthesis to happen under diffuse and direct radiation.

On the diurnal scale, GECROS is a crop growth model based on evaporative demand, which means that the potential photosynthesis is first calculated according to the amount of available photosynthetically active radiation, and then it determines the leaf conductance and the potential transpiration. The actual photosynthesis and transpiration are obtained by evaluating the soil water content: if the available soil moisture is higher than the amount of water needed for potential transpiration, GECROS works at full potential. Otherwise,

GECROS transpires solely the available water supply and reduces its photosynthesis and stomatal conductance accordingly. In addition to water stress, GECROS has a nitrogen cycle implemented that interacts with the carbon cycle, accounting for nitrogen stress. This last feature did not play a role in our study of crop–atmosphere interactions on 4 August 2007.

On the seasonal scale, GECROS simulates its own phenological development based on the accumulation of heat (i.e. growing degree-days). Also, it accumulates carbon into the different crop organs (leaves, stems, roots and storage organs), which determines crop yield. Both of these features, typical of a crop model but not of a DGVM or SVAT model, allow interactions and feedbacks between the crop and the atmosphere to change with crop ageing. This is a potential advantage for a seasonal study of the cropland–atmosphere system.

Modifications to GECROS used in this paper and validation

We analysed the surface energy budget of GECROS and identified two core problems in its original version: (a) the budget of net long-wave radiation was faulty, generating too much outgoing long-wave radiation and consequently too little energy was retained at the surface; and (b) the calculated VPD was too high because it used the humidity at 2 m instead of inside-canopy humidity, stimulating too much latent heat at the expense of sensible heat. In order for GECROS to have realistic heat fluxes to feed to the MXL model, we implemented the following changes to improve its surface energy balance. First we replaced the original net long-wave radiation budget with a simplified multilayer budget:

$$LW_i = \left(\underbrace{\mathcal{E}_{ATMOS} \times \sigma \times T_{ATMOS}^4}_{\text{Incoming radiation}} - \underbrace{\mathcal{E}_i \times \sigma \times T_i^4}_{\text{Outgoing radiation}} \right) \times F_i, \quad (2.2)$$

$$\text{with } F_i = \begin{cases} f_{veg} & \text{if sunlit leaf } (i = 1) \\ 0 & \text{if shaded leaf } (i = 2) \\ 1 - f_{veg} & \text{if bare soil } (i = 3), \end{cases}$$

where \mathcal{E}_{ATMOS} and \mathcal{E}_i are emissivities, T_{ATMOS} and T_i are temperatures, σ is the Stefan–Boltzmann constant and f_{veg} is the vegetation-cover fraction. We assume similar black-body radiation ($\mathcal{E}_1 = \mathcal{E}_2 = \mathcal{E}_3 = 1$) originating from the sunlit leaf, shaded leaf and the underlying soil. As a consequence, we approximate the net long-wave radiation budget of the shaded leaf to be zero. Note that there is no interaction of long-wave radiation between the bare soil and vegetated fractions and thus no reabsorption of emitted long-wave radiation. This approximation for shaded leaves in a multilayer model is supported by Zhao and Qualls (2006).

Then, in order to decrease the allocation of energy into the latent heat flux, we create

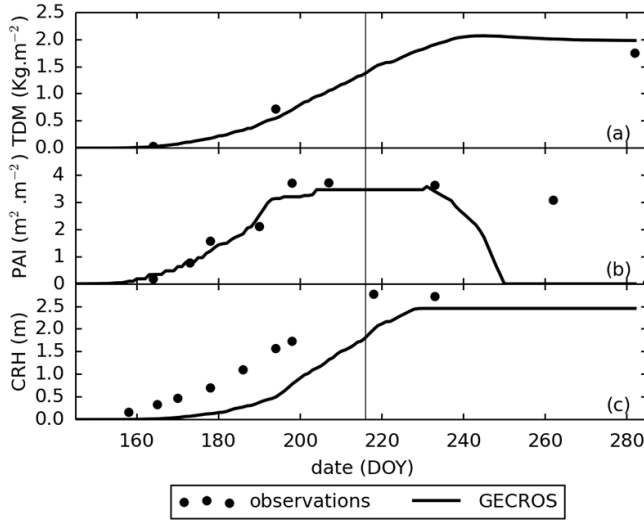


Figure 2.1 – Seasonal evolution of the (a) maize total dry matter (TDM), (b) plant area index (PAI) and (c) crop height (CRH), from sowing to maturity dates. The vertical continuous line represents 4 August 2007, the date at which we dynamically couple both the MXL-GECROS and MXL-A-g_s models (see the assessment of these couplings in Sect. 2.3.1).

a ground heat flux (it was assumed negligible in the original GECROS version). We take a first-order estimate and parameterize it to be 10 % of the net absorbed radiation at the surface (this assumption was validated for short grass by de Bruin and Holtslag, 1982). Finally, we implement a vapour pressure profile in the canopy layer to enable a more realistic description of VPD. In our implementation, the vapour pressure (e) changes linearly from the top to the bottom of the canopy and from the actual vapour pressure at 2 m to the saturation vapour pressure at 2 m. The state of saturation at the bottom of the canopy is adjusted for cases of lighter vegetation cover. This allows the vapour pressure at the bottom always to be larger or equal to $e(2\text{ m})$.

$$e(z) = e(2\text{ m}) + (e_0 - e(2\text{ m})) \times d_{\text{rel}}, \quad (2.3)$$

$$\text{with } e_0 = e(2\text{ m}) + (e_{\text{SAT}}(2\text{ m}) - e(2\text{ m})) \times f_{\text{veg}}.$$

We use the relative canopy depth $d_{\text{rel}} = 0.5$ for shaded leaves and $d_{\text{rel}} = 0.9$ for the soil. Note that, in contrast to the canopy profile for vapour pressure, we do not implement a canopy profile for air temperature. We keep air temperature vertically constant and equal to the 2 m air temperature. We refer to the modified version of the GECROS model from here on.

In order to validate our modified version of GECROS, we performed a standard simu-

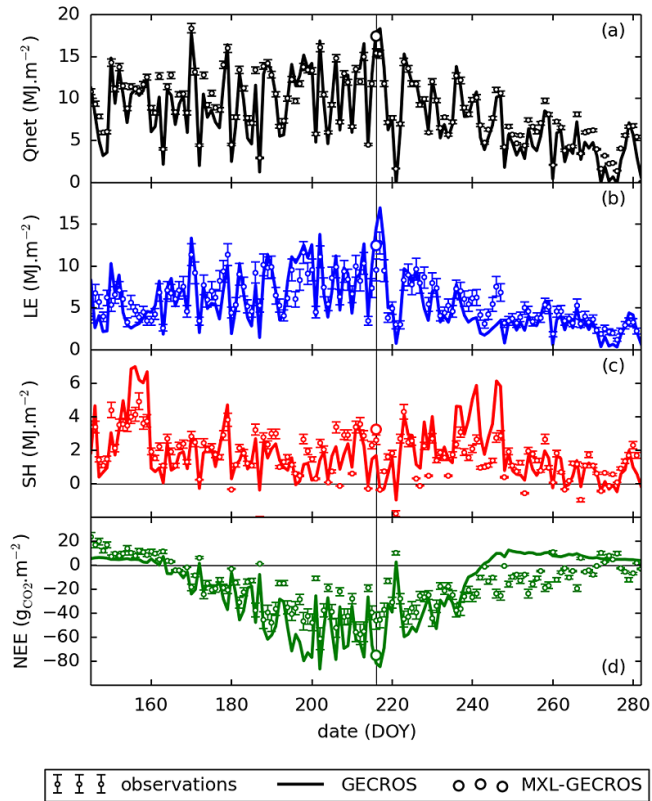


Figure 2.2 – Daily integrated (a) net radiation (Q_{net}), (b) latent heat flux (LE), (c) sensible heat flux (SH) and (d) net ecosystem exchange (NEE) at the maize site, from sowing to maturity dates. The integration is computed each day, using the average daytime flux times the daytime number of seconds. Days with more than 20% measurement gaps are discarded. Errors are computed as a direct sum of the eddy covariance random errors for instantaneous fluxes, which are presented in Sect. 4.4 of Aubinet et al. (2012). The vertical continuous line represents 4 August 2007, the date at which we dynamically couple both the MXL-GECROS and MXL-A-g_s models (see the assessment of these couplings in Sect. 2.3.1).

lation of the maize growth for our location and year of interest (2007) and compared our results to observations. The initial conditions for this experiment are presented in Table A.3. In Fig. 2.1 we show three cumulative variables evolving over the growing season: yield, PAI and crop height. In Fig. 2.1a we find that the GECROS model reproduces the observed maize yield at day 282 within 10% (2 kg m^{-2} simulated vs. 1.8 kg m^{-2} observed), indicating a correct integration of the net primary production (NPP) over the growing season. Moreover, Fig. 2.1b and c show that GECROS also approaches the observed maximum PAI and

crop height, with a $3.5 \text{ m}^2 \text{ m}^{-2}$ PAI and a 2.5 m height vs. an observed $3.8 \text{ m}^2 \text{ m}^{-2}$ PAI and 2.8 m height. This suggests that NPP was also assigned to the correct GECROS carbon pools (stems, leaves, roots) during crop development. This satisfactory agreement for carbon storage was expected and is reassuring since the GECROS model was built as a crop yield model (Yin and van Laar, 2005).

In addition, we show in Fig. 2.2 the seasonal evolution of surface available energy (Q_{net}), latent heat flux (LE), sensible heat flux (SH) and net CO_2 exchange (i.e. net ecosystem exchange; NEE) in daily integrated amounts. Their seasonal means, presented in Table 2.1, are all in agreement with the observations, except for a small overestimation of the mean NEE. This overestimation could be due to a too-low soil respiration. Also, the R^2 between the modelled and observed daily integrated Q_{net} (0.95) is very high, and the R^2 for the daily integrated LE (0.75), SH (0.59) and NEE (0.74) are satisfactory. The high degree to which GECROS reproduces the variability from day to day results from the prescribed meteorological driver data in the seasonal simulation, which provides the model with observed radiation, atmospheric temperature and precipitation data. Note that the mismatch between observations and GECROS on individual days can nevertheless be quite large (cf. the RMSE compared to the observed seasonal means and standard deviations in Table 2.1) despite the improvements we made to its energy balance. Such a mismatch could be produced by the incorrect simulation of key driver variables (e.g. Q_{net} and soil moisture) in GECROS, by the absence of a diurnal-scale weather forcing (only one data input is given per day) or even by the lack of atmospheric feedback. This partly reinforces the aim of our study, which is to focus on understanding the daytime two-way crop–atmosphere interactions.

Table 2.1 – Seasonal statistics of the daily integrated Q_{net} , LE, SH and NEE from Fig. 2.2. Statistics are computed from sowing to maturity dates. We present the observed and modelled means and standard deviations, the root mean squared error (RMSE) between the model and the observations (in the same units as the mean) and the R^2 between the model and the observations. Note that the large error on NEE is partly due to the inability of the model to reproduce the LAI after DOY 240 (see Fig. 2.1).

Variable [units]	Observed		Modelled		RMSE	R^2
	mean	stddev	mean	stddev		
Q_{net} [MJ m^{-2}]	8.9	3.7	8.1	4.4	1.4	0.95
LE [MJ m^{-2}]	5.9	2.5	5.5	3.5	1.8	0.75
SH [MJ m^{-2}]	1.7	1.3	1.8	1.7	1.1	0.59
NEE [$\text{g CO}_2 \text{ m}^{-2}$]	-15.8	19.5	-19.1	28.8	16.0	0.74

A-g_s, a land-surface exchange model

The A-g_s model is a generic meteorological-oriented land-surface model, which was originally published by Jacobs et al. (1996). Its use has been validated for grapevine (Jacobs et al., 1996), C₃ grass, C₄ grass and soybean (Ronda et al., 2001). It is a single-big-leaf model that relates plant CO₂ assimilation to the stomatal conductance ($g_s = 1/r_s$) via a CO₂ gradient (see Eq. 2.4). We use the version of Ronda et al. (2001), where the impact of soil water depletion on g_s is calculated with a linear function from wilting point to field capacity. In A-g_s, the upscaled canopy conductance (g_c) is hence calculated as a function of light, temperature, stomata to atmospheric CO₂ concentration ratio, VPD, soil water stress and LAI. In Eq. (2.4), soil respiration is computed with an Arrhenius-type equation, using the concepts of reference respiration R_{10} and of the activation energy for chemical reactions E_a . In addition to the CO₂ fluxes, A-g_s calculates surface fluxes of latent and sensible heat with the same conductance approach (see Eqs. 2.5–2.6). Finally, the ground heat flux is calculated as the thermal diffusivity of the skin layer times the temperature difference between the soil and skin layers.

$$\underbrace{(\overline{w'c'})_s}_{\text{Net ecosystem exchange}} = \underbrace{\left(\frac{1}{r_a + 1.6 r_s}\right)}_{\text{CO}_2 \text{ conductance}} \times \underbrace{(c_{\text{stomata}} - c_{\text{atmos}})}_{\text{CO}_2 \text{ gradient}} + \text{Soil Respiration}, \quad (2.4)$$

$$\underbrace{(\overline{w'q'})_s}_{\text{Surface moisture flux}} = \underbrace{\left(f_{\text{veg}} \times \frac{1}{r_a + r_s} + (1 - f_{\text{veg}}) \times \frac{1}{r_a + r_{\text{soil}}}\right)}_{\text{water conductance}} \times \underbrace{(q_{\text{sat}}(T_{\text{skin}}) - q_{\text{atmos}})}_{\text{moisture gradient}}, \quad (2.5)$$

$$\underbrace{(\overline{w'\theta'})_s}_{\text{Surface heat flux}} = \underbrace{\left(\frac{1}{r_a}\right)}_{\text{heat conductance}} \times \underbrace{(T_{\text{skin}} - \theta_{\text{atmos}})}_{\text{temperature gradient}}. \quad (2.6)$$

A-g_s adapts its surface fluxes according to the vegetation cover and LAI but simulates neither its own crop phenological development nor carbon accumulation into crop organs. This setup makes the A-g_s model, in the present version, suited for the simulation of surface exchange at the diurnal scale only.

2.2.3 Simulation setup

With the three models presented before, we make two couplings to study the daytime maize–atmosphere system: MXL-A-g_s and MXL-GECROS. We design them as two-way couplings: the surface fluxes given by A-g_s and GECROS are used as surface conditions for the MXL model, and in return, the incoming short-wave radiation, atmospheric temperature, humidity,

wind speed and CO_2 mole fraction are fed to the surface schemes as environmental conditions. The internal calculations of MXL are done on a time step of 1 min. In addition, A-g_s and GECROS feed the surface fluxes to MXL with a frequency of 1 and 5 min respectively. Note that we have checked and validated that the 4 min difference in communication frequency does not affect the coupling. Finally, all calculations start at 06:00 UTC, after sunrise when turbulent convection is already active, and last until 18:00 UTC, thus ensuring the atmosphere is well mixed during that time.

The main settings of our models are presented in Tables A.1–A.3. For MXL-GECROS, we first initialise the uncoupled GECROS model with the maize parameters of Yin and van Laar (2005) and Sinclair and de Wit (1975) (cf. Table A.3). The uncoupled GECROS model is run from emergence date to 4 August 2007 in order to obtain all initial conditions of its internal variables on the coupling date. On 4 August, we initialise all our coupled models following the available soil, crop and atmospheric observations from Jans et al. (2010). Note that we prescribe horizontal heat and moisture advection during the first hours of our numerical experiments to improve the match to observations during the early-morning transition to convective conditions. In addition, we use the C_4 photosynthesis parameters published by Ronda et al. (2001) for the A-g_s scheme.

The data set from Jans et al. (2010) provides the soil volumetric water content on 4 August 2007, but in absence of measurements of the soil wilting point and field capacity we assume typical values for these quantities for our soil type. In light of the uncertainty of the soil moisture measurements and of these soil moisture characteristic points, we decide to adjust the modelled soil volumetric water content to obtain a Bowen ratio similar to the observed one. We perform this adjustment with the two models. The soil moisture index (SMI, see Eq. 3.13) obtained with MXL-GECROS is very low, which suggests a heavy drought situation that was not observed:

$$\text{SMI} = \frac{W_{\text{actual}} - W_{\text{wilting point}}}{W_{\text{field capacity}} - W_{\text{wilting point}}}, \quad (2.7)$$

with W the soil volumetric water content. In consequence, we decide to apply the SMI obtained with MXL-A-g_s (55.5 %) in both cases. In the end, both models operate with the same soil type and SMI (see Appendix Tables A.2 and A.3) but yield different Bowen ratios and surface energy balances because of their difference in water-stress implementation.

In the absence of observations for soil respiration on 4 August 2007, we adjust the MXL-A-g_s soil respiration to be identical to the internally calculated value from MXL-GECROS ($0.2 \text{ mg CO}_2 \text{ m}^{-2} \text{ s}^{-1}$ at 12:00 UTC). This means that for NEE, the only difference between the two models is in their representation of NPP. We execute this by setting the reference respiration R_{10} of MXL-A-g_s at $0.03 \text{ mg CO}_2 \text{ m}^{-2} \text{ s}^{-1}$, a low but realistic number when considering the natural range of variation of R_{10} in the Netherlands (cf. Jacobs et al., 2007a).

Also, the estimate of soil respiration is in the range of observed values at that period of the year (Jans et al., 2010).

Finally, in order to obtain the same input of short-wave radiation as in our observations (25.0 MJ m^{-2}) on 4 August 2007, we prescribe a cloud cover of 22.5 % in our models to match the observed total incoming short-wave radiation (SWin) during daytime. This is because the observations show a significant reduction of SWin compared to the output of astronomic functions for a cloudless day, likely due to haze or fog in the morning. With our two coupled models, we make an intercomparison of their simulations against observations to study the ability of these couplings to reproduce the cropland–atmosphere interactions.

2.2.4 Sensitivity analysis

Related to our first research question, we perform a sensitivity analysis of the daytime cropland–atmosphere system to upper-atmosphere conditions (subsidence) in comparison to surface conditions (soil moisture). We conduct this sensitivity analysis with the model that shows the best performance on the diurnal scale (i.e. MXL-A-g_s, see Results). We design two study cases, stemming from the control case of 4 August 2007 (Sect. 2.2.3), by selecting two drivers to modify separately: (a) the “high-subsidence” case, where we replace the very small horizontal wind divergence ($7 \times 10^{-6} \text{ s}^{-1}$) of the control case by a high one ($4 \times 10^{-5} \text{ s}^{-1}$), representing a realistic case of strong subsidence in the Netherlands; and (b) the “soil moisture depletion” case, where we apply a reduction of soil moisture (from 0.110 to $0.105 \text{ cm}^3 \text{ cm}^{-3}$) equivalent to a 5 % decrease of SMI for that soil type. A decrease of 5 % SMI could happen over several days in a drying phase (e.g. Daly et al., 2004; Betts, 2004). We analyse the impact of these two external forcings on the daytime surface energy balance and NEE, as well as the net effect on the atmospheric CO_2 mole fraction.

2.3 Results

2.3.1 Intercomparison of coupled models against observations

Daytime evolution of the surface fluxes

Figure 2.3 presents three of the four components of the surface energy balance, together with the net surface CO_2 exchange, for 4 August 2007. We identify three phases in the observed surface fluxes daytime diurnal cycle. Phase A corresponds to the early-morning transition from a stable to a convective boundary layer. During Phase A, the SH flux switches from negative to positive (see Fig. 2.3b), and this heat becomes the source of convection which works to break up the thermal stratification built during night-time. Reproducing this observed transition with our models is difficult: firstly because advection of heat and moisture

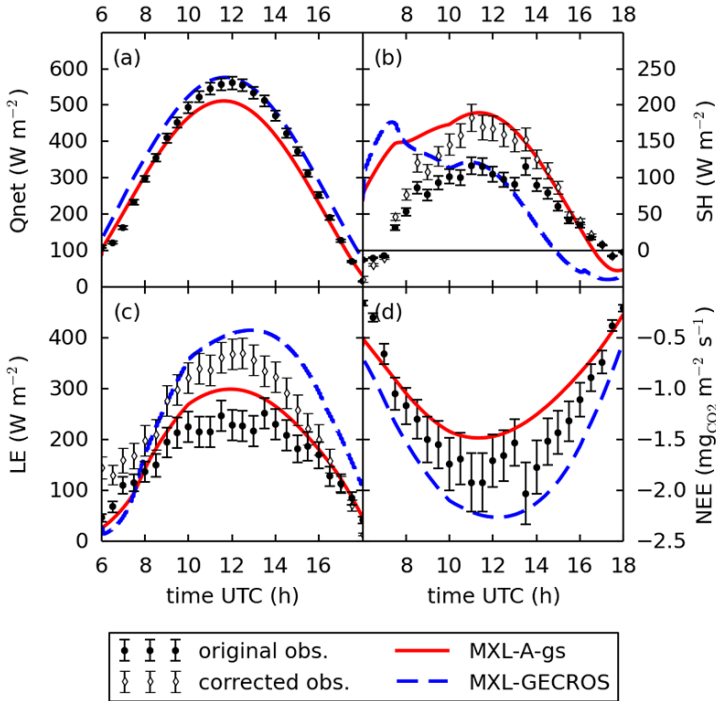


Figure 2.3 – Daytime diurnal cycle of the (a) net radiation (Q_{net}), (b) sensible heat flux (SH), (c) latent heat flux (LE) and (d) net ecosystem exchange (NEE) on 4 August 2007. For comparison with the models we corrected the observations to allocate the residual of the surface energy balance into extra SH and LE (see Sect. 2.2.1). The error bars represent the average eddy covariance random errors of Aubinet et al. (2012, see Sect. 4.4). NEE is negative when CO_2 is being removed from the atmosphere. Differences in NEE between the two couplings directly reflect differences in net plant photosynthesis, as soil respiration is identical between the two models.

plays an important role in this early-morning phase (see next section) and secondly because dew on the vegetation possibly delayed the onset of a positive SH in observations. In addition, when SH is negative, the corrected observed LE flux assumes unrealistically high values (see Fig. 2.3c) due to our correction method. For all these reasons we will exclude the early-morning transition from our model evaluation.

Phase B is the most important part of the day, when fluxes are highest and convection is dominant. During Phase B, MXL-GECROS strongly underestimates the Bowen ratio, with an underestimated SH in accordance with its consistently higher LE flux. As a consequence and due to the coupling with evapotranspiration, photosynthesis is overestimated, as shown in NEE (considering that the soil respiration is low and identical between MXL-GECROS

and MXL-A-g_s). These strong fluxes contribute most to the daily integrated amount, which impacts the atmospheric state. Therefore it is very important to calculate correct surface fluxes during Phase B, which MXL-A-g_s does slightly better than MXL-GECROS.

Finally, Phase C is the late-afternoon transition from a convective to a stable boundary layer. During Phase C, the SH flux changes from positive to negative, causing the convection to cease. Also, evapotranspiration and photosynthesis decrease until fluxes become negligible. The late-afternoon transition for SH occurs much earlier for MXL-GECROS (15:00 UTC) than for MXL-A-g_s (16:45 UTC) and the observations (17:15 UTC), which means the assumption of a convective boundary layer, the basis of the MXL model, ends earlier for MXL-GECROS than for MXL-A-g_s.

Overall, Fig. 2.3 shows that both MXL-GECROS and MXL-A-g_s calculate reasonable magnitudes and temporal evolutions of the surface fluxes for the observed maize crop, but MXL-A-g_s performs slightly better than MXL-GECROS. We find in Fig. 2.3a that both models calculate different amounts of Q_{net} . They benefit from the same amount of incoming short-wave radiation (25.0 MJ m^{-2} integrated over the day) but yield different radiation balances, since they have differently parameterized functions for albedo and long-wave radiation budgets of the leaves and soil. As a result, a different amount of available energy will be partitioned into sensible heat, latent heat and ground heat fluxes. Following Q_{net} , in Fig. 2.3b–d we find that, integrated between 08:00 and 18:00 UTC, MXL-GECROS underestimates SH by a total of 1.3 MJ m^{-2} (38 %) and overestimates LE by 2.1 MJ m^{-2} (22 %) and NEE by $13.0 \text{ g CO}_2 \text{ m}^{-2}$ (25 %, see Table 2.2). On the other hand, MXL-A-g_s overestimates SH by a total of 0.8 MJ m^{-2} (24 %), and underestimates LE by 1.5 MJ m^{-2} (15 %) and NEE by $10.6 \text{ g CO}_2 \text{ m}^{-2}$ (20 %). Considering the three fluxes of heat, water and CO₂, we find that MXL-A-g_s reproduces the observed daytime evolution of the surface fluxes better than MXL-GECROS on 4 August 2007. It is important to remember that we prescribe the initial soil moisture to match the observed Bowen ratio with MXL-A-g_s, which is why we arrive at this better fit for the surface energy balance of this model. We prescribe the same SMI (55.5 %) to both models, which have different water-stress responses and are thus the lesser fit for MXL-GECROS. To see how the differences in magnitudes and timing of heat, water and carbon surface fluxes impact the atmospheric state, we assess the atmospheric mixed

Table 2.2 – Daytime integrals of Q_{net} , LE, SH and NEE from Fig. 2.3, calculated from 08:00 to 18:00 UTC on 4 August 2007.

	Q_{net} [MJ m^{-2}]	LE [MJ m^{-2}]	SH [MJ m^{-2}]	NEE [$\text{g CO}_2 \text{ m}^{-2}$]
Observations	14.4	9.7	3.4	-52.0
MXL-A-g _s	13.1	8.2	4.2	-41.4
MXL-GECROS	15.3	11.8	2.1	-65.0

layer next.

Daytime evolution of the ABL

Figure 2.4 shows that MXL-A-g_s outperforms MXL-GECROS when simulating a fully coupled atmosphere. When comparing observations with the model results, note that we present the modelled mixed-layer (or bulk) values against the 2 m observations for temperature and specific humidity. Considering the general properties of the surface layer (a gradual decrease of temperature and humidity from the surface level to the mixed-layer level), the observed 2 m atmosphere is thus expected to be slightly warmer and moister than the modelled mixed-layer atmosphere. Also, because the negative SH depletes the layer of air close to the surface from heat at the very end of the day, the observed 2 m temperature is expected to decrease at that time. Keeping these expected differences in mind, we find that the MXL-A-g_s model reproduces the observed temperature and moisture values well, while MXL-GECROS calculates a clearly too-high 18:00 UTC humidity (11.2 g kg⁻¹) compared to the observations (9.8 g kg⁻¹). Similarly, MXL-GECROS simulates a too CO₂-depleted atmosphere (-20 ppm) and a too-shallow boundary layer (-250 m) compared to observations, where MXL-A-g_s performs relatively well.

When we relate the integrated heat, water and CO₂ surface fluxes of Table 2.2 to the atmosphere of Fig. 2.4, we observe, as expected, that a lower integrated amount of SH in MXL-GECROS compared to MXL-A-g_s leads to a 2 °C lower maximum temperature (24 instead of 26 °C). Also, a higher integrated LE in MXL-GECROS compared to MXL-A-g_s results in a 1.4 g kg⁻¹ higher specific humidity at the end of the day (11.1 instead of 9.7 g kg⁻¹). Finally, a lower integrated NEE in MXL-GECROS compared to MXL-A-g_s leads to a 22 ppm lower CO₂ mole fraction (333 instead of 355 ppm). However, when we compare the modelled and observed atmosphere we find discrepancies. This is because surface fluxes do not directly translate into a daytime evolution of the atmospheric temperature, humidity and CO₂ mole fraction. For instance, in Fig. 2.4c we find that the daytime overestimation of NEE by MXL-GECROS leads to a too strongly CO₂ depleted atmosphere compared to observations only in the afternoon. Also, despite a daytime underestimated NEE, MXL-A-g_s reproduces satisfactorily the observed CO₂ daily minimum on 4 August 2007. This shows that errors in the surface fluxes can be cancelled by other non-local effects like the advection, entrainment or boundary-layer dilution (e.g. see the role of dry-air entrainment in van Heerwaarden et al., 2009, or CO₂ advection in Casso-Torralba et al., 2008). A full analysis of the daytime diurnal cycle of the atmosphere must thus include the contribution of these processes.

Advection fluxes can change the expected evolution of the atmosphere. The occurrence of heat and moisture advection on 4 August 2007 is noticeable because the observed daytime

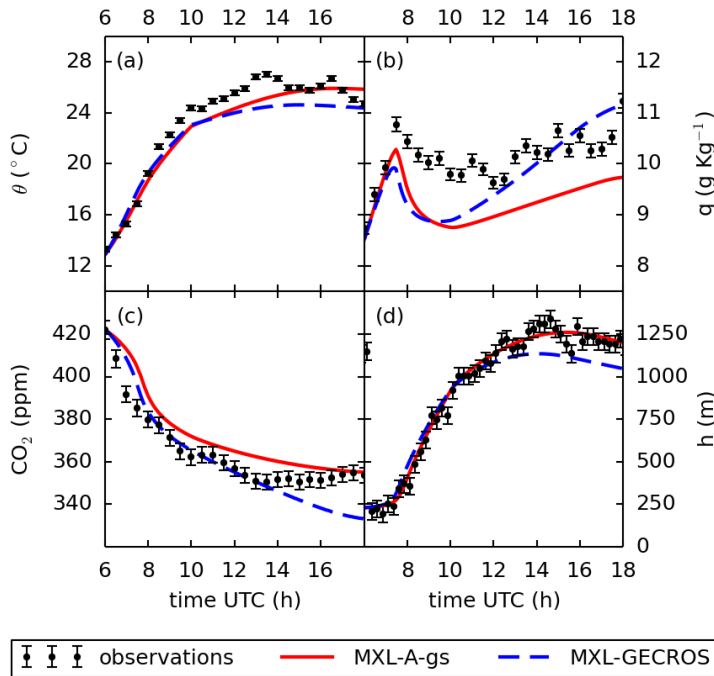


Figure 2.4 – Daytime diurnal cycle of (a) the potential temperature θ , (b) the specific humidity q , (c) the CO_2 mole fraction and (d) the boundary-layer height h at the maize site on 4 August 2007. The errors for the θ , q and CO_2 measurements are obtained based on the factory specifications of the instruments. The error for h is assumed to be constant and equal to 50 m (personal communication, Henk Klein Baltink). Note that, in order to reproduce the early-morning temperature and humidity variations, we prescribed advection of heat until 10:00 UTC and advection of humidity until 07:30 UTC (see settings in Table A.1).

range in temperature and the early-morning increase in humidity are too large to be solely due to realistic crop-sensible heat and evapotranspiration fluxes. We thus prescribed horizontal heat and moisture advection during the first hours of our numerical experiments (see Table A.1). We estimate the contribution of advection for the MXL-A-gs model to the daytime temperature range (DTR, 13 °C) to be 3 °C and the contribution to the early-morning specific humidity increase (1.8 g kg^{-1}) to be 1.2 g kg^{-1} . The observed CO_2 mole fraction stabilisation and increase after 13:00 UTC is also most probably generated by advection because an increase in CO_2 mole fraction could only be due to (a) a positive NEE (which we do not have), (b) strong entrainment of CO_2 -rich air (which is unlikely at the end of the day) or (c) CO_2 advection. Despite this observation, we prescribed no advection of CO_2 in our model runs to more clearly demonstrate the role of surface fluxes in the CO_2 budget.

Finally, entrainment fluxes also alter the state of the boundary layer. The boundary-layer height (h) of Fig. 2.4d can serve as a proxy for measuring the amount of warmer, drier, CO₂-depleted air that is entrained from the free troposphere into the boundary layer in cases where there is no or very little subsidence (our case). In the end, we find in Fig. 2.4d that both models calculate a maximum h that is lower (–150 m for MXL-A-g_s and –250 m for MXL-GECROS) than observed (1400 m). Differences between the models are due to differences in heat input from SH and the subsequent entrainment, since the heat advection, free tropospheric vertical profiles and subsidence are identical between the models. However, in reality there must be discrepancies in all of these variables to create the existing differences between models and observations. Clearly, both boundary-layer dynamics and surface fluxes must be included in atmospheric simulations to properly capture the contribution of the large-scale air masses to the local atmospheric state. We will investigate the relevance of upper-atmosphere conditions in more detail in the next section.

2.3.2 Sensitivity analysis of an upper-atmosphere forcing

We show in the previous sections that MXL-A-g_s performs best to reproduce the daytime diurnal crop–atmosphere coupling on 4 August 2007. As a consequence, we use it to conduct a sensitivity experiment. Our goal here is to quantify the strength of the couplings between the upper atmosphere, the boundary layer and the crop surface. From now on, we refer to the MXL-A-g_s run of the previous sections as the control run, from which we derive our sensitivity analysis runs. We design two case studies: one where we apply a stronger upper-atmosphere forcing (high subsidence) and another where we alter a land-surface forcing (depletion of soil moisture, see Sect. 2.2.4 for a detailed specification of the settings). Both high subsidence and soil moisture depletion are characteristic of a drought period. Figure 2.5 presents the main interactions between carbon, water and energy that result in the state of the land–atmosphere. We use it to summarise the changes linked to increased subsidence, discussed in the next paragraphs.

While the high-subsidence case stimulates the latent heat flux LE through the warming of the boundary layer (red arrows in Fig. 2.5), the soil moisture depletion case decreases LE through the closure of plant stomata. Subsidence is a large-scale forcing that counteracts the growth of the boundary layer and even reduces h once its growth has stopped (see the high-subsidence case in Fig. 2.6a). It enhances the entrainment of warm free tropospheric air and causes a smaller volume of air to be warmed up by the same surface sensible heat flux, thus increasing the atmospheric temperature (+1.5 °C at 18:00 UTC, see Fig. 2.6b). This warming of the atmosphere increases the VPD at the surface (+0.2 kPa at 14:00 UTC, not shown here) and shifts the evaporative fraction ($EF = LE/(SH + LE)$) towards evapotranspiration by 5% on average during the day (see Fig. 2.7a). Finally, this increase in LE results in

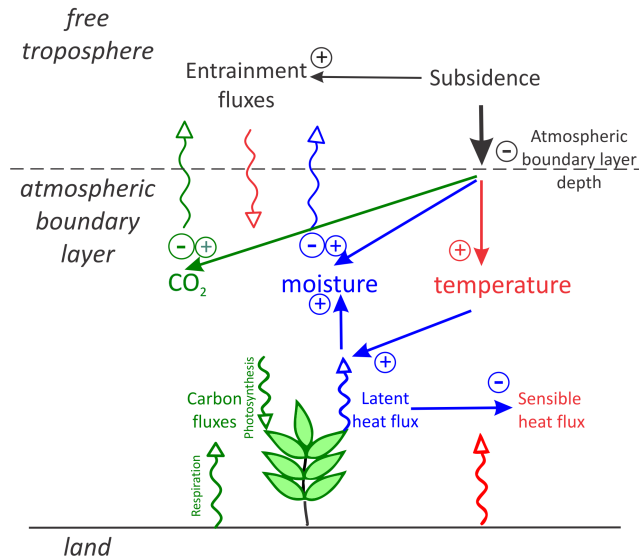


Figure 2.5 – Interactions between the carbon (green), water (blue) and heat (red) cycles in the coupled land–ABL system. Increased subsidence tends to reduce the boundary-layer height, which directly causes the ABL to warm up, dry and become CO_2 -depleted. This in turn affects the land-surface, which feeds back on the ABL by shifting its Bowen ratio towards more evapotranspiration.

a moistening of the atmosphere that counteracts the initial atmospheric drying caused by a short-term enhancement of dry-air entrainment (not shown here). In Fig. 2.6c we find that the specific humidity, which is first lower than in the control run, becomes higher than in the control run after 14:00 UTC due to the stimulation of LE.

On the other hand, for the lower soil moisture case, the decreased availability of soil moisture generates a decrease in surface conductance g_s on average by 1 mm s^{-1} during the day (see Fig. 2.6d). This decrease in surface conductance leads to a reduction of EF of 5 % throughout the day (see Fig. 2.7a) and finally to a reduction of h of 40 m (see Fig. 2.6a). As a result, we find that both cases affect the energy partitioning at the surface with equivalent magnitude. It is thus important to consider both the effect of high subsidence and of soil moisture depletion on evapotranspiration in the context of drought response. Moreover, it is interesting to analyse how the net surface carbon uptake is affected by them.

High subsidence and soil moisture depletion have different impacts on the net CO_2 flux at the surface. While the high-subsidence case shows no difference in photosynthesis and respiration compared to the control case, the reduced soil moisture case presents a reduction in photosynthesis ($-0.2 \text{ mg CO}_2 \text{ m}^{-2} \text{ s}^{-1}$ at midday in Fig. 2.9a). This is because while

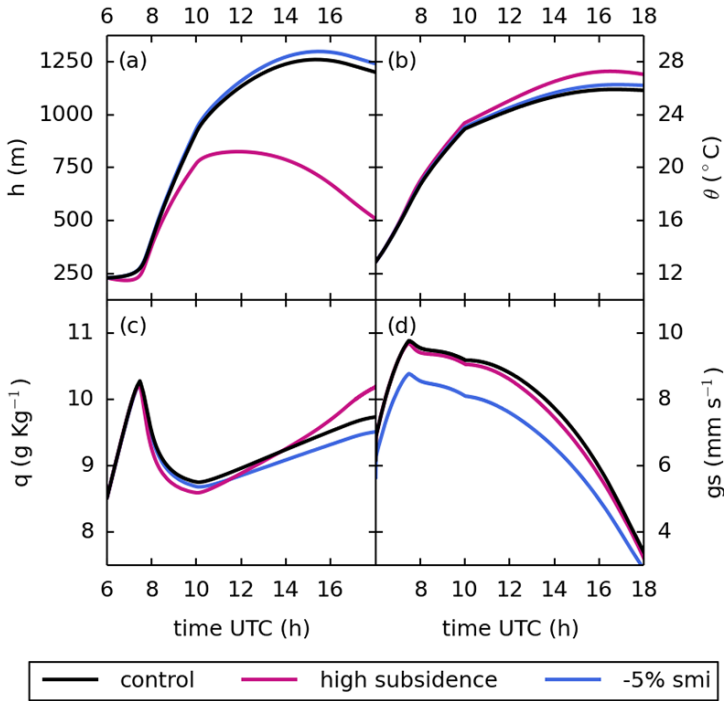


Figure 2.6 – Boundary layer and surface response to high subsidence and soil moisture depletion. High subsidence, an upper-atmosphere forcing, directly impacts the boundary-layer height h and affects the specific humidity q and the potential temperature θ . This contrasts with soil moisture depletion, a surface forcing, which acts through the stomatal conductance g_s to impact the evapotranspiration and q .

the reduced soil moisture case generates a clear stomata closure in response to water stress (-1 mm s^{-1} at 14:00 UTC in Fig. 2.6d), the high-subsidence case generates only a slight change of stomata opening in response to the increased VPD (-0.3 mm s^{-1} at 14:00 UTC in Fig. 2.6d), which is entirely compensated by a slight increase in the surface CO_2 gradient ($+8 \text{ ppm}$ at 14:00 UTC, not shown here). Thus, as a result of two very different feedback mechanisms on net photosynthesis and evapotranspiration (see previous paragraph), we obtain an increase in intrinsic water-use efficiency ($\text{iWUE} = \text{NPP} / g_s$) of 11 and 18 $\mu\text{mol CO}_2 \text{ mol}^{-1}_{\text{H}_2\text{O}}$ for the high-subsidence and soil moisture depletion cases respectively compared to the control case (i.e. $+3$ and $+6\%$ on average, see Fig. 2.7b). This means both forcings make plant carbon exchange, and by extension plant carbon storage, slightly more water efficient. While a reduction in soil moisture has an immediate impact on the daily crop yield (integrated decrease of NPP of 1.2 g C m^{-2}), high subsidence does not. However, high

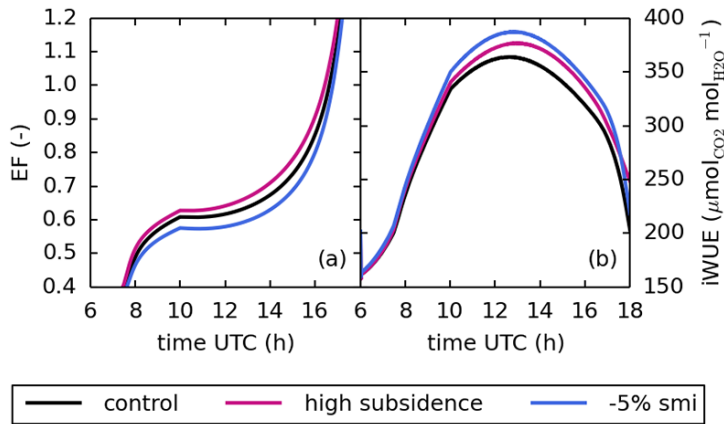


Figure 2.7 – The response of surface exchange to high subsidence and soil moisture depletion. High subsidence and soil moisture depletion both shift the evaporative fraction ($EF = LE/(SH + LE)$) by 5% on average, and both increase the intrinsic water use efficiency ($iWUE = NPP/g_s$) by 3 and 6% respectively on average, as a result of two different mechanisms (respectively an increase of VPD and a stomata closure).

subsidence worsens soil moisture depletion (-1% SMI) because it increases EF by 5%, as we described earlier. This suggests that subsidence could ultimately contribute to a yield decrease if the drought situation is prolonged. It is therefore interesting to extend our sensitivity analysis to a larger range of SMI and subsidence in order to verify the response of the system.

We perform a more detailed sensitivity analysis of $iWUE$ and EF to soil moisture and subsidence, which is presented in Fig. 2.8. We start our 10 201 experiments with identical initial conditions to the control case (point C in Fig. 2.8), except that we vary both the initial SMI by 20% (on x axis) and the large-scale divergence by $4 \times 10^{-5} \text{ s}^{-1}$ (D , on y axis). Note that the variable D is related to the subsidence velocity (w_s) through the ABL height ($w_s = -D \times h$). Thus, the full range of D explored in Fig. 2.8 represents a subsidence velocity of 0 to 0.04 m s^{-1} , the maximum being typical of stationary high-pressure systems. By studying these ranges, we cover small fluctuations of drivers around the control case as well as conditions associated with drought (i.e. much dryer soil with high subsidence). Figure 2.8 shows that EF and $iWUE$ are more dependent on changes in SMI than variations of D . However, note that day-to-day changes in SMI do not exceed 2–3%; thus the full range presented here corresponds to a long-term drying of the soil, whereas the full range of D can be explored short-term. Thus, on a diurnal scale, subsidence is as important as soil moisture.

As discussed earlier, increasing subsidence (e.g. moving from point C to point H) directly reduces the maximum ABL height (from 1250 to 825 m) and thus causes the atmosphere to become warmer and moister at the end of the day. Increasing soil moisture (e.g. moving from

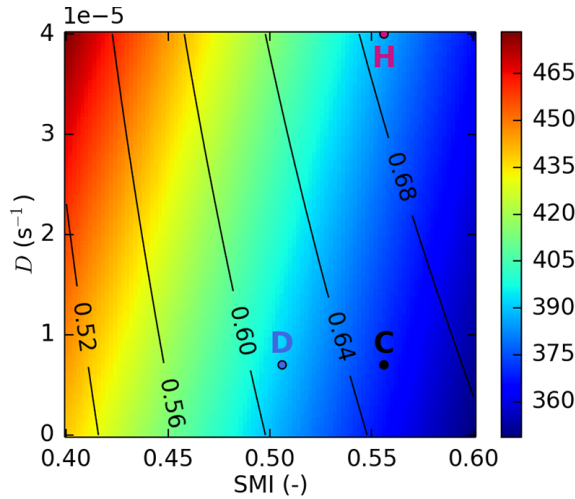


Figure 2.8 – Response of the 14:00 UTC $iWUE$ ($\mu\text{mol}_{\text{CO}_2} \text{mol}_{\text{H}_2\text{O}}^{-1}$, in colours) and EF (unitless, in contours) to seasonal variations of SMI and the large-scale divergence (D). Scatter points represent the control case (C), the dry (-5% SMI) case (D) and the high-subsidence case (H) of Figs. 2.6 and 2.7.

point D to point C) stimulates evapotranspiration and carbon exchange and generates a cooler, wetter atmosphere at the end of the day. As the figure shows, a simultaneous change of SMI and D (e.g. when we move from the lower-right corner to the upper-left corner of Fig. 2.8) leads to a 3.5 K increase in the daytime maximum atmospheric temperature and a 0.5 g kg^{-1} decrease in the daytime average atmospheric humidity. These atmospheric conditions, together with the lower availability of soil moisture (-20% SMI), enhance the 14:00 UTC $iWUE$ by $130 \mu\text{mol}_{\text{CO}_2} \text{mol}_{\text{H}_2\text{O}}^{-1}$ and reduce the 14:00 UTC EF by 14.4% . These results are in accordance with studies that state droughts enhance the plant intrinsic water-use efficiency for carbon exchange (e.g. Maseyk et al., 2011) and switch the partitioning of the surface energy balance towards SH at the expense of LE (e.g. Jongen et al., 2011).

We find in Fig. 2.8 that the positive feedback of subsidence on soil moisture depletion, discussed earlier, is slightly lessened under a prolonged drought. Figure 2.8 shows that when we increase subsidence (i.e. when we move along the full range of the y axis), the resulting change in EF is smaller at SMI 0.40 (3.0%) than at SMI 0.60 (4.5%). This is a direct consequence of having less soil moisture available for evapotranspiration. The positive feedback of subsidence on soil moisture is an extension of the feedback loops on evapotranspiration discussed by van Heerwaarden et al. (2010). Our findings indicate that although the stimulation of EF by subsidence is less important under drought, it still contributes to a faster soil moisture depletion and decrease in crop yield over the days. Moreover, from a carbon cycle

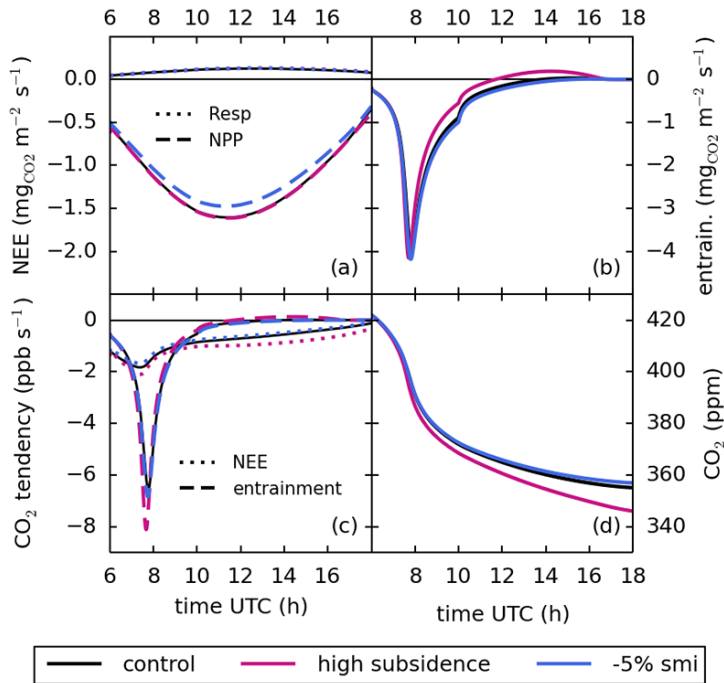


Figure 2.9 – Contributions of the surface and entrainment fluxes to the atmospheric CO_2 budget. Net photosynthesis (NPP) and soil respiration (Resp) combine at the surface to form NEE, while the entrainment of CO_2 takes place at the top of the boundary layer. All these fluxes are negative when CO_2 is being removed from the boundary layer. The CO_2 tendencies, which determine the daytime diurnal cycle of CO_2 , are obtained by dividing these CO_2 fluxes by the instantaneous boundary-layer height.

perspective it is interesting to analyse in more detail how the atmospheric CO_2 budget can be affected by surface and upper-atmosphere modifications.

Figure 2.9 presents the daytime atmospheric CO_2 budget. In Fig. 2.9c we see that the boundary-layer CO_2 tendency receives equivalent contributions from the surface and from entrainment, but their distribution in time differs. The contribution of entrainment to the overall CO_2 drawdown (-32 ppm in the control case) happens in the morning, before 09:00 UTC (i.e. 11:00 LT). On the other hand, the contribution of the surface uptake to the overall CO_2 drawdown (-34 ppm in the control case) is more constant throughout the day. In the high-subsidence case, even though the entrainment of CO_2 -depleted air is lower (cf. Fig. 2.9b) and the NEE is unchanged (cf. Fig. 2.9a), both the surface and entrainment CO_2 tendencies are higher due to the lower boundary-layer volume (see Fig. 2.6a). This is because the tendencies are inversely proportional to the boundary-layer height in the mixed-layer framework,

as shown by Pino et al. (2012). Consequently, the atmospheric CO₂ mole fraction is even more reduced in the high-subsidence case (−12 ppm at 18:00 UTC relative to the control and soil moisture depletion cases; Fig. 2.9d). Because the larger CO₂ drawdown is caused solely by the reduction in boundary-layer height in the high-subsidence case, it is very important to consider the effect of increased subsidence in high-pressure systems when interpreting measurements of the boundary-layer CO₂ mole fraction.

2.4 Discussion

2.4.1 On the importance of upper-atmosphere processes

In our study we compare two coupled models, MXL-A-g_s and MXL-GECROS, against a complete set of surface and boundary-layer observations. Related to our first research question, we hypothesise that entrainment and subsidence are essential processes which contribute to the determination of the carbon, water and energy budgets of the daytime crop–atmosphere system. Our findings indeed confirm our hypothesis: we show that entrainment and subsidence have a non-negligible impact on the daytime surface fluxes (iWUE and EF) as well as the atmospheric quantities (temperature, humidity and CO₂ mole fraction).

Previous studies have often put emphasis on surface processes. They have shown the importance of calculating correct surface fluxes of heat, water and CO₂, to improve numerical weather predictions (e.g. Boussetta et al., 2013; Moreira et al., 2013; Smallman et al., 2013; Hong et al., 2009), atmospheric CO₂ modelling (e.g. Corbin et al., 2010; Schuh et al., 2010; Tolk et al., 2009) and crop yield forecast (e.g. de Wit and Van Diepen, 2007). Studies involving two-way coupled models like ours (e.g. Santanello et al., 2013; Tao et al., 2013; Chen and Xie, 2011 and Kohler et al., 2010) have stressed the importance of slowly evolving surface forcings such as soil moisture, vegetation cover and LAI, which drive the surface exchange and strongly impact atmospheric properties like boundary-layer height. Also, interpretations of observed CO₂ mole fractions in the ABL often focus on the role of NEE, typically a large contributor to the atmospheric CO₂ budget (Tolk et al., 2009). While we agree that these surface processes and drivers are all key to the carbon, water and energy budgets, we have shown that atmospheric processes occurring at the top of the ABL also need to be taken into account.

A few studies have explored the importance of the upper-atmosphere processes in the vegetation–atmosphere system. For instance, van Heerwaarden et al. (2009) and Ek and Holtslag (2004) have shown the impact of the ABL–top moisture inversion and the tropospheric temperature lapse rate on surface fluxes, relative humidity at the top of the ABL and the boundary-layer cloud formation. With our sensitivity analysis, we additionally emphasise the importance of another large-scale atmospheric forcing, subsidence, which affects surface

fluxes and changes boundary-layer properties like temperature, moisture and CO₂ mole fraction.

Our results agree with Canut et al. (2012), Williams et al. (2011), McGrath-Spangler and Denning (2010), van Heerwaarden et al. (2009), Casso-Torralba et al. (2008) and Vilà-Guerau De Arellano et al. (2004), who found ABL growth and entrainment were key controls of the atmospheric CO₂ budget at the diurnal scale. However, the observation-based work of Williams et al. (2011) also showed that during longer time periods than the typical 10-day synoptic scale, NEE and large-scale atmospheric transport are the most important contributions to the atmospheric CO₂ mole fractions observed in the ABL. Day-to-day variations of ABL growth rates and associated entrainment were less important when interpreting weekly to seasonally averaged CO₂ budgets. Here, we show that NEE is impacted by the daytime diurnal coupling of the fluxes of water and heat at the top of the ABL to the crops growing at the surface, possibly at time scales of weeks and longer. This is because crops such as wheat and maize have sensitive periods of less than 2 weeks (e.g. crop germination, anthesis/flowering, ripening) in which crop yield can decline if heat or water stress is applied (Eitzinger et al., 2013; Sánchez et al., 2014). Thus, using a diurnal scale coupled framework to calculate the fluxes of heat, water during those specific periods of crop development could be important even if the direct contribution of entrainment to the CO₂ budget becomes smaller at longer time scales. A further investigation of the interactions identified in this work, focusing on the synoptic and seasonal time scales described in Williams et al. (2011), is therefore planned as a follow-up study.

To conclude, we know that the daytime diurnal cycles of heat, water and CO₂ are joined in a coupled system: through (a) the canopy stomatal control on CO₂ exchange and transpiration, which in turn determines the amount of sensible heat flux in the surface energy balance; and through (b) the large-scale conditions at the top of the boundary layer, which control the daytime boundary-layer development and thus the entrainment and volume dilution of heat, water and CO₂. Our findings show these surface and upper-atmosphere controls are of equivalent importance on a diurnal scale for the atmospheric CO₂ budget. We recommend using a fully coupled land–atmosphere framework to study the daytime atmospheric CO₂ budget, as we confirm that the land-induced boundary-layer growth has an important impact due to both volume dilution and CO₂ entrainment.

2.4.2 On the performance of our models

Related to our second research question, we hypothesise that the MXL-GECROS model can best reproduce the daytime crop–atmosphere interactions because of the higher level of crop biology detail embedded in the model. However, we show that neither of our models is able to simultaneously reproduce the daytime heat, water and CO₂ surface fluxes. MXL-A-g_s

simulates the crop interactions more satisfactorily overall, but it underestimates NEE.

The performance of our two models strongly depends on the sensitivity of the water-stress function to soil moisture. While GECROS only reduces its conductivity, and hence evaporation, close to wilting point, $A-g_s$ linearly decreases stomatal conductance from field capacity to wilting point. These are similar water-stress responses as for the CLM3.5 and JULES models shown in Powell et al. (2013). We have confirmed that these differences in water-stress functions are responsible for the overestimation of latent heat by MXL-GECROS compared to MXL- $A-g_s$. We conclude, in agreement with Eitzinger et al. (2013) and Powell et al. (2013), that these differences in water-stress implementation could lead to significant differences in simulated crop yield. Studies like that of Verhoef and Egea (2014) can help to validate the water-stress representations of surface models.

The satisfactory performance of our models also depends on the correct initialization of key surface and upper-atmosphere variables, as suggested by Sabater et al. (2008). In our study, we lacked measurements of the soil moisture characteristic points (wilting point, field capacity and saturation point). Thus, we estimated them and allowed the MXL- $A-g_s$ model to profit from the explicit initialization of soil moisture using the observed Bowen ratio. This was our best estimation possible. We advocate the use of complete sets of observations, including not only soil, vegetation and lower atmosphere but also boundary layer and free troposphere, to evaluate the performance of coupled land-atmosphere models. These proved to be of utmost importance for the validation of the modelled interactions.

For the prospect of going from a diurnal to a seasonal scale study, we regard data assimilation of soil moisture values, as done by e.g. Boussetta et al. (2013); Hong et al. (2009) and de Wit and Van Diepen (2007), as a promising solution. Data assimilation of LAI, as done by Huang et al. (2013), Zhao et al. (2013), Sus et al. (2010) and Jégo et al. (2012), could also help transform our daytime diurnal land-surface scheme $A-g_s$ into a capable seasonal surface scheme, as previously done within ISBA- $A-g_s$ (Barbu et al., 2011). Albergel et al. (2010) and Ines et al. (2013) suggest joint assimilation of LAI and soil moisture yields the best results. As an alternative, the MXL- $A-g_s$ model could also benefit from a satisfactory crop phenology module to interactively calculate LAI, like GECROS, as a replacement for LAI data assimilation (e.g. Lokupitiya et al., 2009).

To conclude, we recommend using meteorological-oriented (surface exchange) models, such as MXL- $A-g_s$, for simulations of the daytime crop-atmosphere interactions, as long as the crop is not nitrogen-stressed. However, to simulate longer periods of crop-atmosphere interactions, we recommend adopting a merging strategy to use the distinct advantages of both the generic meteorological-oriented land-surface models (sound surface energy balance) and the specialised crop carbon storage-oriented models (crop phenology, nitrogen stress implementation and prognostic carbon pools). The performance of such models is linked to their correct initialization, which can only be achieved thanks to complete observational data

sets. It is also linked to their crop water-stress representation, which conditions the surface energy balance and carbon exchange under shortages of soil moisture.

2.5 Conclusion

In this work, we use a process-based coupled framework to investigate the daytime interactions of CO₂, water and heat in the crop–atmosphere system. Our framework strength lies in the relative simplicity of the model that still represents the essential processes of the system. For example, the sensitivity analysis of Fig. 2.8 and the CO₂ budget of Fig. 2.9 could not easily have been produced using a full meso-scale land–atmosphere model. Using it, we are able to study the relevant interactions of the ABL with the surface and to allow a direct comparison to observed ABL and surface variables. Our results show that upper-atmosphere processes and drivers (entrainment and subsidence) are as important as surface processes and drivers (surface fluxes, soil moisture, LAI) to determine the daytime budgets of heat, water and carbon of the crop–atmosphere system. Therefore, ABL dynamics need to be considered when interpreting observations of atmospheric CO₂ mole fractions over crops. Using correct estimates of the large-scale forcings are also of key importance. Our modelling framework and its modular design describe these dynamics and allows an extension to other processes, such as the impact of aerosols (Barbaro et al., 2014), clouds (Vilà-Guerau de Arellano et al., 2012) or ozone on the budgets of carbon, water and heat. Although we have demonstrated that the daytime diurnal scale interactions are well described by a meteorology-oriented coupled model like MXL-A-g_s, the development of the crop and soil hydraulics at the seasonal scale are likely to be important given the nonlinear response of the coupled system across a wide range of large-scale forcings, as shown in this paper.

This research was funded by the Netherlands Organisation for Scientific Research through VIDI grant no. 864.08.012 and by the China Exchange Program of the Dutch Royal Academy of Research (KNAW) through travel grant no. 12CDP006. The authors acknowledge Xinyou Yin (Wageningen University) and Kees Rappoldt (EcoCurves BV) for their expert help with the GECROS model. We also thank Henk Klein Baltink (KNMI) and Fred Bosveld (KNMI) for providing the Cabauw data, Eduardo Barbaro (Wageningen University) for his help with the radiation formulation, and Denica Bozhinova (Wageningen University) for her help with programming a part of the analysis code.

Edited by: N. Zeng

3

Plant water-stress parameterization determines the strength of land-atmosphere coupling

Land-surface models used in studies of the atmosphere and vegetation during droughts usually include an underlying parameterization that describes the response of plants to water stress. Here, we show that different formulations of this parameterization can lead to significant differences in the coupling strength (i.e. the magnitude of the carbon and water exchange) between the land surface and the atmospheric boundary layer (ABL). We use a numerical model that couples the daytime surface fluxes typical for low vegetation to the dynamics of a convective ABL, to systematically investigate a range of plant water-stress responses. This modeling framework is a conceptual, but typical example of a combined carbon assimilation – stomatal conductance ($A-g_s$) approach used in many coupled models. We find that under dry soil conditions, changing from a sensitive to an insensitive vegetation response to water stress has the same impact on the land-atmosphere (L-A) coupling as a strong increase in soil moisture content. The insensitive vegetation allows stomata to remain open, partitions more available energy towards latent heat than the sensitive vegetation ($+150 \text{ W m}^{-2}$), and subsequently has lower atmospheric heating (-3.5 K) and ABL growth (-500 m). It also switches the dominant term in the CO_2 budget, reducing the dilution of ABL CO_2 by entrainment and increasing the dilution by net surface CO_2 uptake in vegetation. During the progressive development of a dry spell, the insensitive response will first dampen atmospheric heating because the vegetation continues to transpire a maximum of 4.6 mm day^{-1} while soil moisture is available. In contrast, the more sensitive vegetation response reduces its transpiration by more than 1 mm day^{-1} to prevent soil moisture depletion. But when soil moisture comes close to wilting point, the insensitive vegetation will suddenly close its stomata causing a switch to a L-A coupling regime dominated by sensible heat exchange. We find that in both cases, progressive soil moisture depletion contributes to further atmospheric warming up to 6 K , reduced photosynthesis up to 89% , and CO_2 enrichment up to 30 ppm , but the full impact is strongly delayed for the insensitive vegetation. The difference between the two L-A coupling regimes furthermore causes a different sensitivity of the coupled model to errors in the simulation of the atmospheric conditions during droughts. Our study illustrates and quantifies the impact of a chosen representation of plant water stress response in a coupled L-A model of carbon, water, and energy.

This chapter is published as Combe, M., Vilà-Guerau de Arellano, J., Ouwersloot, H. G., and Peters, W.: Plant water-stress parameterization determines the strength of land-atmosphere coupling, *Agricultural and Forest Meteorology*, 217, 61-73, doi:10.1016/j.agrformet.2015.11.006, 2016.

3.1 Introduction

Diurnal land-atmosphere (L-A) interactions have been shown to impact cloud formation (Vilà-Guerau de Arellano et al., 2014, 2012; Ek and Holtslag, 2004), precipitation (Santanello et al., 2013), as well as the build up of heat waves and droughts (Miralles et al., 2014; Teuling et al., 2010). Over vegetated surfaces, the diurnal cycles of carbon, water and energy are coupled at the surface through stomatal control (Berry et al., 2010; Leuning et al., 1995; Collatz et al., 1991; Jarvis, 1976) and at the top of the atmospheric boundary layer (ABL) through the entrainment of air from the free troposphere (McGrath-Spangler and Denning, 2010; van Heerwaarden et al., 2009). The exchange of carbon for example affects both the CO₂ mole fractions (Combe et al., 2015; Pino et al., 2012) and the amount of carbon stored in vegetation. Little attention has been given so far to the impact of conditions in the free troposphere and upper ABL on surface carbon exchange. However, through the vegetation response to atmospheric conditions, important variables such as the net primary production (NPP) or the surface water-use efficiency can be under strong atmospheric control.

In the diurnal L-A system, upper-atmosphere and surface processes typically together determine conditions in the ABL. At the surface both plant phenology (Richardson et al., 2013; Peñuelas et al., 2009) and soil moisture (Seneviratne et al., 2010; Koster, 2004) have been shown to be key drivers of the surface fluxes of water and CO₂, as well as the surface energy balance. Among these surface drivers, the impact of plant water-stress response on the strength of the L-A coupling remains an open question. Observations show that water-stress responses can differ between plant species and varieties (Calvet et al., 2004; Tardieu and Simonneau, 1998) and various plant water-stress parameterizations are now used in land-surface models. But there is little observational evidence to support their realism over the wide range of conditions they are applied to (Powell et al., 2013).

While a few attempts to mechanistically represent plant water stress have been made (Verhoef and Egea, 2014), the majority of land-surface models use a simple parameterization of plant water stress. They most often scale down net assimilation, stomatal and/or mesophyll conductance, or other photosynthesis parameters such as the maximum carboxylation rate. The scaling factor depends on the levels of soil moisture relative to field capacity and wilting point, and various response curve shapes are used ranging from linear (e.g. the CTESSEL and JULES models in Boussetta et al., 2013; Best et al., 2011) to highly non-linear (e.g. SiB3 and ORCHIDEE in Baker et al., 2008; Krinner et al., 2005). Observational studies suggest that the linear response might not be a realistic assumption for C₄ crops like maize (Verhoef and Egea, 2014), and crop models often use a strongly non-linear response to water stress by downregulating photosynthesis with the ratio of actual to potential transpiration (e.g. GECROS, WOFOST, SUCROS in Yin and van Laar, 2005; van Ittersum et al., 2003). Powell et al. (2013) showed that the shape of the water-stress response function can make

large differences for the simulation of diurnal and seasonal surface CO₂ fluxes under dry soil conditions. Van der Molen et al. (2011) and Combe et al. (2015) also speculated about such an impact on modeled L-A interactions. An extensive exploration of the effects of plant water-stress parameterizations on the coupled L-A system has yet to be performed.

The primary aim of our study is therefore to systematically assess the impact of differing plant water-stress parameterizations on the strength of the L-A coupling. We perform a sensitivity analysis of the coupled L-A system using a diurnal L-A modeling framework, called the MXL-A-g_s model, as a continuation of the studies of Combe et al. (2015), van Heerwaarden and Teuling (2014), and van Heerwaarden et al. (2009). In this work we introduce an adjustable plant water-stress function into the model, allowing us to explore a wide range of water stress responses. Our model represents the daytime surface fluxes of carbon, water, and energy coupled to the dynamics of a convective boundary layer. Its strength is to include the essential diurnal processes of the L-A in a concise manner. With this system we address three research questions:

1. What is the impact of changing the plant water-stress response function from a sensitive to an insensitive formulation on the simulated atmospheric boundary-layer of a coupled land-atmosphere (L-A) system?
2. How does this choice of plant water-stress response function affect the development of a dry spell over time?
3. How are the interactions of the diurnal L-A system, as well as its sensitivity to model errors, affected by the choice of plant water-stress response function?

We base our sensitivity analysis on a control case that represents a grown maize crop field during a sunny summer day in the Netherlands. This control case has been validated with observations and discussed in Combe et al. (2015), and is generally representative of short vegetation. In Sect. 3.3.1, we first modify the conventional representation of soil water stress (i.e. the linear response) in our model, and explore the impact of a range of other, non-linear water-stress response curves on the mixed-layer budgets of CO₂, water, and heat. We next turn to the development of a dry spell in Sect. 3.3.2, and investigate the impact of two different plant water-stress responses on the coupled L-A system, during the dynamic soil drying of a three-week period. Finally, we show in Sect. 3.3.3 that the impact of errors in the simulated early-morning temperatures, cloud cover conditions and large-scale air motions can be large, small, and even of opposite sign depending on the choice of water-stress response function. The implications of these findings are discussed in Sect. 3.4.

3.2 Research strategy

3.2.1 Conceptual view of the land-atmosphere system

Figure 3.1 presents a schematic view of a coupled land-ABL system. This figure was extended to include the carbon cycle from the work of van Heerwaarden and Teuling (2014) and van Heerwaarden et al. (2009) (hereafter H14 and H9), who focused on the water and heat cycles only. Figure 3.1a represents a well-watered short vegetation surface coupled with a convective ABL under no subsidence. Figure 3.1b then shows the changing interactions under large-scale subsidence.

In H9, the authors presented three negative feedback loops that regulate evapotranspiration (LE) under well-watered conditions: a heating feedback, a drying feedback and a moistening feedback (see the blue shaded part of Fig. 3.1). We refer to H9 for their full description. This description of the feedbacks excluded the possibility for plants to regulate their transpiration flux. In H14, the authors thus added the concept of an adaptable surface conductance (g_s), which could additionally modify LE (see the brown shaded part of Fig. 3.1a). Knowing that this representation of the water and heat cycles is more correct for vegetated lands, we expanded this picture to carbon dioxide as it is controlled by many of the same processes, as shown in Fig.3.1a.

From H14, we first added the net surface flux of CO_2 or net ecosystem exchange (NEE). This variable is determined by the net primary production (NPP) from plants and the heterotrophic respiration (R_{het}). While NPP is controlled both by the canopy conductance (g_s) and by the stomatal demand for CO_2 (c_i/c ratio), R_{het} is known to be a function of soil temperature (Karhu et al., 2014; Davidson and Janssens, 2006). In that way, g_s acts as a coupling point for the carbon cycle, the water, and the heat cycles previously described by H9 and H14 (see Fig. 3.1a). This coupling point is directly controlled by surface drivers such as the soil moisture index (SMI) and the leaf area index (LAI) (Ronda et al., 2001).

From H14, we then added the entrainment flux of CO_2 at top of the ABL and the mixed-layer CO_2 mole fraction. The latter is affected by all boundary fluxes of CO_2 , as well as the volume dilution due to the growth of the ABL during the day (Pino et al., 2012). Both the entrainment velocity (w_e) and volume dilution are related to changes in h , which is determined by the amount of energy that is partitioned into sensible heat at the surface and by subsidence (see Eqs. 1-2). In that way, h acts as the second coupling point of the L-A system as it joins the carbon, water and heat water cycles at top of the ABL (see Fig. 3.1a). This second coupling point is directly influenced by the free-tropospheric processes and ABL-top conditions, such as subsidence (w_s) and the free-troposphere temperature lapse rate (γ_θ) (Ek and Holtslag, 2004; Williams et al., 2011). As a result of the coupling of the carbon, water and heat cycles at the surface (g_s) and at the top of the ABL (h), it is necessary to consider the L-A system as

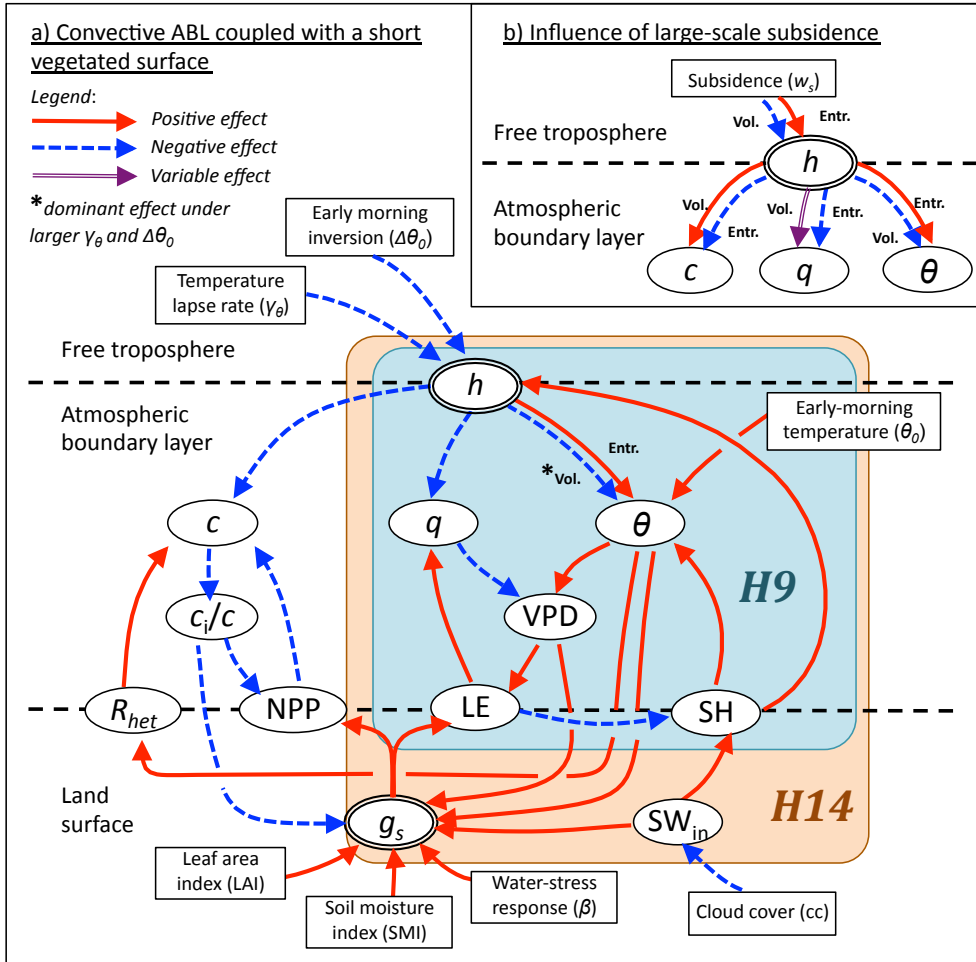


Figure 3.1 – Interactions of the vegetated land-ABL system, based on the studies of H9 and H14. Each arrow represents the impact of an increase in variable “x” on another variable “y”. Boundary and initial conditions explored in this study are presented in squared boxes. Model variables (encircled) are from the surface to the top of the ABL: the surface conductance (g_s), net surface shortwave radiation (SW_{net}), sensible heat flux (SH), latent heat flux (LE), net primary production (NPP), heterotrophic respiration (R_{het}), the internal to external CO_2 concentration ratio (c_i/c), the surface vapor pressure deficit (VPD), the ABL potential temperature (θ), specific humidity (q), CO_2 mole fraction (c), and the ABL height (h). Changes in h are related to changes in ABL volume (Vol.) and entrainment flux (Entr.) and these are separated when divergent.

a whole to understand variations in specific parts of the carbon, water or heat cycles.

3.2.2 Description of the MXL-A-g_s model

We focus on the case of a well-grown short vegetation surface that interacts with a convective ABL, in the mid-latitudes. We choose to model the interactions of the coupled land-atmosphere system with a simple process-based modeling framework: the MXL-A-g_s model. This model consists of a zero-order model for the convective ABL (Tennekes, 1973), coupled with a simple radiation scheme using a net sky transmissivity (Stull, 1988), a land-surface scheme using a stomatal conductance approach (Jacobs et al., 1996), and a modified two-layer force-restore soil model (Duynkerke, 1991; Noilhan and Planton, 1989). We introduce hereafter the equations of the MXL-A-g_s model that describe the ABL dynamics, the mixed-layer CO₂ mole fraction, and the net surface flux of CO₂. In addition, we refer to Appendices A and B for the complementary equations describing the heat and water cycles and the full surface conductance formulation.

Atmospheric convective boundary layer

The mixed-layer model (MXL) calculates the diurnal evolution of the atmospheric state variables and CO₂ in a convective boundary layer. The mixed-layer state variables (also called "bulk" variables) do not vary with height due to the intense convective turbulent mixing. First, under convective conditions the diurnal evolution of the ABL height (h) can be described as follows:

$$\frac{dh}{dt} = w_e + w_s, \quad (3.1)$$

$$w_e = -\frac{\overline{(w'\theta'_v)_e}}{\Delta\theta_v} = \beta_{\theta_v} \frac{\overline{(w'\theta'_v)_s}}{\Delta\theta_v}, \quad (3.2)$$

with w_e the entrainment vertical velocity, w_s the negative vertical subsidence velocity to include the effect of large-scale subsidence motions, β_{θ_v} the ratio between the entrainment turbulent flux of virtual heat ($\overline{(w'\theta'_v)_e}$) and the surface turbulent flux of virtual heat ($\overline{(w'\theta'_v)_s}$), and $\Delta\theta_v$ the virtual potential temperature jump at the inversion height, as we assume that the inversion layer is infinitesimally thin. With this formulation, entrainment is thus parameterized as function of $\overline{(w'\theta'_v)_s}$, and turbulent motions do not need to be resolved.

To complete Eqs. 3.1 and 3.2, we need a budget equation for the ABL virtual potential temperature (θ_v) and for the evolution of the virtual potential temperature jump at the inversion height ($\Delta\theta_v$), which we present in Appendix A. The diurnal evolution of all ABL state variables (i.e. the potential temperature θ , the specific humidity q , and the wind speed u) and of the atmospheric compounds (e.g. CO₂) can be expressed as a function of their boundary

fluxes (i.e. the surface, entrainment and advection fluxes) and of the ABL volume. For the CO₂ mole fraction (c), the physical interpretation is as follows if we neglect the horizontal advection of CO₂:

$$\begin{aligned} \frac{dc}{dt} &= \frac{1}{h} \times \left(\underbrace{\overline{w'c'_s}}_{\text{Surface turbulent flux of CO}_2} - \underbrace{\overline{w'c'_e}}_{\text{Entrainment turbulent flux of CO}_2} \right), \\ &= \frac{1}{h} \times \left(\frac{\text{NEE}}{\rho_{air}} + w_e \Delta c \right), \end{aligned} \quad (3.3)$$

with NEE the net ecosystem exchange in $\text{mg}_{\text{CO}_2} \text{ m}^{-2} \text{ s}^{-1}$, ρ_{air} the density of the air, and Δc the CO₂ jump at the inversion height. Note that h controls the dilution of the CO₂ mole fraction in Eq. 3.3. The gradient Δc evolves in time due to the growth of the ABL into the free troposphere and to the evolution of the mixed-layer CO₂. This expression reads:

$$\frac{d\Delta c}{dt} = \gamma_c w_e - \frac{dc}{dt}, \quad (3.4)$$

with γ_c the free-troposphere lapse rate of CO₂. At Eq. 3.3, we represent the entrainment as the entrainment velocity (see Eq. 3.2) times the instantaneous gradient of CO₂ at top of the ABL (see Eq. 3.4). We refer to Appendix A for similar atmospheric equations to Eqs. 3.3 and 3.4 for θ and q .

Land-surface

The A-g_s model expresses the net surface fluxes of heat (SH), water (LE) and CO₂ (NEE) as the temperature, moisture and CO₂ gradients times their corresponding surface conductance, except for NEE where we have to add the contribution of the heterotrophic respiration (R_{het}):

$$\text{NEE} = \overbrace{\rho_{air} g_{s,c} (c_i - c)}^{\text{NPP}} + R_{het}, \quad (3.5)$$

$$g_{s,c} = \frac{1}{r_a + r_c}, \quad (3.6)$$

with $g_{s,c}$ the surface conductance for CO₂ transfer, c_i the CO₂ concentration in the plant substomatal cavities, r_a the aerodynamic resistance, r_c the canopy stomatal resistance to CO₂ transfer. R_{het} is calculated as the product of a reference respiration constant with a soil water-stress factor and an exponential function of the surface temperature. We refer to Appendix A for the complementary equations for the surface heat and moisture fluxes.

We describe the aerodynamic resistance as an inverse function of wind speed and a drag

coefficient for heat, which is a function of the surface roughness and atmospheric stability. This formulation is issued from the Monin-Obukhov similarity theory. At the origin of the r_c formulation, Jacobs et al. (1996) expresses the net leaf assimilation A_n (i.e. the net flux of CO_2 through the stomata of a leaf) as the sum of gross leaf assimilation (A_g) and leaf dark respiration (R_{dark}):

$$A_n = \frac{1}{r_{l,c}} (c - c_i) = \beta A_g^* - R_{dark}, \quad (3.7)$$

with $r_{l,c}$ the leaf stomatal resistance to CO_2 transfer, β the plant water stress factor and A_g^* the unstressed gross leaf assimilation. R_{dark} is parameterized as 11 % A_g^* . Note that A_n is not equal to NPP as (a) the CO_2 still has to transfer through the leaf boundary-layer (i.e. experience r_a) and (b) the CO_2 assimilation has to be upscaled to the canopy level, before we obtain NPP. Jacobs et al. (1996) uses an empirical response function of A_g^* to light, CO_2 and temperature, which allows us to rewrite Eq. 3.7 as follows:

$$A_g^* = (A_m + R_{dark}) \left[1 - \exp\left(-\frac{\text{LUE } K_x \text{ PAR}_t e^{-K_x L}}{(A_m + R_{dark})}\right) \right], \quad (3.8)$$

with A_m the primary productivity under high light conditions, LUE the light-use efficiency constant, K_x the light extinction coefficient, PAR_t the photosynthetically active radiation at an instant t , and L the integrated LAI at a specific depth within the canopy (we integrate from 0 at top of the canopy to the total LAI at bottom). A_m is a function of the internal CO_2 concentration c_i , of the CO_2 compensation point Γ , of the maximum productivity $A_{m,max}$, and of the mesophyll conductance g_m , all later three parameters being dependent on the leaf temperature (T_{sk}). Jacobs et al. (1996) also found that the c_i/c ratio is a function of the vapor pressure deficit (VPD) at the leaf surface:

$$\frac{c_i - \Gamma}{c - \Gamma} = f_0 \left(1 - \frac{\text{VPD}}{\text{VPD}_0} \right) + f_{min} \frac{\text{VPD}}{\text{VPD}_0}, \quad (3.9)$$

with f_0 and f_{min} respectively the maximum and minimum values of $(c_i - \Gamma)/(c - \Gamma)$, and VPD_0 the value of VPD at which the stomata close. Combining Eqs. 3.7, 3.8 and 3.9, the leaf stomatal resistance for CO_2 transfer $r_{l,c}$ can be rewritten as:

$$\frac{1}{r_{l,c}} = g_{min,c} + \frac{a_1 A_g^* \beta}{(c - \Gamma) \left(1 + \frac{\text{VPD}}{\text{VPD}_*} \right)}, \quad (3.10)$$

with $g_{min,c}$ the cuticular conductance for CO_2 transfer. a_1 is $1/(1-f_0)$ and VPD_* is $\text{VPD}_0/(a_1 - 1)$. To upscale $r_{l,c}$ from the leaf to the canopy level (i.e. to obtain r_c), we integrate Eq. 3.10 over LAI (see the full derivation in Appendix B). In the end, and to summarize, the A-gs

formulation from Jacobs et al. (1996) expresses r_c as a function of PAR, T_{sk} , the c_i/c_a ratio, VPD, the plant water stress (β , our main point of investigation in this study) and LAI. Note that in the rest of the manuscript, we analyze the variations of g_s (i.e. the surface conductance for water transfer) which is equal to $g_{s,c}/1.6$. The variations in g_s thus reflects the variations in both r_a and r_c .

Soil water budget

We use the soil water budget from the two-layer force-restore model of Noilhan and Planton (1989). It describes water flow as follows:

$$\frac{dw_1}{dt} = \underbrace{\frac{C_1}{\rho_w d_1} (Pr - \frac{LE_{evap}}{L_v})}_{\text{input - output atmosphere}} - \underbrace{\frac{C_2}{\tau} (w_1 - w_{1eq})}_{\text{diffusion into the ground}}, \quad 0 \leq w_1 \leq wsat, \quad (3.11)$$

$$\frac{dw_2}{dt} = \frac{1}{\rho_w d_2} (Pr - \frac{LE_{transpi}}{L_v}), \quad 0 < w_2 \leq wsat, \quad (3.12)$$

with w_1 and w_2 the volumetric soil moisture content of the first and second soil layers, ρ_w the density of liquid water, d_1 and d_2 the depths of the first and second soil layers, Pr the input of water from precipitation, LE_{evap} the output of water from soil evaporation, $LE_{transpi}$ the output of water from plant transpiration, L_v the latent heat of vaporization, C_1 and C_2 are two coefficients related to the Clapp and Hornberger parameterization (Clapp and Hornberger, 1978), w_{1eq} the soil moisture content at which the capillary forces balance the gravity forces and no diffusion of water occurs to the second layer, and τ the time-scale of that return to equilibrium.

The force-restore model neglects the diffusion of water between the second layer and the deeper – non-modeled – soil layers, and the diffusion of water from the second soil layer to the upper layer by capillarity. All soil evaporation is done from the first soil layer (first 10 cm), and all plant transpiration is taken from the second layer (lower 1.5 m). We thus neglect the roots water extraction from the upper superficial layer. We refer to Combe et al. (2015) for the constants of the soil model used in our study.

Updated plant water-stress parameterization

As mentioned in Sect.3.2.2, in the A- g_s model, the plant water-stress factor (β) is directly multiplied with the leaf gross assimilation A_g^* . The standard β function of MXL-A- g_s is the linear one, and is equal to the soil moisture index (SMI) of the second soil layer:

$$SMI = \frac{w_2 - w_{wp}}{w_{fc} - w_{wp}}, \quad (3.13)$$

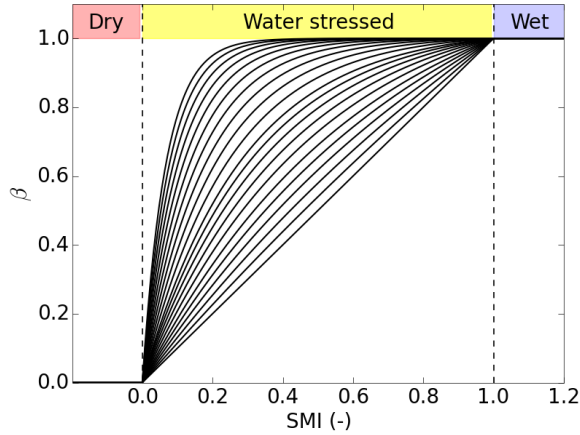


Figure 3.2 – Range of soil water-stress (β) response functions modeled in this study. The soil water content is expressed on the x-axis with the soil moisture index (SMI, see Eq. 3.13), thus wilting point and field capacity are respectively represented as the $SMI = 0$ and $SMI = 1$ dashed lines. Below wilting point, plants are incapable of taking water up from the soil. Above field capacity, the maximum amount of water is being stored in the soil pores. Plant water-stress occurs in between those two points.

with w_{wp} and w_{fc} the volumetric water contents at wilting point and field capacity. To vary the curvature (C_β) of this response function we implemented a new exponential function suggested by Ronda et al. (2001):

$$\beta = \frac{1 - \exp(-P(C_\beta) \times SMI)}{1 - \exp(-P(C_\beta))}, \quad (3.14)$$

$$\text{with } P(C_\beta) = \begin{cases} 6.4 \times C_\beta & \text{for } 0 \leq C_\beta < 25 \%, \\ 7.6 \times C_\beta - 0.3 & \text{for } 25 \leq C_\beta < 50 \%, \\ 2^{(3.66 \times C_\beta + 0.34)} - 1 & \text{for } 50 \leq C_\beta \leq 100 \%. \end{cases}$$

With Eq. 3.14, we vary the curvature of the response function (C_β) from 0 (sensitive) to 100 % (insensitive) to obtain the range of β response functions plotted in Fig. 3.2. This range encompasses a large variety of β response functions currently used in land-surface models (e.g. see Powell et al., 2013). Note that at a fixed $SMI < 1$, we obtain a higher β value and thus higher g_s with the non-linear responses.

3.2.3 Diagnostic variables

We calculate two supplementary diagnostic variables to help analyze the state of the diurnal L-A system. Firstly, we calculate the ratio of the entrainment to surface CO₂ tendencies (R_c), which quantifies how much of the total daytime CO₂ tendency is driven by entrainment, in comparison to the surface NEE:

$$R_c = \frac{\int_{t=6:00 \text{ UTC}}^{t=18:00 \text{ UTC}} (-\overline{w'c'_e}/h) dt}{\int_{t=6:00 \text{ UTC}}^{t=18:00 \text{ UTC}} (\overline{w'c'_s}/h) dt}. \quad (3.15)$$

A ratio of 1 means that the surface and ABL-top processes contributed equally to the daytime mixed-layer CO₂ tendency.

Secondly, we calculate the evaporative fraction (EF) at 14:00 UTC, which quantifies the partitioning of energy at the surface going into evapotranspiration:

$$EF = \frac{LE}{LE + SH}. \quad (3.16)$$

We calculate the 14:00 UTC value as the surface fluxes of water and heat are high and the ABL is fully convective.

3.2.4 Sensitivity analysis

In order to quantify the interactions between the land surface and the ABL, we design a sensitivity analysis with our MXL-A-g_s model. We use a recently published control case (Combe et al., 2015) that is based on observations of the soil, plants and ABL, over a maize field grown in Wageningen (the Netherlands) on 4 August 2007 (Jans et al., 2010). Using this comprehensive set of observations to design our control case gives us confidence that we are representing a realistic situation. The main initial and boundary conditions of our control case can be found in Table C.1, in Appendix.

We first focus on the influence of the type of plant water-stress response function on the two key coupling points presented in Sect. 3.2.1. For this, we perform a series of sensitivity experiment where we simultaneously vary SMI from 0 to 1 and C_β from 0 to 100 %, performing 100×100 cases. We then analyze the response of g_s , R_c , EF and h to these combined variations of SMI and C_β . The results of this series of experiments are presented in Sect. 3.3.1.

We then analyze the impact of the plant water-stress response on the time evolution of a dry spell (i.e. here: a 21-day continuous soil moisture depletion). We start two sensitivity experiments with the control case of Combe et al. (2015), only changing the curvature of the plant water stress response function. We use two extreme plant water stress responses: our

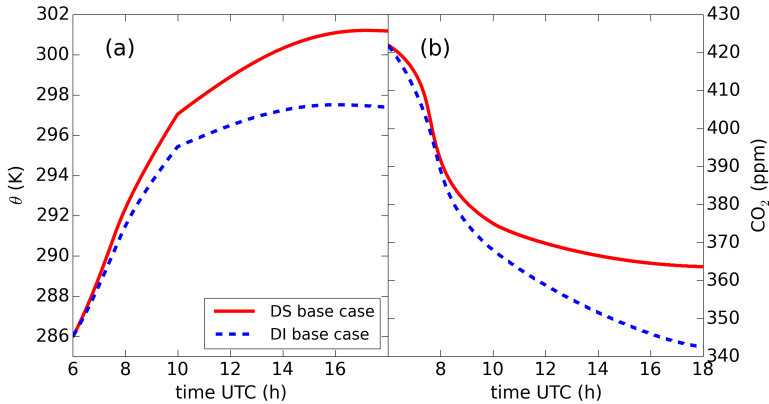


Figure 3.3 – Diurnal cycles of c and θ for the dry soil ($SMI = 0.2$) base cases of the sensitive (DS) and insensitive (DI) vegetated surfaces.

most sensitive response ($C_\beta = 0\%$) and our most insensitive response ($C_\beta = 100\%$). Over a 21-day period, we transfer the soil moisture depletion caused by evapotranspiration (LE) from one day to the next, while we reinitialize all other variables identically to the control case. This is a similar approach to Daly et al. (2004), except we do not represent the nocturnal boundary-layer and nighttime surface fluxes. The results of this analysis are presented in Sect. 3.3.2.

Finally, because our previous experiment does not include variations in the daily atmospheric initial conditions that occur during a dry spell, we assess the impact of atmospheric model errors on the carbon and heat cycles. We define two new base cases that are identical to the one of Combe et al. (2015) except for their $SMI (= 0.2)$ and the curvature of their plant water stress response function ($C_\beta = 0\%$ and 100%). These values generate the largest differences in plant water stress factor β (see Fig. 3.2) and surface coupling g_s between our two plant water stress responses. We illustrate the two generated base cases in Fig. 3.3, which we respectively name DS (dry soil - sensitive to water stress) and DI (dry soil - insensitive to water stress). Note that the diurnal cycles of CO_2 and temperature presented in Fig. 3.3 reach two characteristic values: a diurnal minimum for CO_2 (c_{min}) and a diurnal maximum for temperature (θ_{max}). These are the two characteristic values that we hereafter focus our analysis on.

We select four initial and boundary conditions that vary from day-to-day during a dry spell: the subsidence velocity (w_s), the free-troposphere temperature lapse rate (γ_θ), the early-morning ABL potential temperature (θ_0), and the cloud cover (cc , see Fig. 3.1). For each of these variables we define a model error (see Table 3.1). Note that for θ_0 we create a set

Table 3.1 – Explored model errors.

Variable [units]	Initial value	Change
w_s [s^{-1}]	0.7×10^{-5}	$+3.3 \times 10^{-5}$
γ_θ [$K km^{-1}$]	8	+3
cc [%]	22.5	-22.5
θ_0 [K]	286	+4

of consistent initial conditions for each run: (a) we conserve the temperature differences between the soil layers and the atmosphere, effectively shifting the entire temperature profile, and (b) we conserve the initial VPD of the base case (94 %) by adapting the initial q . We subsequently apply all our defined model errors first one-by-one, then all at once on our two base cases (DS and DI) and analyze their impact on c_{min} and θ_{max} . The result of these experiments is presented in Sect. 3.3.3.

3.3 Results

3.3.1 Coupling points

The atmospheric budget of CO_2 can switch from being dominated by surface fluxes to dominated by entrainment depending on the stomata aperture, which is controlled by the soil moisture level and the vegetation sensitivity to water stress. This is illustrated in Figure 3.4a, which presents the response of the surface coupling point (g_s) and of the mixed-layer CO_2 budget (through R_c) to the assumed curvature of the plant water-stress response function (C_β on the y-axis) and soil moisture level (SMI on the x-axis). If we first focus on soil moisture at a given water-stress response ($C_\beta = 0$), we find two opposite regimes of the CO_2 budget indicated by two dots marked WS (wet soil – sensitive to water stress) and DS (dry soil – sensitive to water stress). The non-stressed vegetation of the WS case has a g_s of 12 mm s^{-1} which enables high photosynthesis rates and a large contribution of NEE to the CO_2 budget ($R_c = 0.5$) while the stressed vegetation of the DS case has a g_s of 3 mm s^{-1} , which almost fully inhibits photosynthesis and reduces the coupling between the vegetation and the atmospheric CO_2 budget ($R_c = 3$). This reduced coupling of the ABL carbon budget from the surface fluxes is important for the interpretation of observed mixed-layer CO_2 mole fractions under drought conditions as it is often assumed that CO_2 measurements in the ABL predominantly reflect vegetation carbon exchange – which is clearly not true in this example. Further reducing soil moisture below $SMI = 0.2$ would lead to an exponential R_c increase and even weaker surface coupling.

However, we can again increase the vegetation influence on ABL CO_2 at low soil moisture

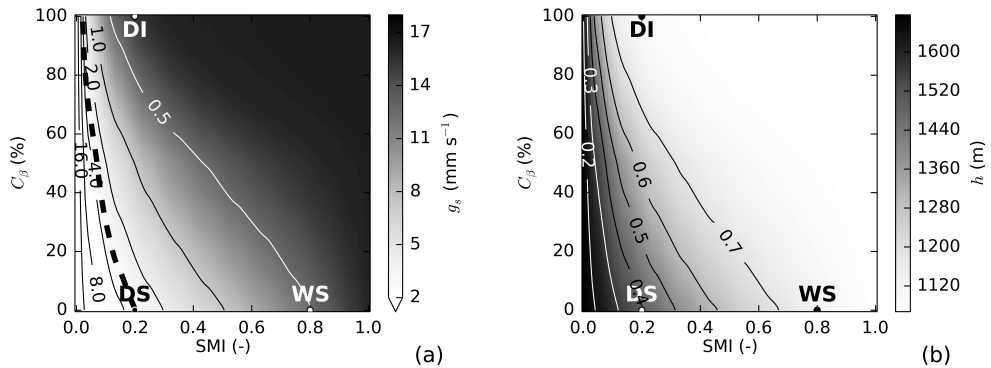


Figure 3.4 – Values of key variables in the coupled land-atmosphere system as a function of soil moisture index (SMI, x-axis) and of curvature of the water-stress function (C_β , y-axis). Shown are (left) diurnal average g_s in grey scale with R_c in contours and (right) ABL height in grey scale and evaporative fraction in contours. We highlight where $R_c = 3$ with a thick dashed line, which corresponds roughly where $g_s = 3 \text{ mm s}^{-1}$. Three specific points are indicated: a wet soil case simulated with the sensitive water-stress response function (WS), a dry soil case simulated with the sensitive water-stress response function (DS), and a dry soil case simulated with an insensitive water-stress response function (DI).

by changing the assumed vegetation sensitivity to water stress. In Figure 3.4a, the point marked DI (dry soil – insensitive to water stress) is a simulation at the same soil moisture level as the DS point. It maintains high conductance, high carbon assimilation and evaporation rates, and thus conserves a strong influence of surface carbon exchange on atmospheric CO_2 . The R_c -value at this point is even below 0.5, while conductance remains close to 15 mm s^{-1} confirming that downregulation of photosynthesis has not yet started, in agreement with the $\text{SMI} = 0.2$ and $\beta = 0.95$ point in Fig. 3.2. We tentatively define the threshold of $g_s = 3 \text{ mm s}^{-1}$ shown as the thick dashed line in Fig. 3.4a as the point where we enter a very weakly coupled regime for CO_2 in the ABL. We note that this threshold shifts towards very low values of SMI if C_β (and thus β) increases in our analysis, and a similar effect occurs if we apply the linear β function on the mesophyll conductance instead of on the gross primary production, as done by Calvet et al. (1998) and as suggested by Keenan et al. (2010a) (not shown here). This will be discussed further in Sect. 3.4.

The weakly coupled regime of surface CO_2 is always correlated with high ABL growth and high entrainment of dry and warm air, which will ultimately feed back on surface conditions. This is illustrated in Fig. 3.4b that presents the response of the coupling point at the top of the ABL (h) and of the evaporative fraction (EF) to the variation of the curvature of the water-stress response function (y-axis) and SMI (x-axis). We first see the complementarity of Figs. 3.4a and b, and how low g_s switches the surface energy budget towards the

release of sensible heat. From the WS to the DS case, the 10 mm s^{-1} drop in g_s causes EF to decrease from 0.74 to 0.39, and thus the ABL height to increase from 1131 m to 1494 m. Then from the DS to the DI case, the 12 mm s^{-1} increase in g_s reverts EF and h back to 0.76 and 1120 m. These substantial differences in ABL height and surface energy balances are relevant for both numerical weather prediction and climate modeling, as simulated temperatures near the surface as well as cloud formation and precipitation rates now depend on plant water-stress response.

We find that water-stress sensitive and insensitive vegetated surfaces can behave identically from a carbon, water, and heat exchange point of view, despite a large difference in their hydrological state. In Fig. 3.4a, the vegetation of the DI case has the same g_s ($12\text{-}15 \text{ mm s}^{-1}$) as the vegetation of the WS case. In Fig. 3.4b this leads them to have a similar surface energy budget ($EF \approx 0.75$) and ABL growth ($h \approx 1130 \text{ m}$). Specifically for coupled land-surface simulations such as done in climate models, it is important to realize that in addition to their effects on local conditions mentioned above, the differing sensitivities ultimately feed back on the larger scale atmospheric state. This shows that the choice of plant water stress representation in land-surface models could be an important area of model improvement.

3.3.2 Temporal evolution of a dry spell

We find that vegetation insensitive to water-stress depletes soil moisture faster than the sensitive vegetation because it does not downregulate g_s and LE until the soil moisture is very close to wilting point. Even on the first day when $SMI = 0.55$ the sensitive response downregulates LE to 300 W m^{-2} whereas the insensitive response keeps evapotranspiring at potential level ($LE = 400 \text{ W m}^{-2}$) (Fig. 3.5). The accumulated amount of water transpired from the deeper soil layer - where the maize roots are located - over the 21-day period is much greater for the insensitive response (78 mm) than for the sensitive response (57 mm). As a result, the SMI for the insensitive response drops below wilting point and is much lower than for the sensitive response. The insensitive response is similar to observed C_3 and C_4 grasses over Europe, while the sensitive response is more conservative of water resources as observed over forests (Wolf et al., 2013; Teuling et al., 2010).

Our simulations illustrate how vegetation insensitive to water-stress delays atmospheric warming. Figures 3.5c and d show this vegetation conserves a high $g_s > 14 \text{ mm s}^{-1}$, thus a low maximum $SH \approx 100 \text{ W m}^{-2}$ and a low θ_{max} of 298 K over the first 14 days. Between days 14 and 19 in Fig. 3.5c it switches suddenly to a low $g_s < 1 \text{ mm s}^{-1}$, and subsequently a high maximum SH flux of 400 W m^{-2} and a high θ_{max} of 303 K. In contrast, vegetation sensitive to water-stress evolves gradually towards a warmer atmospheric state over the 21 days, but without ever reaching the same range of temperature increase (from 299 to 302 K). Our finding is thus in agreement with Teuling et al. (2010); van Heerwaarden and Teuling

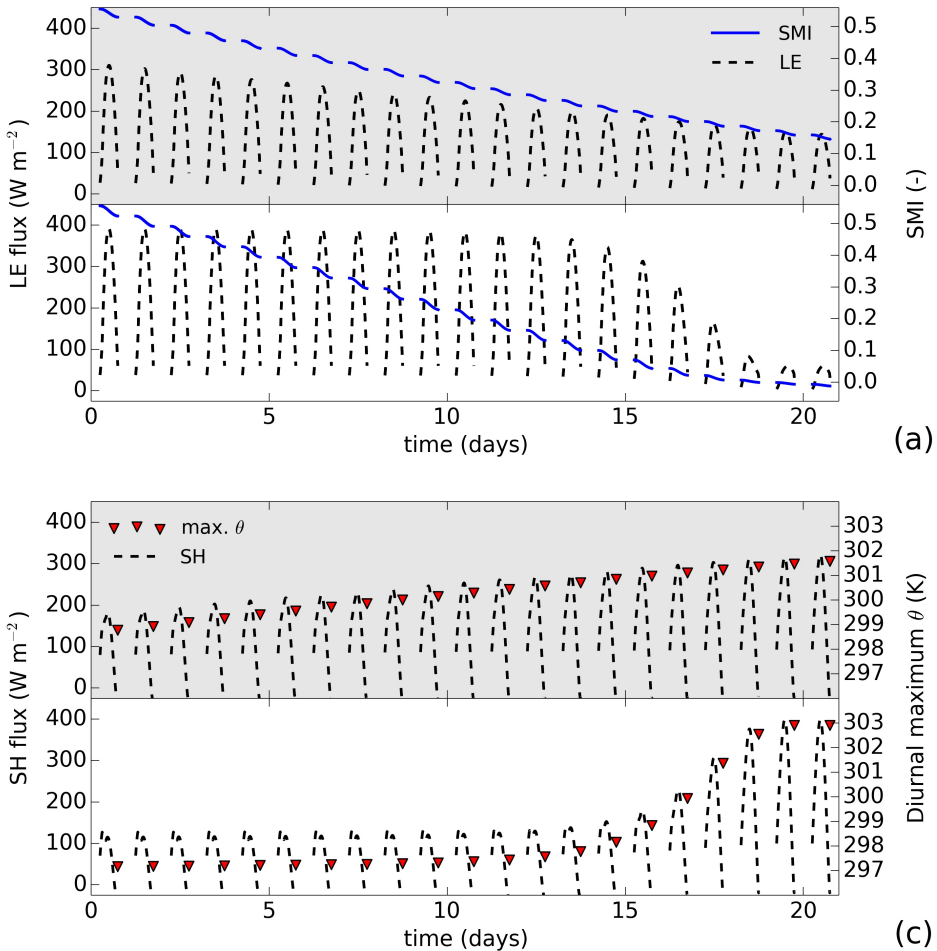


Figure 3.5 – The effect of soil moisture depletion over a 21-day dry period under two different plant water-stress representations. Results using the sensitive response are shown with a grey background, while the results with an insensitive response are shown with a white background. Both simulations start at SMI = 0.55. Variables shown here are (a) LE and SMI, and (c) SH and θ_{max} .

(2014), who showed that during the European 2003 heatwave forests downregulated their transpiration sooner than grass and were showing increases in air temperature earlier in time. Our result shows that the choice of water stress representation in a land-surface model is important to simulate the build-up of heat waves, and is an additional factor to take into account in heat waves studies like Miralles et al. (2014).

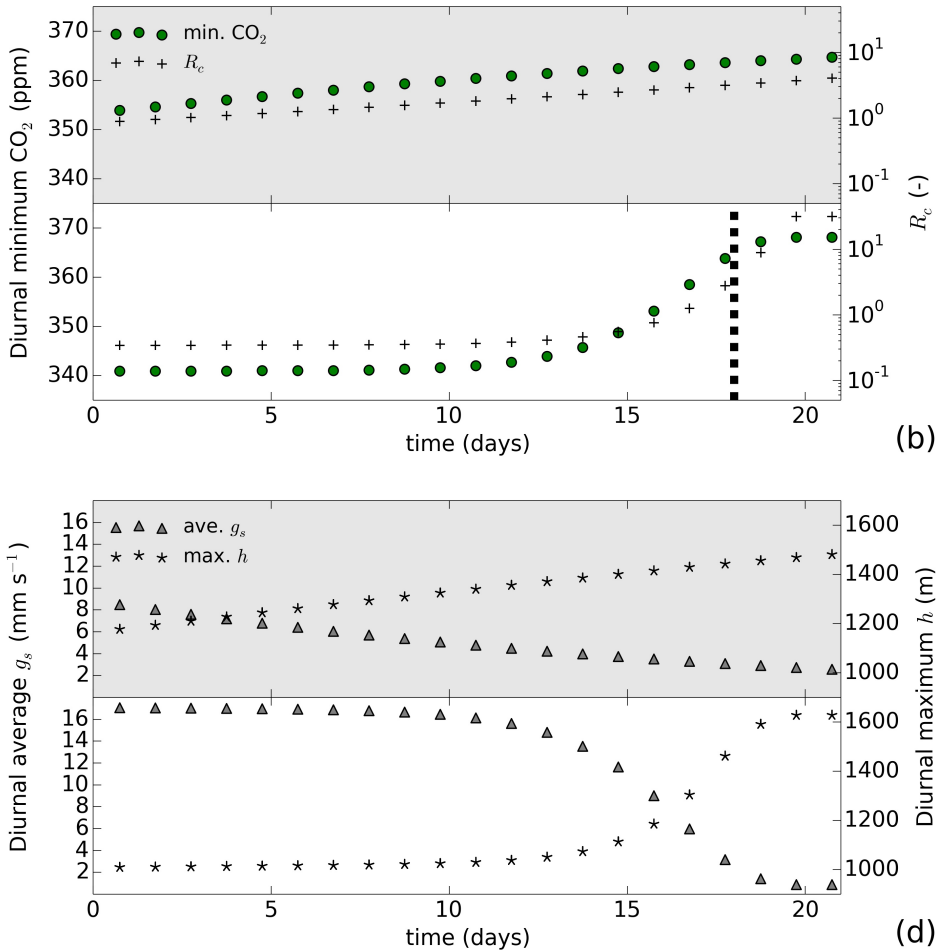


Figure 3.5 – (continued) – Variables shown here are (b) c_{min} and R_c , and (d) g_s and h . The surface coupling threshold for the CO₂ budget at $g_s = 3 \text{ mm s}^{-1}$ is shown by the thick dashed line in panel (b).

Finally, when we look at the mixed-layer CO₂ mole fraction, we find the insensitive water-stress response consistently generates lower CO₂ mole fractions than the more sensitive response over the first 15 days. After day 17, this difference reverses as the insensitive response abruptly decreases g_s , reducing the coupling between land and atmosphere for the carbon cycle. In Fig. 3.5b we find the diurnal minimum CO₂ mole fraction for the sensitive response evolves linearly from 354 to 362 ppm, whereas the diurnal minimum CO₂ mole

fraction for the insensitive response switches abruptly from 341 to 368 ppm between day 12 and 19. As a consequence, it reaches the weakly coupled CO₂ regime that we tentatively defined in Sect. 3.3.1 at $g_s = 3 \text{ mm s}^{-1}$. Any model interpretation of observed CO₂ mole fractions under water-stressed conditions thus needs to consider the type of water stress response to explain (a) the temporal evolution pattern of CO₂ mole fractions, and (b) the relative importance of the entrainment process and of large-scale conditions in the ABL CO₂ budget.

3.3.3 Sensitivity to model errors

The long-term temperature and CO₂ increases from Sect. 3.3.2 can be regarded as a lower-bound estimate during such drought, as we have currently only carried over the effects on soil-moisture from one day to the next. Additional cumulative effects can be expected for example from increasing early-morning temperatures (which increases g_s , VPD and R_{het} , see Fig. 3.1), reduced absolute humidity (which increases VPD), reduced cloud cover (which increases PAR). However, these cumulative changes cannot be modeled readily with our framework, as we cannot simulate nighttime conditions, meso-scale air circulation or cloud formation. But we can assess the effects of possible errors in these variables (i.e., a deviation from their true state) that can occur in our simulations or in other models that do not correctly capture the dynamics of the land (e.g. LAI), or atmosphere (e.g. meso-scale air circulation), or their interaction.

Errors in simulated atmospheric conditions can have significant impacts on the ABL CO₂ mole fraction and ABL temperature on a single day. We show this in Fig. 3.6 where we present the change in the daily minimum c (y-axis) and in the daily maximum θ (x-axis) resulting from prescribed errors in the atmospheric initial conditions of the DI and DS base runs. All prescribed errors listed in Table 3.1 cause a positive or negative change in c_{min} larger than 1 ppm, and an always positive change in θ_{max} larger than 0.5 K independent of the assumed plant water stress response. For example, overestimates in simulated early morning temperature of the mixed-layer (+4 K θ_0) translate to almost identical overestimates in the daytime maximum temperature (+3 to +3.5 K θ_{max}). Similar positive impacts on the maximum temperature are seen from overestimates in large-scale subsidence rates (+1 to +2 K) or temperature lapse-rates (+0.5 to +1 K), as qualitatively illustrated in our conceptual Fig. 3.1. Our examples thus clearly illustrate that simulated conditions in the atmospheric boundary layer during dry spells are very sensitive to both its boundary and initial conditions. Their errors, as well as the simulated coupling strengths thus determine the accuracy of a simulated heatwave.

Moreover, depending on the assumed vegetation sensitivity to water-stress the effect of such model errors on the CO₂ mole fraction and ABL temperature can double, or half, or even reverse sign. For instance in Fig. 3.6, a switch from a sensitive to an insensitive plant response

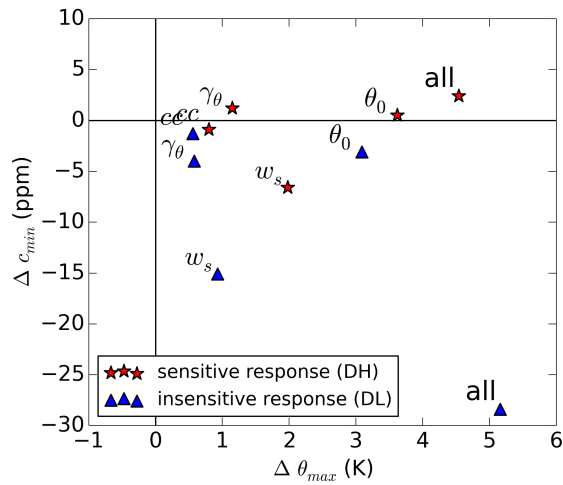


Figure 3.6 – Contrasted response of the ABL CO_2 and temperature to atmospheric model errors for two contrasted plant sensitivity to water stress, under severe water deficit ($SMI = 0.2$). In Fig. 3.3, the sensitive (DS) and insensitive (DI) base cases reached two different c_{min} (364 ppm for DS and 343 ppm for DI) and θ_{max} (301 K for the DS and 297 K for DI) due to their contrasted responses to water stress. We present here the deviations from these base cases c_{min} and θ_{max} , after applying changes to the runs initial conditions (see Table 3.1).

to water stress causes the impact of an error in simulated subsidence rates to be twice as large on c_{min} , but half as large in θ_{max} . Also overestimates in simulated γ_θ causes a 2 ppm higher c_{min} when assuming the sensitive response or a 4 ppm lower c_{min} when assuming the insensitive response. The key difference when switching from the sensitive to the insensitive water-stress response cases is the increase in surface coupling and the subsequent 4 K lower temperature regime of the ABL (see Fig. 3.3). The assumed plant water-stress sensitivity in the model puts us on opposite sides of the optimum temperature for photosynthesis (298 K): while the leaf temperature of the DI base case is consistently below this optimum throughout the day, the one of the DS base case is consistently above this optimum. The extra warming then generated by each model error (from +0.5 to +3.5 K for cc , γ_θ , w_s , and θ_0) causes the insensitive vegetation to increase its assimilation rate and the sensitive vegetation to decrease its assimilation rate, generating consistently higher c_{min} for the sensitive cases compared to their corresponding insensitive cases. Our results highlight the importance of the representation of plant-water stress not just for the temporal evolution of the mean atmospheric conditions as in Sect. 3.3.2, but also for directing the impact of errors in a coupled model for carbon, water, and energy. We will further discuss this in Sect. 3.4.

Finally, we see that simultaneous errors in variables associated with the development of

a dry spell add non-linearly to affect the CO_2 minimum and ABL temperature. In Fig. 3.6 we find that a combination of reduced cloud cover with an increased subsidence rate, free-troposphere temperature lapse rate, and early-morning temperature of the boundary layer, can amount to an error in θ_{max} of 4.6 to 5.2 K and in c_{min} of -27 to $+2$ ppm. Interestingly, the small effect on CO_2 in the sensitive vegetation case is not equal to the sum of the individual model error effects, and this is also true for the total temperature error. This especially illustrates the inter-dependence of the effects triggered by the combined model errors (see Fig. 3.1). Their combination reflects a model where all drivers during a drought are overestimated but in the sensitive vegetation response CO_2 is hardly affected, while in the insensitive case the modeled daytime CO_2 minimum is too low by almost 30 ppm. The implications of this finding will be discussed in the next section.

3.4 Discussion

The modularity of the atmospheric model (MXL) has allowed its users to add many processes to explore their importance for the diurnal simulation of the the ABL temperature, moisture and CO_2 . This includes a number of processes not considered in this study, such as the effect of shear-driven turbulence (Pino et al., 2006), residual boundary layers (Ouwersloot et al., 2012), shallow-cumulus formation and surface shading (van Stratum et al., 2014; Vilà-Guerau de Arellano et al., 2012), large-scale advection of heat (Miralles et al., 2014) and heating of the ABL by aerosols (Barbaro et al., 2014). Guided by the observations, we chose here to focus on the most important processes for a convective boundary-layer when coupled to a vegetation model that includes carbon exchange. On the atmospheric side of our framework this includes entrainment, subsidence, boundary-layer growth, free-tropospheric conditions, and horizontal heat advection. In our land-surface model (A-g_s) this includes the coupling of the carbon and water cycles through stomatal conductance. Its formulation has been validated for a number of surfaces with low vegetation such as maize (Combe et al., 2015), C₃ and C₄ grass, soybean (Ronda et al., 2001), and grapevine (Jacobs et al., 1996). We specifically note that to extend it to high vegetation (i.e. forests), the disturbance of the turbulence by the canopy should be included in the model. Such extension for the MXL model is being done at the moment, following the principles of Harman and Finnigan (2007). To additionally include the effect of meso-scale circulations, nighttime turbulent exchange, topography, or cloud dynamics requires a more explicit 3-D modeling framework, which would add considerable complexity to the study. We simply represent those as large-scale forcings by imposing vertical and horizontal advection of heat and moisture (Pietersen et al., 2015).

The range of water-stress responses and soil moisture index explored here is representative of a specific range of observed situations. A soil moisture index of 0.2 is a typical water

deficit observed during summer in Southern Europe (e.g. southern France and Portugal as shown in Barbu et al., 2011; Jongen et al., 2011) that can also occur in wetter regions during prolonged droughts. Our findings are thus relevant for those cases, as the replenishment of soil water by precipitation or irrigation will largely diminish our contrasted plant water stress responses effect on the stomatal conductance. Moreover, note that here we are exploring the spectrum of water stress responses existing between the linear and the very non-linear insensitive responses. We chose that spectrum as it was representative of a number of land-surface water-stress responses (SiB3, CTESSEL, JULES, CLM, A-g_s, see Boussetta et al., 2013; Powell et al., 2013; Ronda et al., 2001). However, there is a second half of the spectrum, between the linear and the non-linear very sensitive response, the later being representative of plants that shut their stomata as soon as there is a small soil moisture deficit (Calvet et al., 2004; Tardieu and Simonneau, 1998). By extension of our results, we expect the decoupling of the L-A water and carbon exchange (and the corresponding high L-A heat exchange) to happen at higher SMI and thus earlier in time during dry spells for this very sensitive non-linear response to water stress.

The plant water stress parameterization we investigated here is not the only approach taken in land-surface models. Several studies (Egea et al., 2011; Keenan et al., 2010a; Calvet et al., 1998) have suggested that in addition to downregulation of stomatal conductance, the mesophyll conductance and/or the maximum carboxylation rate should also be downregulated. The latter would account for non-stomatal effects, such as the decline in leaf nitrogen content (Grassi and Magnani, 2005) and the hardening of mesophyll cell walls (Keenan et al., 2010b). Even in models that use the beta-function as employed here, it is not clear which shape to choose because as argued by Joetzjer et al. (2014) the physiological response to water stress itself is not well understood. It will vary between species, and is observed to even be different for different varieties of crops (Zhou et al., 2013; Carmo-Silva et al., 2007; Calvet et al., 2004; Tardieu and Simonneau, 1998). As an alternative, mechanistic approaches were proposed (Verhoef and Egea, 2014; McDowell et al., 2013) that describe plant internal hydraulics. Such models in turn require more complex model input, with variables difficult to acquire (e.g. root density, soil hydraulic conductivity). For both water-stress response approaches, Powell et al. (2013) showed that a full drought response of vegetation should moreover include a change in respiration, LAI, plant mortality, carbon allocation, root adaptation, and even reproduction strategies (also see van der Molen et al., 2011). A possible extension of our study could be to repeat our experiments with our coupled MXL-A-g_s model but introducing the mechanistic water-stress approach, to observe which type of sensitivity to water stress and which L-A coupling it can model.

The idea of a coupling strength in climate models has been raised before. For example, Koster (2004) and Dirmeyer et al. (2006) looked at the hydrological cycle to define a coupling strength between the atmosphere and land, specifically using soil moisture and precipitation.

The fraction of explained variance in soil moisture by variations in precipitation allowed a quantification of this strength, and the separation of different coupling regimes. Seneviratne et al. (2010) summarizes similar approaches, amongst others for the soil moisture-temperature coupling strength. More similar to our use of a coupling strength, Santanello et al. (2009) analyzed the local land-atmosphere coupling state of heat and water showing that there are three surface energy balance regimes depending on the soil wetness (dry, intermediate, wet). Our study expands this analysis also to the surface carbon fluxes, and through R_c moreover accounts for CO_2 entrainment at the top of the PBL. This coupling strength at the top of the boundary layer is often not considered in coupled land-surface modeling, but forms an important connection to the larger atmospheric scales that control for example the development of heat waves.

Our study of the development of a heat wave is highly simplified due to the impossibility of the model to run through nighttime that led us not to change atmospheric conditions from day-to-day. This simplification can be partly supported by the fact that a heatwave typically develops in a synoptic situation that is relatively stable, with high-pressure, few clouds, strong subsidence, and little precipitation. However, variations in other variables are likely to occur over the 21-day period: heat and moisture advection, temperature lapse rates, and CO_2 in and above the ABL typically also change over synoptic scales (5-10) days (Miralles et al., 2014). These variations are partly offset by the rapid adaptation of the short time scale processes of ABL growth to the long term variations (e.g., subsidence, soil moisture). In our results we therefore specifically isolated the effect of progressive soil moisture depletion on the land-atmosphere coupling and obtained a reasonable soil moisture depletion over the 21 days of 30-55 % in SMI. This is on the high side compared to the SMI decrease observed by Wolf et al. (2013) during a 30-day drought in Switzerland (-20 % SMI) but can be partially explained by the observed replenishment of soil moisture by precipitation, which is absent in our model. Our findings agree with Joetzjer et al. (2014) that the choice of plant water-stress response can strongly affect the dynamic simulation of soil moisture in a land-surface model.

Although our study is conceptual in nature, its results can be generalized to a large number of other models that use the same principle of coupled photosynthesis-conductance modeling, and moisture-stress induced reductions of leaf assimilation. This includes for example the version of the Integrated Forecast System built by ECMWF used in the Copernicus project (Boussetta et al., 2013). In its coupled land-surface model (CTESSEL) the stomatal conductance, and hence energy and water balance, will respond very similarly to what we have shown here to the atmospheric and surface drivers, and to errors therein. The skill of this numerical weather prediction system therefore is tied partially to the vegetation state and its response to water-stress. A similar argument can be made for Earth System Models used in coupled carbon-climate simulations (Meir et al., 2006; Friedlingstein et al., 2006; Booth et al., 2012), which instead simulate the long-term fate of vegetation and soil carbon pools

based on this L-A coupling. With the tropics as dominant region for carbon-climate feedbacks, Joetzjer et al. (2014) illustrated the effect of different drought response function on the simulation of carbon fluxes in the Amazon in one such model (ISBA). As hypothesized by Berry et al. (2010) and in agreement with our study, large effects on stomatal conductance lead to large variations in evaporation and carbon assimilation. These authors stressed the need to include drought effects on plant mortality, in addition to a better understanding of the mechanisms of drought response as is also advocated in van der Molen et al. (2011).

3.5 Conclusion

We systematically evaluated the sensitivity of a coupled land-atmosphere system to the plant water-stress response under drought conditions. Using various responses from linear (sensitive) to non-linear (insensitive) within the MXL-A- g_s model, we quantified the differences in the simulated budgets of carbon, water, and heat in the daytime ABL. The strength of our framework is that it includes the essential processes of the diurnal convective ABL coupling with the surface characteristics of low vegetation, similar to larger, more complex, and more widely used land-surface models. We use our conceptual framework to answer three research questions.

Firstly, we find that under low soil moisture conditions the use of a sensitive plant water-stress response in a land-surface model can strongly decrease the diurnal exchange of carbon and water at the surface and increase the exchange of heat. This increases ABL growth and entrainment, contributes to further warming and drying of the ABL, and shifts the dominant processes in the ABL CO_2 budget away from surface CO_2 exchange. Misspecification of this simulated water-stress response can lead to errors in simulated temperatures, a misinterpretation of observed CO_2 mole fractions, but also leads to errors in coupled land-atmosphere simulations with climate models for longer integration times (drought, heatwaves).

Secondly, during the development a dry spell, plants that are insensitive to water stress will delay atmospheric warming at the expense of a faster depletion of soil moisture. This will create a sudden switch in surface coupling strength, CO_2 mole fractions, and temperature when approaching wilting point. On the contrary, plants that are more sensitive to water-stress will immediately contribute to increased atmospheric warming by reducing evaporation to preserve soil water resources. These contrasting vegetation responses are important to model the onset of heat waves and the development of droughts in numerical weather prediction models, which are starting to rely on coupled photosynthesis-evaporation formulations for stomatal conductance.

Thirdly, we find that the nonlinear interactions between water-stress sensitivity, stomatal conductance, and atmospheric dynamics create a wide range of system responses in which

errors in initial and boundary conditions for the ABL can affect the ABL budgets of carbon, water, and heat very differently, and even non-linearly. This means that a coupled model's sensitivity to errors in simulated drought conditions can shift strongly due to underlying assumptions. This is especially relevant for models used in numerical weather prediction, and models used to simulate droughts in a future climate.

This research was funded by the Netherlands Organization for Scientific Research (NWO) through the VIDI grant number 864.08.012. We thank two anonymous reviewers for their helpful comments on the manuscript.

4

Grain yield observations constrain cropland CO₂ fluxes over Europe: method and validation

Carbon exchange over croplands plays an important role in the European carbon cycle over daily to seasonal time scales. Not only do crops occupy one eighth of the global land area, but their photosynthesis and respiration are large and affect CO₂ mole fractions at nearly every atmospheric CO₂ monitoring site. A better description of this crop carbon exchange in terrestrial biosphere models – most of which currently treat crops as unmanaged grasslands – could strongly improve their terrestrial carbon cycle. Available longterm observations of crop yield, harvest, and cultivated area allow such improvements, when combined with the new crop-modeling framework we present. This framework models the carbon fluxes of the major European crops on a 25 x 25 km grid and daily time-step. The development of this framework is twofold. Firstly, we optimize crop growth using the process-based World Food Studies (WOFOST) agricultural crop growth model. Modeled yields are downscaled to match regional crop yield observations from the Statistical Office of the European Union (EUROSTAT) by estimating a yearly regional parameter for each crop species: the yield gap factor. This optimization step allows us to better represent crop phenology, to reproduce the observed multiannual European crop yields, and to construct realistic time series of the crop carbon fluxes (gross primary production, GPP, and autotrophic respiration, R_{aut}). Secondly, we combine these GPP and R_{aut} fluxes with a soil respiration model to obtain the total ecosystem respiration (TER) and net ecosystem exchange (NEE). We assess the model's ability to represent the seasonal GPP, TER and NEE fluxes using observations at 7 European FluxNet cropland sites and compare it with the fluxes of the current terrestrial carbon cycle model of CarbonTracker Europe: the Simple Biosphere - Carnegie-Ames-Stanford Approach (SiBCASA) model. We find that the new model framework provides a detailed, realistic, and strongly observation-driven estimate of carbon exchange over European croplands. Its products will be made available to the scientific community through the ICOS Carbon Portal, and serve as a new cropland component in the CarbonTracker Europe inverse model flux estimates.

4.1 Introduction

Even though croplands occupy about 12 % of the Earth land surface (1990s estimate from Ramankutty et al., 2002), they are usually considered not to contribute to the global land carbon sink (see the neutral balance assumption in Smith et al., 2014 or Gray et al., 2014). This neutral contribution is justified by a lack of long-term carbon storage in crop biomass and in intensely used agricultural soils (Lal, 2004), in contrast to forests (Pan et al., 2011). Crop harvests are rapidly consumed, their residues are incorporated into the cropland soils, and thus most of their stored CO₂ is respired back into the atmosphere within a few years. However, seasonally, crop productivity still strongly impacts measured atmospheric CO₂ concentrations.

Croplands have a different seasonal cycle compared to natural vegetation, their seasonal CO₂ uptake being shorter in time and larger in magnitude (Corbin et al., 2010). It is thus understandable that they strongly impact measured CO₂ concentrations locally (Tolk et al., 2009). Recently, Gray et al. (2014) and Zeng et al. (2014) have also shown that the footprint of croplands can be found in the 25% increase in the seasonal amplitude of atmospheric CO₂ over remote and naturally vegetated sites. This increase can be explained by the 200% rise in crop productivity since the green revolution (Pingali, 2012), a trend that is likely to continue as roughly 9 billion people are expected to be fed by agriculture by 2050 (Roberts, 2011). Given the large impact of cropland CO₂ exchange on atmospheric CO₂ mole fractions on daily to seasonal scales, croplands CO₂ exchange must be properly represented in atmospheric CO₂ models and coupled carbon-climate models. Proper representation of this short-term cropland CO₂ exchange should furthermore help to reduce the uncertainty in inverse model estimates of the total land carbon sink, the most variable and uncertain sink of the global carbon budget (Le Quéré et al., 2015).

To model land-surface CO₂ exchange, a vast majority of terrestrial biosphere models (TBMs) use the concept of plant functional type (PFT). A good example of this approach is given by SiBCASA (Schaefer et al., 2008), a model that has been used in studies of atmospheric CO₂ (Alden et al., 2016; Peters et al., 2010), CO₂ isotopes (van der Velde et al., 2014), and carbon-climate interactions (Hope and Schaefer, 2015; Richardson et al., 2011). TBMs with PFTs simplify croplands as unmanaged grassland in a unique PFT, or go as far as separating it into two types for C₃ and C₄ photosynthesis (e.g. the ORCHIDEE model in Krinner et al., 2005). Over croplands, all PFT models neglect the effect of key processes such as crop phenology (the timing of crop maturation), crop management (tillage, irrigation, fertilization, etc), or the lateral transport of carbon after the harvest. The absence of key crop growth processes in TBMs can sometimes be remedied with data assimilation. For instance in past studies, crop phenology has been constrained with the assimilation of remotely-sensed NDVI, although such data contains large uncertainties (Lokupitiya et al., 2009). But crop

processes that cannot be replaced by data assimilation need to be modeled. This is why agricultural crop growth models, which were developed to represent species-dependent crop growth processes, become a good alternative to classical TBMs for modeling cropland CO₂ exchange.

In this study, we aim at improving the representation of the diurnal to seasonal cropland CO₂ exchange in the SiBCASA model. Contrarily to Lokupitiya et al. (2009), our strategy is not to add processes to SiBCASA to create a better cropland PFT, but to replace it entirely with a specialized agricultural model, WOFOST-WLP (Supit et al., 1994). This crop growth model computes the daily water-limited photosynthesis and respiration fluxes, crop phenology, and crop yield. We combine it with a soil respiration model that depends on temperature to obtain the net surface CO₂ exchange over croplands. We then assimilate European grain yield observations (EUROSTAT 2015) to constrain crop productivity from the modeled water-limited to the actual crop production level. By optimizing crop growth, we attempt to bridge the gap between model and observed crop productivity that is due to the non-modeled processes (here: fertilization, pests and diseases). To our knowledge, we become the first to use the readily available grain yield stream of data to constrain a model for cropland net CO₂ exchange, useful to the biogeosciences and atmospheric sciences. Our modeling framework makes moreover use of a complete database for European crop calendars, crop species, and a detailed European soil map (Boogaard et al., 2013). It is operational for the European domain, for the ten most-grown crop species, and has a spatial resolution of 25 km.

We use our novel model-data integration framework, which we name WOFOST-opt, to address three research questions:

1. How well does our framework capture the diurnal to seasonal cropland productivity and respiration over the European domain?
2. To what extent does the integration of yield data constrain the net cropland CO₂ exchange?
3. Can our framework capture the spatial and temporal patterns of cropland net CO₂ exchange during agricultural droughts?

With these research questions, we thus address the performance of our framework under normal to water-limiting conditions. We first answer research questions 1 and 2 by comparing our CO₂ exchange product to independent observations from the FluxNet community (Baldocchi et al., 2001) and to model estimates by SiBCASA, at 6 cropland sites across Europe located within three contrasting climate zones. We then answer our third research question by modeling the total cropland CO₂ exchange during the 2005 drought over the Iberian peninsula, and by analyzing the effect of water-stress on the net cropland CO₂ exchange. Doing this, we demonstrate the capacity of our methodology to produce high-resolution hindcasts of cropland CO₂ exchange, which can be used as boundary conditions in atmospheric models.

4.2 Model description

4.2.1 Crop photosynthesis and respiration

We use the WO^rld FO^od ST^udies water-limited production model (WOFOST-WLP) version 7.1 to represent the crop gross primary production (GPP) and autotrophic respiration (R_{aut}) during the growing season. WOFOST is an agricultural crop growth model from the Wageningen school of models (Supit et al., 1994; van Ittersum et al., 2003). Its original purpose is to compute the accumulation of carbon inside the grains or storage organs of the plant. To do this, WOFOST models the crop CO₂ exchange with the atmosphere on a daily time step. The atmosphere is treated here as a boundary condition, as six daily weather variables (the incoming short-wave radiation, minimum and maximum air temperature, atmospheric vapor pressure, precipitation, and wind speed) are provided as input to the crop photosynthesis and respiration models (see Sect. 4.3.1).

WOFOST calculates the instantaneous gross assimilation rate of a leaf layer ($A_l(z, t)$, in kgCO₂ ha_{leaf}⁻¹ hr⁻¹) using a two big-leaf light-use efficiency approach:

$$\begin{aligned} A_{sha}(z, t) &= A_m \left(1 - e^{-\varepsilon \frac{PAR_{a,sha}}{A_m}} \right), \\ A_{sun}(z, t) &= A_m \left\{ 1 - \frac{(A_m - A_{sha})}{\varepsilon \times PAR_{a,sun}} \times \left(1 - e^{-\varepsilon \frac{PAR_{a,sun}}{A_m}} \right) \right\}, \\ A_l(z, t) &= f_{sun} A_{sun} + (1 - f_{sun}) A_{sha}, \end{aligned} \quad (4.1)$$

with A_{sha} and A_{sun} respectively the instantaneous gross assimilation rates of shaded and sunlit leaves, A_m the maximum leaf assimilation rate at light saturation that is dependent on the air temperature and the development stage of the crop, ε the light-use efficiency in kgCO₂ ha_{leaf}⁻¹ hr⁻¹ / (W m⁻²), $PAR_{a,sha}$ and $PAR_{a,sun}$ the amount of photosynthetically active radiation absorbed by respectively the shaded and the sunlit part of the leaf layer in W m⁻², and f_{sun} the fraction of sunlit leaf area. Within the canopy, A_l varies along height due to the extinction of light caused by the leaves self-shading, and along time following the diurnal course of radiation and temperature. We upscale A_l to its canopy level (A_c , in kgCO₂ ha_{ground}⁻¹ hr⁻¹) with a Gaussian integration (Scheid, 1968) of A_l over three leaf layers:

$$A_c(t) = \int_{z=0}^{z_{top}} A_l(z, t) dz \approx LAI \times \frac{A_l(z_0, t) + 1.6 A_l(z_1, t) + A_l(z_2, t)}{3.6}, \quad (4.2)$$

with LAI the leaf area index in ha_{leaf} ha_{ground}⁻¹. We then compute the daily potential canopy GPP (GPP_p , in kgCO₂ ha_{ground}⁻¹ d⁻¹) with the same Gaussian integration approach over three

points in time:

$$\text{GPP}_p = \int_{t=\text{sunrise}}^{t=\text{sunset}} A_c(t) dt \approx l_{\text{day}} \times \frac{A_c(t_0) + 1.6A_c(t_1) + A_c(t_2)}{3.6}, \quad (4.3)$$

with l_{day} the daylength in hours. We then account for the effect of water-stress and all other limitations to growth (e.g. weeds, pests, diseases) by multiplying GPP_p with two empirical factors: (a) a water-stress factor (f_{stress}) that varies in time following the amount of available soil moisture, and (b) a fixed yearly yield gap factor (f_{gap}) that is based on observations of crop yields, and that allows us to regulate the modeled crop production further down to its actual level. We obtain the actual canopy GPP (in $\text{g}_C \text{ m}^{-2} \text{ d}^{-1}$) with the following expression:

$$\text{GPP} = \text{GPP}_p \times C_e \times f_{\text{stress}} \times f_{\text{gap}}, \quad (4.4)$$

with C_e the conversion factor of $\text{kg}_{\text{CO}_2} \text{ ha}^{-1}$ to $\text{g}_C \text{ m}^{-2}$, and both f_{stress} and f_{gap} dimensionless and ranging from 0 to 1. We explain the computation of f_{stress} and f_{gap} respectively in Sect. 4.2.2 and 4.3.2. When applying Eq. 4.4, it is important to realize that the yearly value of f_{gap} scales down crop growth as well as the coupled evapotranspiration, which will interact with the evolution of f_{stress} along the growing season. We will come back to this issue in the discussion.

The assimilated matter is allocated to plant organs (leaves, stems, roots and storage organs) once the autotrophic respiration (R_{aut} , in $\text{g}_C \text{ m}^{-2} \text{ d}^{-1}$) has been computed (see Eq. 4.7). R_{aut} is composed of two respirations. First, maintenance respiration (R_{maint}) represents the energy cost of maintaining the plant cell structural material. Second, growth respiration (R_{grow}) is the energy cost to transform any left-over assimilates into structural plant cell material. The following expressions are used to parameterize both processes:

$$R_{\text{maint}} = R_{m,25} \times Q_{10}^{(T_{\text{air}}-25)/10}, \quad (4.5)$$

$$R_{\text{grow}} = (\text{GPP} + R_{\text{maint}}) \times (1 - r_{\text{conv}}), \quad (4.6)$$

$$R_{\text{aut}} = R_{\text{maint}} + R_{\text{grow}}, \quad (4.7)$$

with $R_{m,25}$ the reference maintenance respiration rate at 25°C in $\text{g}_C \text{ m}^{-2} \text{ d}^{-1}$, related to the size of plant carbon pools to maintain and their age, Q_{10} the relative increase in R_{maint} with each 10°C increase, T_{air} the daily mean air temperature in $^\circ\text{C}$, and r_{conv} the species-dependent conversion efficiency of carbon into dry matter.

Finally, note that carbon exchange and storage in the plant organs is computed per m^2 of ground area, which means that WOFOST is not spatially explicit. We use soil, crop and weather information at a 25 km resolution (see Sect. 4.3.1) to allow the spatial representation of crop GPP and R_{aut} .

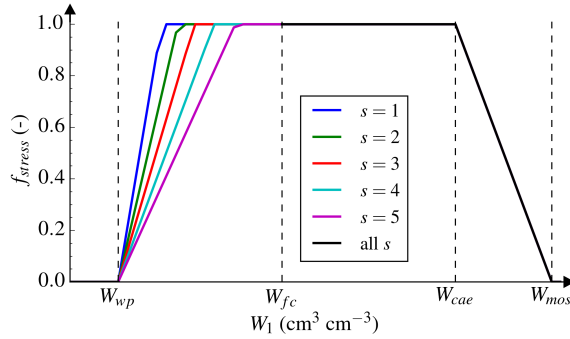


Figure 4.1 – Water-stress downscaling factor of daily GPP and transpiration. Key soil moisture contents are indicated as W_{wp} the wilting point, W_{fc} the field capacity, W_{cae} the critical point for aeration, and W_{mos} the maximum oxygen stress point. In WOFOST-WLP, crops are categorized in groups from drought-sensitive ($s = 5$) to drought-resistant ($s = 1$). Potatoes, sunflower, peas and beans are generally in crop group 3, cereals in group 4 or 5, and maize in group 5. Above field capacity, all drought sensitivity groups assume the same water-excess stress response.

4.2.2 Crop water-stress response

WOFOST-WLP is coupled to a simple soil moisture model to evaluate the effect of water-stress on crop growth (see f_{stress} in Eq. 4.4). Two soil layers are defined: (1) the upper “rooted” soil layer and (2) the lower explorable soil layer expanding down to the maximum rooting depth (a soil- and crop-dependent parameter). Note that the depth of the rooted layer (RD, in cm) increases along time as the crop roots accumulate carbon and expand downwards. To compute the crop water stress, we evaluate the volumetric soil moisture content from the upper layer (W_1 , in $\text{cm}^3 \text{cm}^{-3}$) every day as the result of the previous day’s content ($W_{1,i}$), and of the daily incoming and outgoing water fluxes (all in cm d^{-1}): precipitation (P), evapotranspiration (ET), free drainage (D) and runoff (R):

$$W_1 = W_{1,i} + \frac{P - ET - D - R}{RD} \Delta t, \quad (4.8)$$

with Δt the time step of one day. We assume here no irrigation, no capillary rise from the groundwater, and no lateral transport of water between the grid cells. For every individual crop growth run, we initialize soil moisture to be at field capacity at sowing date before allowing it to vary in time with the local incoming and outgoing fluxes of water. Every day, W_1 is used to estimate a dimensionless water-stress factor f_{stress} – shown in Fig. 4.1 – that directly downregulates daily GPP and R_{growth} . We note that under water-limited conditions (i.e. below field capacity), the type of water-stress response is dependent on the crop species.

4.2.3 Soil respiration and resulting net ecosystem exchange

To complete the CO₂ exchange budget at the surface, we use a modified version of the Lloyd and Taylor (1994) exponential function of temperature to model the instantaneous soil respiration ($R_s(t)$, in mg_{CO₂} m⁻² s⁻¹) taken from Jacobs et al. (2007a):

$$R_s(t) = R_{10} \times \exp\left(\frac{E_a}{283.15 R^*} \times \left(1 - \frac{283.15}{T_s}\right)\right), \quad (4.9)$$

with R_{10} the base respiration rate at 10°C, E_a the ecosystem sensitivity coefficient in K, R^* the universal gas constant, and T_s the upper soil layer temperature in K. In contrast to Jacobs et al. (2007a) and for practicality, we assume here no dependence of soil respiration on water stress. We use an R_{10} of 0.08 mg_{CO₂} m⁻² s⁻¹, and an E_a of 53 kJ kmol⁻¹, two reasonable values measured over grassland sites in the Netherlands (Jacobs et al., 2007b). We also replace the soil temperature with the 2-meter air temperature, assuming the error introduced by the larger diurnal amplitude of T_{air} will average out as we compute the daily total soil respiration. We finally compute the daily soil respiration (R_{soil} , in g_C m⁻² d⁻¹) by integrating R_s over a day and converting it from mg_{CO₂} to g_C with a conversion factor (C_f):

$$R_{soil} = C_f \int_{t=00:00 \text{ LT}}^{t=23:59 \text{ LT}} R_s(t) dt. \quad (4.10)$$

The total exchange of CO₂ at the surface (or net ecosystem exchange – NEE – in g_C m⁻² d⁻¹) is finally the result of all daily fluxes of photosynthesis and respiration:

$$\begin{aligned} \text{NEE} &= \text{GPP} + \text{TER}, \\ &= \text{GPP} + R_{grow} + R_{maint} + R_{het}, \end{aligned} \quad (4.11)$$

with TER the total ecosystem respiration and R_{het} the heterotrophic respiration generated by soil microbial activity. We note that in practice, the R_{10} and E_a constants from Eq. 4.10 were computed from night-time eddy-covariance NEE measurements, when no GPP and no R_{growth} occur (see Jacobs et al., 2007b). As a result, R_{soil} does not only represent R_{het} as originally intended but also the whole plant maintenance respiration, both variables dependent on the 2-meter air temperature. Since we cannot extract R_{het} from the soil respiration model and to avoid double counting R_{maint} , in this study we compute NEE by adding R_{soil} to the GPP and R_{grow} from the WOFOST-WLP model:

$$\text{NEE} = \text{GPP} + R_{grow} + R_{soil}. \quad (4.12)$$

4.3 Material and methods

4.3.1 Model input data and spatial implementation

To model crop growth, we provide three types of input data to the WOFOST-WLP model: crop parameters, soil parameters, and weather data. As mentioned earlier, WOFOST-WLP is not spatially explicit as it represents crop growth per m² of ground area. This means that the spatial resolution and domain of the model are set entirely by the input data itself. In our study, we provide the WOFOST-WLP model with spatially-varying crop and soil parameters taken from the Crop Growth Monitoring System (CGMS, see Boogaard et al., 2013). The CGMS database contains crop calendars and variety parameters for the 10 most grown crop species in Europe (wheat, barley, grain and fodder maize, sugar beet, potato, rye, rapeseed, sunflower, and field beans) on a 25 x 25 km grid. It also contains soil types information on an even finer 1:1 000 000 scale, and thus several soil types are listed in each 25 km² grid cell. The CGMS database for crop and soil parameters currently covers a large European domain, extended to Russia up to the Ural mountains, to Anatolia and to the Maghreb. For this study though, we only include regions for which EUROSTAT crop yield observations are available (see Sect. 4.3.2). Our restricted domain hence covers the 28 European Union (EU) member states, the EU candidate countries (Montenegro, Macedonia, Albania, Serbia, Kosovo, Bosnia-Herzegovina, Turkey), and the European Free-Trade Association countries (Iceland, Norway, Liechtenstein, Switzerland).

In addition to initializing the model with crop and soil parameters from the CGMS database, we provide it with weather driver data. We use the 1 x 1° ERA-Interim reanalysis weather data from the European Centre for Medium-Range Weather Forecasts (ECMWF) model (Dee et al., 2011), which we transfer onto the finer CGMS grid without downscaling. With this combination of data, we assume homogeneity of crop parameters and weather conditions over one 25 km² CGMS grid cell, but heterogeneity of soils below the 25 km scale, as several soil types are available per grid cell.

4.3.2 Crop growth optimization

The WOFOST-WLP model represents the crop potential growth in a given weather and soil environment, and its possible reduction by water-stress. The model thus neglects the impact of additional limiting factors such as nutrients, weed, pests, diseases, and other disturbances. To bridge the gap between the modeled and the actual levels of crop production, we integrate grain yield observations to optimize a crop growth scaling factor, the yield gap factor (see f_{gap} in Eq. 4.4). One optimum f_{gap} is computed per year, crop and observed region as described below. In this study, we use the observed yields from the Statistical Office of the European Union (EUROSTAT 2015). The EUROSTAT yields of all major European crop species are

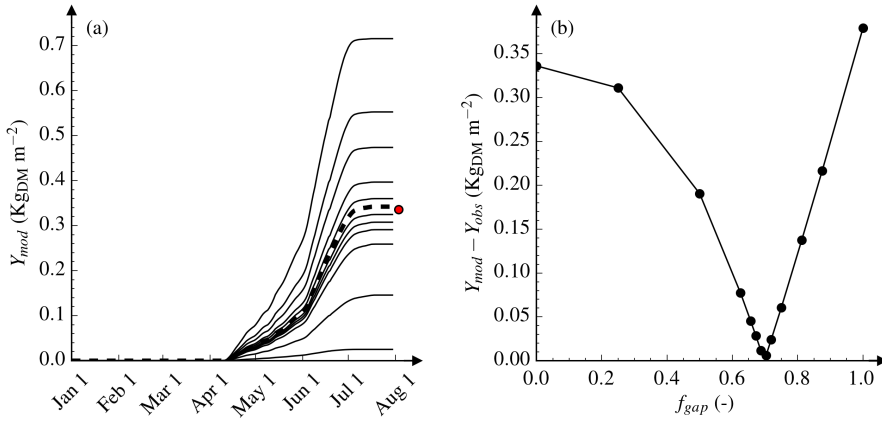


Figure 4.2 – Example optimization of the winter wheat growth in Spain, 2013. Figure 4.2a presents the evolution along time of Y_{mod} for the 13 tested values of f_{gap} . Figure 4.2b then presents the absolute $Y_{mod} - Y_{obs}$ difference for these 13 runs. We find the optimum run (thick dashed line in Fig. 4.2a) is the one that reaches the observed yield (red circle) best, resulting in the lowest $Y_{mod} - Y_{obs}$ residual in Fig. 4.2b.

reported by the EU member and candidate member states at four administrative regional levels, the so-called NUTS 0 (national) and NUTS 1, 2, and 3 (sub-national) levels. Reports of grain yields are only compulsory at the NUTS 0 level. We use the NUTS 2 records in order to obtain a higher spatial resolution on the optimized crop growth where observations are available. Otherwise in NUTS 2 regions and years where observed records are missing, we use instead the upper NUTS level records (NUTS 1 or if fails, NUTS 0) to estimate the optimum f_{gap} .

Because the EUROSTAT observations are reported on a larger scale than the model grid scale, the first step of the optimization is to aggregate the gridded yields to the same spatial resolution as the observations. For that, we execute an ensemble of 30 runs per NUTS region with the WOFOST-WLP model, for a given crop and year. This ensemble is created by selecting the top 10 grid cells containing the most arable land in a NUTS region, and the top 3 soil types that are most present within these grid cells. The modeled regional yield is then approximated by a weighted average of the 30 yields, using soil type areas as weighing factors:

$$Y_{mod} = \frac{\sum_{i=1}^{30} (a_i \times y_i)}{\sum_{i=1}^{30} a_i}, \quad (4.13)$$

with Y_{mod} the aggregated modeled yield, y_i the single run yield, and a_i the soil type area

of the same run. The difference between Y_{mod} and the reported regional yield (Y_{obs}) is then computed to determine the optimum f_{gap} . We iteratively explore 13 values of f_{gap} between 0 and 1, every time dividing its exploration range by two, and retain the optimum as the value that minimizes the absolute $Y_{mod} - Y_{obs}$ difference (see Fig. 4.2). Note that the optimum f_{gap} cannot be greater than 1. Our assumption is then that by regulating crop yield, we regulate crop growth and crop CO₂ exchange down to their actual levels. We repeat that f_{gap} is directly coupled to plant development and evapotranspiration, and therefore influences the value of f_{stress} . We evaluate our method by comparing the modeled crop CO₂ fluxes against independent observations.

4.3.3 Model Validation

Independent CO₂ flux observations

We validate the fluxes of GPP, TER, and NEE generated by the optimized WOFOST-WLP model (hereafter referred to as WOFOST-opt) with independent observations at seven FluxNet sites. These sites are located within three important climate zones of Europe: a Mediterranean (Csa), a temperate (Cfb), and a cold zone (Dfb, see Table 4.1), and they were active in various periods between 2000 and 2014. All sites measured NEE on a half-hourly basis using the eddy-covariance technique and following the FluxNet protocol. Measurements of NEE were filtered for low friction velocities using a yearly variable threshold, then gap-filled and partitioned into TER and GPP using the night-time method of Reichstein et al. (2005). More information about the crop rotation and management of the different sites can be found in appendix Table D.1. All the sites have been fully described in previous publications (see the reference papers cited in Table 4.1).

Table 4.1 – List of selected FluxNet sites. Climates were classified using the Köppen-Geiger classification from Peel et al. (2007).

Site ID	Country	Lon	Lat	Climate	NUTS 2 region	CGMS grid cell ID	Reference papers
BE-Lon	Belgium	4.74	50.55	Cfb	BE35	100094	Moureaux et al. (2006)
DE-Kli	Germany	13.52	50.89	Cfb	DED2	102119	Prescher et al. (2010)
FI-Jok	Finland	23.51	60.90	Dfb	FI1C	148139	Lohila et al. (2004)
FR-Gri	France	1.95	48.84	Cfb	FR10	94086	Loubet et al. (2011)
IT-BCi	Italy	14.96	40.52	Csa	ITF3	56126	Vitale et al. (2007)
NL-Dij	Netherlands	5.65	51.99	Cfb	NL31	107097	Jans et al. (2010)
NL-Lan	Netherlands	4.90	51.95	Cfb	NL33	106095	Moors et al. (2010)

The SiBCASA global vegetation model

We use the SiBCASA model (Schaefer et al., 2008) as our benchmark. SiBCASA is a typical example of a terrestrial biosphere model that uses the concept of plant functional types. For our study, we compute fluxes of GPP, TER, and NEE for the seven grid cells where the FluxNet sites are located, using the cropland PFT parameters. We drive SiBCASA with the $1^\circ \times 1^\circ$ soil moisture and meteorological data from the ERA-Interim reanalysis (Dee et al., 2011). We start all our runs from steady-state, which is obtained once the yearly average NEE flux equals less than 1% of the yearly average GPP flux, hence generating stable soil carbon pools over time after steady state.

4.4 Results

4.4.1 Grain yield optimization

The optimization of the crop growth scaling factor (f_{gap}) in WOFOST-opt allows us to reproduce the inter-annual variability of regional observed grain yields from EUROSTAT. The upper time series in Fig. 4.3a presents the modeled grain yields before and after optimization of f_{gap} for spring barley over the NUTS regions of Castilla y León in Spain. After optimiza-

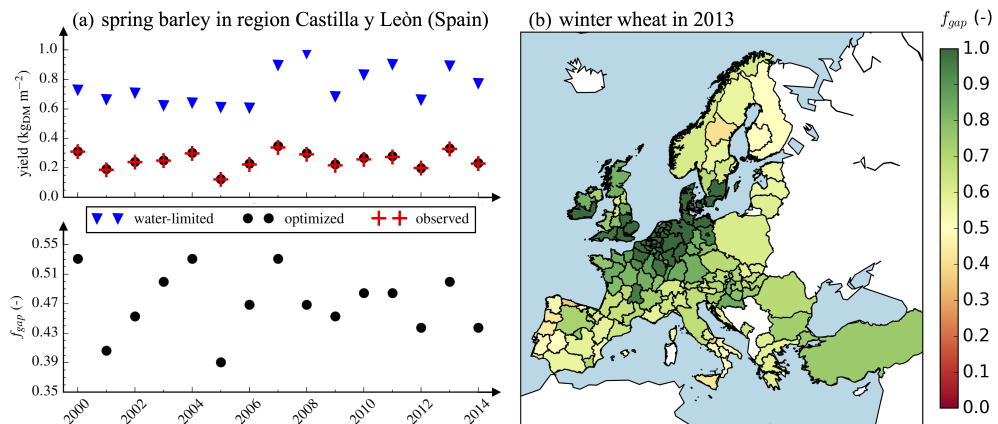


Figure 4.3 – Inter-annual and spatial variability of grain yield and f_{gap} . Figure (a) presents on top the modeled (water-limited and optimized) and the observed grain yields for the example of spring barley in the Spanish NUTS 2 region Castilla y León, and on the bottom the optimum f_{gap} values of each year. NB: the optimum f_{gap} can range from 0 to 1 and directly multiplies daily GPP throughout the season, as shown in Eq. 4.4. Figure (b) presents the spatial variability of the optimum yield gap factor for the example of winter wheat in year 2013.

tion, the remaining difference between optimized and observed yields is only about 2% on average over the years 2000-2014. In few occasions, the optimization corrects year-to-year variations of grain yield (e.g. the yield variation from 2002 to 2003 is changed from decreasing to increasing). The long-term upward trend in the observed grain yields (i.e. the linear yield increase of $+11.33 \times 10^{-4} \text{ kg}_{\text{DM}} \text{ m}^{-2} \text{ yr}^{-1}$ from 2000 to 2014) is also captured after the optimization. This trend, referred to as the technology trend by de Wit et al. (2010), can be explained by the ongoing improvements in farming techniques and industrial crop management. Note that low yields in the timeseries indicate agricultural drought years, like 2005 (confirmed in Spinoni et al., 2015), and we study this example in more detail in Sect. 4.4.4. Finally, the optimum value of f_{gap} of Fig. 4.3a ranges from 0.39 to 0.53 and demonstrates the large gap that can occur between the water-limited and the actual level of crop production.

In addition to year-to-year changes, our optimization captures a substantial spatial variability of observed grain yields and yield gap factors. Fig. 4.3b shows the optimum f_{gap} over Europe for winter wheat in 2013, the most well-covered crop at the NUTS 2 level in EUROSTAT. After optimization, the highest modeled yields and f_{gap} are in Western Europe, and the lowest are in Scandinavia and Southern Europe, which is a typical spatial pattern for wheat and barley (see also Bondeau et al., 2007). The optimum f_{gap} varies from 0.48 to 1.0 across Europe, which implies that using an average value of f_{gap} across the continent will result in significant spatial errors on the optimized yields. With the spatiotemporal variability driven by the EUROSTAT yield records, we expect our WOFOST-opt model to have well-constrained crop carbon accumulation locally, and a more reliable representation of cropland GPP, TER, and NEE over the growing season. To validate this, we analyze next the modeled crop CO₂ fluxes that lead to these optimized grain yields.

4.4.2 Daily CO₂ exchange

We find that the WOFOST-opt model represents the crop-specific growing season length (a short 2-3 months length) and magnitude of the productivity (from 10 to 30 $\text{g}_\text{C} \text{ m}^{-2} \text{ d}^{-1}$) very well above croplands. This is shown in Figures 4.4a-f for a subset of the available years and sites from the FluxNet database. Across three very different climate zones of Europe, and for six of the most grown crops in Europe (winter wheat, grain maize, spring barley, potato, sugar beet and winter rapeseed) we see the correspondence of GPP and TER to daily observations is visually satisfactory, and also clearly much better than the SiBCASA model estimates at these locations. This improvement is most evident in the phenology as WOFOST-opt matches the local growing season length, except for a small overestimation at all potato sites (e.g. 6 weeks in Fig. 4.4a). WOFOST-opt also captures the strong interspecies differences in terms of maximum GPP much better (e.g. highest is 20-30 $\text{g}_\text{C} \text{ m}^{-2} \text{ d}^{-1}$ for maize, lowest is 8-10 $\text{g}_\text{C} \text{ m}^{-2} \text{ d}^{-1}$ for barley). An exception is seen for the Italian site

where we find an overestimation of GPP by WOFOST-opt (cf. panel f), which is further discussed in Sect. 4.4.4.

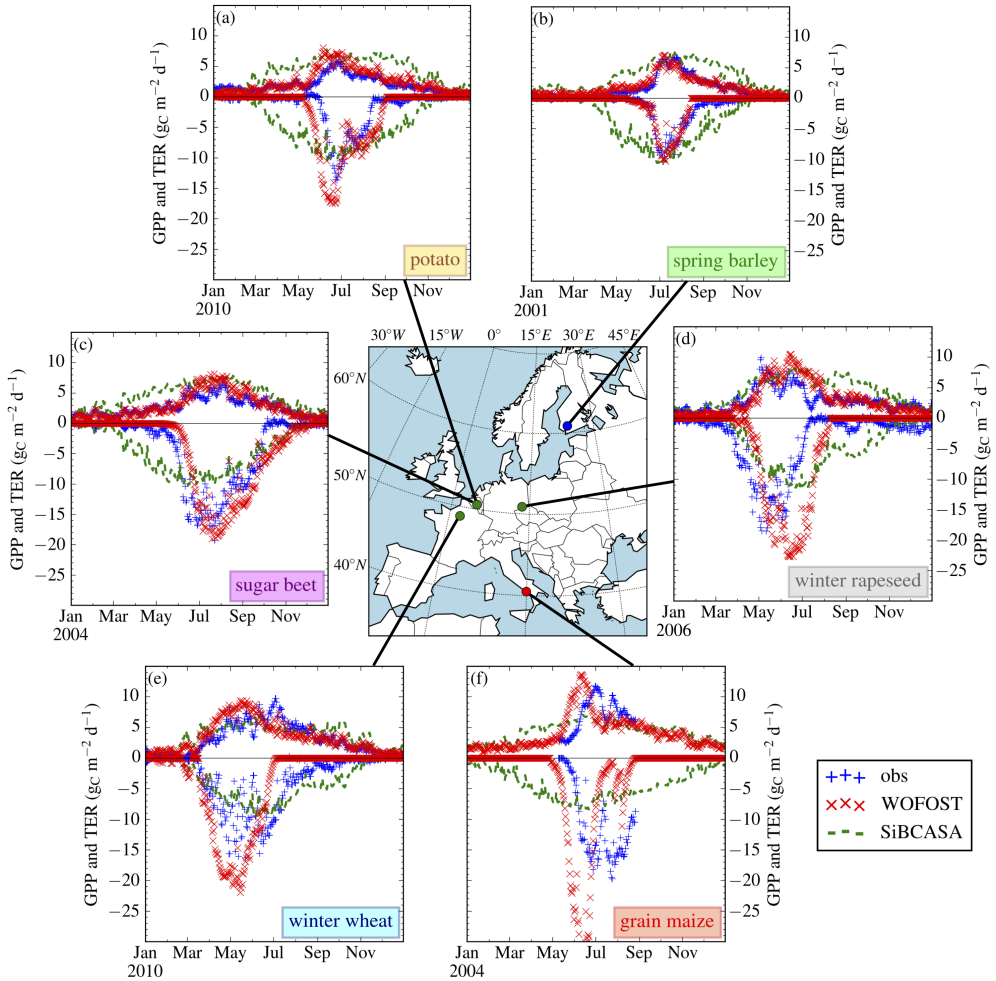


Figure 4.4 – One year of modeled and observed daily GPP and TER fluxes ($g_C m^{-2} d^{-1}$) at five FluxNet sites located in three major European climate zones: Mediterranean (IT-BCi, the red dot on the map), Temperate (BE-Lon, FR-Gri, DE-Kli, green dots), and Cold (FI-Jok, blue dot). In this figure, we present our best model match (panel b) and our worst (panel f) among all 40 campaign years we modeled (see Table D.1 on page 120).

The improved phenology and seasonal cycle of GPP and TER translates into much higher values of the coefficient of determination (R^2) for NEE for WOFOST-opt than for SiBCASA across 15 of the 17 crops and sites in Table 4.2. In terms of RMSE, the better performance

of WOFOST-opt is less obvious, partly as a result of remaining differences in the timing of the growing season, which carry a high penalty in RMSE (e.g. BE-Lon in panel a of Fig. 4.4). WOFOST-opt has a smaller RMSE than SIBCASA at 7 out of 17 crops and sites, and a smaller RMSE than the non-optimized WOFOST at 14 out of 17 (the remaining 3 showing no improvement due to a computed optimum f_{gap} of 1.0). The higher R^2 values of WOFOST-opt nevertheless demonstrates that our optimization framework, even though it is not based on observations of GPP, TER, and NEE, still improves the daily CO₂ exchange estimates at a large number of sites across Europe. This novel application of reported yield data in carbon cycle modeling thus puts new constraints on the CO₂ exchange over European cropland. To complete and extend our analysis, we demonstrate next how the crop phenology of WOFOST-opt better represents the crop rotation effects on the CO₂ exchange for the case of a well-watered location in Belgium.

4.4.3 Decadal CO₂ exchange

The WOFOST-opt model optimized with EUROSTAT grain yield data is able to represent the inter-annual variability of crop CO₂ exchange that is driven by the crop rotation on a field. This is because the crop model accounts for inter-species differences in phenology and photosynthetic rates. Figure 4.5 on page 90 compares the WOFOST-opt GPP, TER and NEE fluxes against 10 years of observations at the BE-Lon FluxNet site in Belgium. This site conserves a sugar beet / winter wheat / potato / winter wheat crop rotation from 2004 to 2014, with one exception of a grain maize year. Over this decade, we computed an optimum f_{gap} that ranges from 0.69 (in 2014) to 1 (in 2006 and 2010), using EUROSTAT crop yields. Doing so, WOFOST-opt captures the timing of local growing season and the amplitude of the GPP and TER fluxes well every year from crop to crop at site BE-Lon, although differences with the observations in terms of maximum fluxes (up to one third of the observed maximum) can be observed. Note that small shifts in the growing season not exceeding 2 weeks for this particular site can occur, the largest shift occurring in early spring 2007. Twice in this decade (in 2009 and 2013), mustard was planted after the harvest of winter wheat, just before the following winter period (see Kutsch et al., 2010). But this is a local feature that cannot be captured by our crop model, as it only represents the growth of one crop sown on site. Despite these local variations, the overall performance of the regionally optimized WOFOST-opt is high at the Belgian site, with a 10-year RMSE of 2.58 g_C m⁻² d⁻¹ for GPP and 1.21 g_C m⁻² d⁻¹ for TER, not exceeding 10 % of the max-min range of the observed respective variables, and an R^2 of 0.80 and 0.71 for GPP and TER over the decade. This translates into a NEE with a correct inter-annual pattern ($R^2 = 0.67$) as can be seen in Fig. 4.5. Finally, we note that this inter-annual variability is typically not included at all in TBMs that use the concept of PFT as they use the same cropland constants every year, which is obvious for SiBCASA in

Table 4.2 – Statistics of the NEE models when compared to our FluxNet observations: (a) SiBCASA (SIB), (b) original WOFOST (WOF), and (c) optimized WOFOST (OPT). Note that these statistics have been computed for the subset of years modeled by all models (2000-2011).

	Number of years	Climates	RMSE on NEE ($\text{gC m}^{-2} \text{d}^{-1}$)			R ² of NEE model (-)			min - max optimum f_{gap} range
			SIB	WOF	OPT	SIB	WOF	OPT	
<i>Winter wheat</i>									
BE-Lon	4	Cfb	3.77	2.90	2.32	0.38	0.78	0.75	0.69 - 1.00
DE-Kli	2	Cfb	2.33	5.74	2.42	0.53	0.21	0.64	
FR-Gri	2	Cfb	3.40	2.66	2.62	0.27	0.77	0.76	
<i>Grain maize</i>									
IT-BCi	4	Cfa	5.84	10.54	10.54	0.12	0.09	0.09	0.70 - 1.00
FR-Gri	2	Cfb	3.21	5.75	4.09	0.37	0.02	0.58	
NL-Lan	1	Cfb	2.83	6.07	4.90	0.17	0.43	0.44	
<i>Fodder Maize</i>									
IT-BCi	2	Cfa	6.31	11.96	11.96	0.23	0.30	0.30	1.00 - 1.00
DE-Kli	1	Cfb	2.66	6.28	5.57	0.10	0.21	0.67	
FR-Gri	1	Cfb	3.81	5.62	4.26	0.59	0.04	0.49	
NL-Dij	1	Cfb	5.12	5.05	5.05	0.14	0.78	0.78	
<i>Winter barley</i>									
DE-Kli	2	Cfb	3.57	4.90	2.00	0.13	0.55	0.77	0.69 - 0.73
FR-Gri	2	Cfb	3.52	8.26	2.36	0.14	0.01	0.87	
<i>Spring barley</i>									
DE-Kli	1	Cfb	1.63	6.97	2.18	0.44	0.38	0.69	0.69 - 0.70
FI-Jok	1	Dfb	1.82	1.66	0.80	0.17	0.69	0.74	
<i>Winter rapeseed</i>									
DE-Kli	2	Cfb	2.48	8.23	2.64	0.34	0.10	0.70	0.92 - 0.98
<i>Potato</i>									
BE-Lon	2	Cfb	2.07	2.79	2.79	0.31	0.30	0.30	0.69 - 1.00
<i>Sugar beet</i>									
BE-Lon	2	Cfb	4.59	2.71	2.82	0.29	0.77	0.67	0.84 - 0.86

Fig. 4.5. We conclude our model is better suited than a TBM like SiBCASA to represent the temporal variations of cropland CO₂ exchange, from the diurnal to the seasonal and decadal scales. While this is true at most locations, we find the performance of WOFOST-opt drops under extreme water-stress (e.g. in Italy, see Fig. 4.4f), which we assess next.

4.4.4 Cropland CO₂ exchange during droughts

We showed in Sect. 4.4.1 that our modeling framework is able to capture the reduced yield of reported drought years, such as over the Iberian peninsula in 2005 (see Spinoni et al., 2015). We further investigate this case as it links closely to the poorer representation of the Italian site in Fig. 4.4f and Table 4.2. For this we optimize crop growth for the top 8 crop

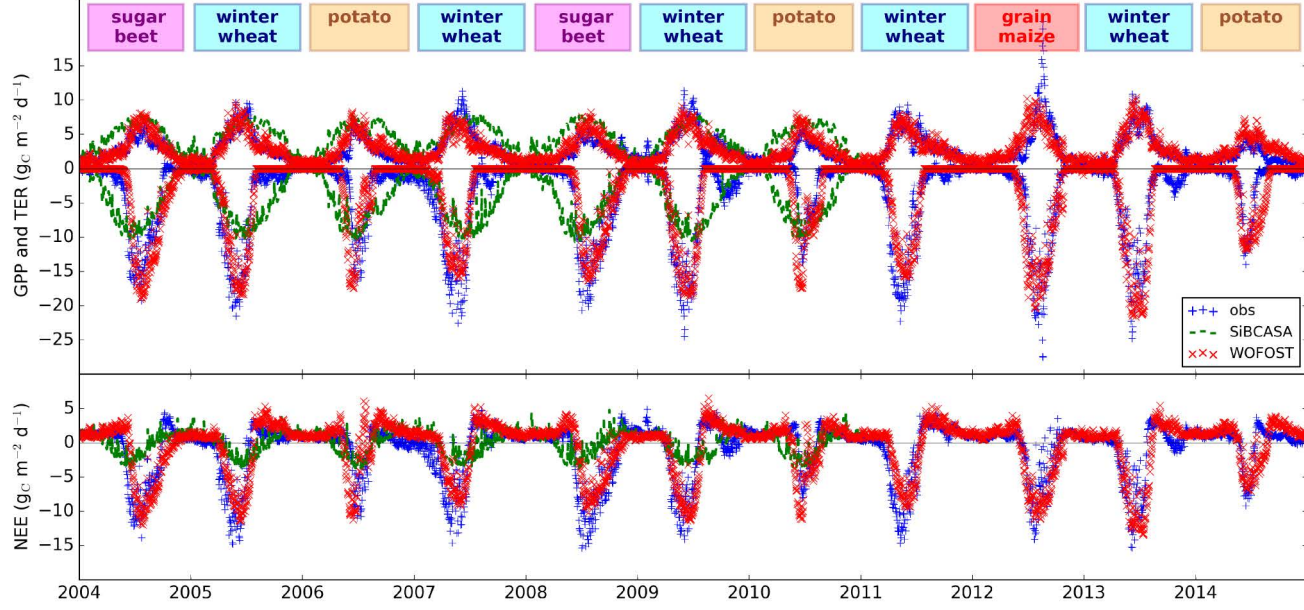


Figure 4.5 – 10 years of observed and modeled GPP, TER, NEE fluxes at the Belgian FluxNet site BE-Lon.

species of Spain and Portugal, and present in Fig. 4.6a-b on page 92 their area-weighted average NEE from April to June, for years 2004 and 2005. Over the Peninsula, the largest contribution to these NEE fluxes hence comes from (1) spring barley (42 % of the total flux), (2) winter wheat (28 %), (3) winter barley (11 %), and (4) grain maize (9 %). For both 2004 and 2005, it is not surprising to see positive NEE values over April-May-June because NEE is then the balance of a consistently high TER and of a short-lived GPP, which peak can occur outside or at the limit of this period depending on the crop species and region. When we compare panels a and b in Fig. 4.6, we see there is a rise in cropland NEE from 2004 to 2005 ($+1.04 \times 10^{-8} \text{ kg}_C \text{ m}^{-2} \text{ s}^{-1}$ on average over the Peninsula). This rise is generated by a decrease in absolute GPP of $-0.75 \times 10^{-8} \text{ kg}_C \text{ m}^{-2} \text{ s}^{-1}$ and by an increase in TER of $+0.29 \times 10^{-8} \text{ kg}_C \text{ m}^{-2} \text{ s}^{-1}$. While TER responded to the higher 2-meter air temperatures ($+0.8 \text{ K}$ in 2005), GPP was the trade-off between the maximum crop growth (controlled with the yearly f_{gap}) and the seasonal development of water stress (calculated as f_{stress}), as we show in Eq. 4.4. In 2005, the large decrease in modeled crop productivity is mostly driven by the large drop in reported EUROSTAT yields of straw cereals in Portugal and Spain, which decreased by 56 % (barley) and 42 % (wheat) from 2004 to 2005.

The forced downscaling of crop productivity with f_{gap} reduced the severity of water stress in 2005. Fig. 4.6c and d show the values of GPP and f_{stress} during the 2004 and 2005 growing seasons as modeled with WOFOST-opt (thick continuous lines). They clearly show the decrease in GPP from a maximum of 12 to 3 $\text{g}_C \text{ m}^{-2} \text{ d}^{-1}$. The larger GPP in 2004 is the likely cause for its more important water stress (f_{stress} going down to 0.2 in 2004), as a result of its higher f_{gap} (0.58) compared to in 2005 (0.39). To demonstrate the yield-imposed constraint on GPP through f_{gap} , we repeat the 2005 case imposing the 2004 value of f_{gap} . In this experiment (dotted red line) we find a strongly increasing GPP and water stress (f_{stress} drops from 0.5 to 0.2). Our findings illustrate the interaction of the carbon and water cycles, as a relatively larger crop growth depletes soil moisture faster. But a remaining question is how realistic is the less severe modeled water-stress for the reported 2005 drought year (see Sect. 4.5). We note in Fig. 4.6d that the water stress started a full month earlier in 2005 due to less cumulated precipitation, and that aspect does seem to correspond to an observed early Spring drought (Spinoni et al., 2015). Finally, it is interesting to note that in the second 2005 experiment (dashed red lines), the early and extreme water stress prevented the crop to accumulate much carbon in the grains, during the later part of the growing season. Such extreme cases make it impossible for the model to match observations.

This leads us to analyze the occurrences of such extreme water stress in 2005 over the peninsula, which can be detected with the harvest index (cf. the dark red patches in Fig 4.6e). The harvest index is the ratio of the grain to aboveground crop dry matter. When this index becomes very low (e.g. below 5 % like in the Extremadura region indicated by a star in Fig 4.6e), it indicates water stress has prevented the crop to accumulate carbon inside the

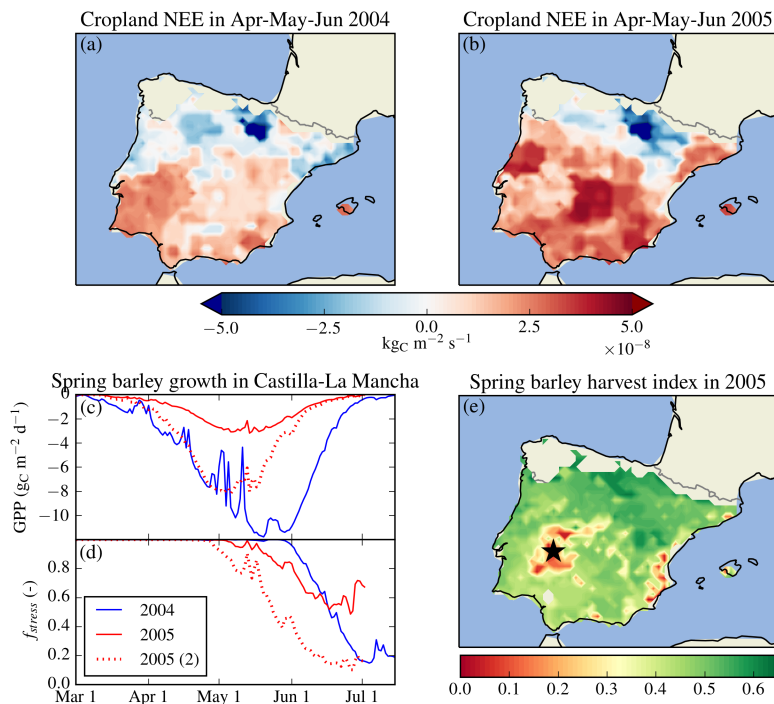


Figure 4.6 – Drought representation in the WOFOST-opt model: the case of 2005 in the Iberian peninsula. Panels (a) and (b) present the monthly average cropland NEE during April-May-June in years 2004 and 2005, showing a major drought (more positive NEE in dark red) in 2005. The displayed cropland average flux is constituted of the individual crop fluxes, with spring barley contributing to 2/5th of it. In panels (c) and (d), we thus zoom in on the 2004 and 2005 growth pattern of spring barley within a high agricultural region of the south of the peninsula (Castilla-La Mancha). The second 2005 run (index 2) uses the 2004 optimum f_{gap} (0.58) instead of the 2005 optimum (0.39) to show the impact of the optimization procedure on the drought simulation. Finally, to diagnose the severity of the early water stress in 2005 in some parts of the peninsula, we present the 2005 harvest index (i.e. grain weight over aboveground plant weight) of spring barley in panel (e). When extremely low (e.g. below 5%, see the Extremadura region indicated with a star) it indicates a critical drought stress that prevents carbon accumulation in the grains.

grains during the late growing season. This is in fact the same that occurred at the Italian FluxNet site IT-BCi, where we poorly matched GPP, TER, and NEE in Fig. 4.4f and obtained high RMSEs in Table 4.2. In these extreme stress cases, it is impossible for the model to close the yield gap between model and observations, but the model minimizes this gap (i.e. maximizes the modeled yield) by setting an optimum f_{gap} of 1. Fig. 4.4f shows that the high

f_{gap} applied throughout the year first overpredicts GPP in the early growing season, but as this leads to high evapotranspiration and enhances water stress, it then leads to the underprediction of GPP in the later water-stressed part of the growing season. These extreme water-stress cases do not seem to be very frequent in our 2005 estimates (see the proportion of red patches in Fig 4.6e). But their occurrence and the unmatched observed yields suggest that some irrigation must have taken place in reality in these locations, in order to alleviate the effects of heavy water stress that a normally developing crop would have otherwise experienced. This irrigation is currently not part of our WOFOST-opt framework, but its implementation is under discussion (see Sect. 4.5). In any case, for future use of our framework we advocate monitoring the frequency of extreme water-stress cases with the harvest index or the modeled to observed yield gap, which will inform on the quality of the simulation in drought situations.

Finally, we find the modeled reduction of crop growth is combined with a realistic shortening of the growing season under warmer conditions in 2005. For instance, we see in Fig. 4.6c that the final date of crop growth (i.e. when $GPP = 0$) occurs on average 14 days earlier than in 2004 in region Castilla-La Mancha for spring barley. We find this to be true for other cereal crops (e.g. -8 and -7 days for respectively winter wheat and winter barley in Castilla-La Mancha) and for other regions in Spain, although the magnitude of the shortening differs between the species and regions. This change in growing season length can be explained by the faster maturation of the crops during the warmer year of 2005, as we assume the sowing dates to be fixed from year to year. This shortening of the season concurs with the combined downscaling of f_{gap} and f_{stress} to reduce the accumulation of carbon inside the crop.

4.5 Discussion

4.5.1 Performance and limits of the framework

While croplands are by definition a homogeneous land surface at the crop field scale, it is not true between the crop field and our sub-grid scale (i.e. 25 km scale). To account for the sub-grid variability of cultivated crop species, we apply a “mosaic” approach where we compute each crop species over the spatial domain independently from each other. We then compute a cropland area-weighted average of NEE, using cultivation areas from EUROSTAT. This method is better suited to address the impact of sub-grid crop variability on the NEE fluxes than the “tiling” method (i.e. computing the fluxes from the dominant species only in each grid cell), which is for instance currently used in SiBCASA.

In our study we do not explicitly model the effects of nitrogen limitation, pests, diseases, or long-term crop breeding improvements on crop growth. These effects are likely responsible for the modeled to observed yield gaps ($Y_{obs} - Y_{mod}$). Instead, we account for these

effects with the yearly optimization of the yield gap factor, following observations of crop yield. This optimization changes the overall yearly production, but does not allow modifications of the seasonal crop growth pattern. We however do represent explicitly the effect of water stress in the model but we do not implement any intervention of the farmers to mitigate water-stress (i.e. irrigation). This assumption is clearly unrealistic for Southern regions like the Mediterranean where irrigation is needed and frequent (Wriedt et al., 2009a) and it almost certainly leads to more occurrences of water stress in our model. Possible misrepresentations of the seasonal cycle of NEE could hence partly be avoided by either developing irrigation rules within the model (e.g. trigger irrigation once soil moisture reaches a given threshold, as done by de Noblet-Ducoudré et al., 2004) or by supplying full irrigation information (cf. the high-resolution European irrigation map from Wriedt et al., 2009b). Moreover with the current setup of our framework, we do not perform a continuous simulation of soil moisture. Instead, we simply initialize it to be at field capacity every year at sowing date. This “wet soil” assumption is unrealistic for the dry regions of Europe such as the Mediterranean, especially for the case of spring crops that are sown later in the year, as we could be neglecting important soil moisture depletion happening before the start of the growing season. We can solve this issue by using soil moisture data – for instance the ERA-Interim re-analysis product (Dee et al., 2011) or perhaps remotely-sensed data like in de Wit and Van Diepen (2007) – to initialize our model.

The WOFOST model has been extensively used for research on crop yield and yield gap all over the world, notably in Europe (Bussay et al., 2015; Kogan et al., 2013; Eitzinger et al., 2013; Foltescu, 2000), Africa (Wolf et al., 2015; Bregaglio et al., 2014; Kassie et al., 2014), Middle-East (Sargordi et al., 2013), India (Dua et al., 2013), and China (Wang et al., 2011). However, to our knowledge we are the first to use WOFOST to estimate surface carbon exchange fluxes, and to verify these against observations of GPP, TER and NEE. Related to our first research question, we show the WOFOST-opt model to be a good match to the observed GPP, TER and NEE at the seven FluxNet sites, which we demonstrate with high R^2 values. Interestingly, we find lower RMSEs are obtained for TER (with an RMSE of $1.8 \text{ g}_C \text{ m}^{-2} \text{ d}^{-1}$ over all 40 years of Table D.1, about 8 % the observed min-max range for TER) than for GPP and NEE (respectively 5.0 and $3.9 \text{ g}_C \text{ m}^{-2} \text{ d}^{-1}$, about 16-17 % the observed min-max range of both variables) indicating that most of the efforts to further improve NEE should be done on improving GPP. We verified that lower RMSEs are obtained for NEE by imposing local sowing dates in the simulations of the FluxNet sites (from 3.9 to $3.2 \text{ g}_C \text{ m}^{-2} \text{ d}^{-1}$, or from 17 % to 13 % of the observed min-max range of NEE), because these effectively remove the shift in the modelled growing season as seen e.g. in Fig. 4.4 (not shown here). Our findings indicate that our framework represents the average regional NEE fluxes of croplands, rather than a point-location estimate of it. Finally, detailed features like the impact of cover crops, grass regrowth after harvest (e.g. winter wheat in 2009 and 2013 in Fig. 4.5, as described by

Kutsch et al., 2010) cannot be represented with our setup, confirming that we are modeling the average seasonal behavior of the dominant crop on field. In the end, we conclude the more realistic seasonal patterns obtained by WOFOST-opt are a clear improvement compared to the SiBCASA approach.

Related to our second research question, we show that the additional integration of crop yield data into the model produces large spatial variations in the f_{gap} scaling factor, which effectively increases the spatial variability of the modeled cropland GPP and NEE towards reported levels (see European crop productivity patterns in Bondeau et al., 2007). At a number of FluxNet sites in Table 4.2, we observe a systematic improvement of the RMSE and R^2 of NEE when switching from the non-optimized to the optimized version of the WOFOST model, with the one exception of sugar beet. Moreover, the RMSE of WOFOST-opt is not systematically lower than the one of SiBCASA because of two factors: (a) the remaining shift in the growing season between WOFOST-opt and observations and (b) the Western-Europe location of the sites, where mostly high yield gap factors occur (they are always greater than 0.7, and often close to 1, see Table 4.2). Larger improvements are to be expected for regions with higher $Y_{obs} - Y_{mod}$ differences, such as in Scandinavia and the Mediterranean basin (see the spatial pattern of f_{gap} in Fig. 4.3b). While we show it is true for the Finnish site (see Table 4.2), we did not demonstrate this for the Italian site since we did not take into account the irrigation practices that occurred there. As a result we obtained a substantially different seasonal cycle from reality, which was also switched earlier in time due to an earlier modeled sowing date (see Fig. 4.4f).

Finally, and related to our third research question, we allow for the regional constraint of GPP, TER and NEE by crop yield observations, which to a certain extent constrains the spatial variability of the carbon fluxes. By extension of Fig. 4.3b, where we present the yield gap factor map for year 2013, we find that the winter wheat growth will be downscaled much more in the South and in Scandinavia, where the lowest grain yields are observed. This downscaling pattern is also the case for other cereal crops: maize, barley (not shown here). This explains part of the overall cropland NEE spatial variations, as most of the summer crop carbon uptake occurs over Western to Central Europe, in the mid-latitudes. Moreover and for water-stressed situations, in Sect. 4.4.4 we demonstrated our framework can capture the year-to-year regional reduction in NEE caused by an agricultural drought, with some limitations on the realism of its seasonal cycle. However, improvements in the soil moisture initialization and the added representation of irrigation should remedy these limitations in water-stressed areas. Further validation of the drought response of the model could then be done by investigating the FluxNet soil moisture and evapotranspiration observations alongside the NEE measurements, where available.

4.5.2 Potential applications of WOFOST-opt

Our successful validation of modeled European cropland NEE fluxes therefore opens up new possibilities for the application of WOFOST-opt in the field of carbon cycle studies, crop forecasts, land-atmosphere interactions and coupled carbon-climate experiments. First, in an uncoupled mode, WOFOST-opt can supply satisfactory past, present, and once modified as suggested in Sect. 4.5.1, satisfactory future NEE boundary fluxes for atmospheric CO₂ studies. For instance, we show WOFOST-opt performs much better than SiBCASA when modeling GPP, TER and NEE, the latter having no crop rotation and thus little inter-annual variability. Our model thus offers an excellent alternative for croplands in the CarbonTracker inverse modelling framework of Peters et al. (2010). The use of the WOFOST-opt model would allow us to integrate an additional stream of data into the atmospheric CO₂ inversions. As a fixed prior flux, it could allow to reduce the uncertainty on the posterior NEE estimates of other biomes, such as forest and grassland. Such analysis of the impact of WOFOST-opt fluxes is scheduled in a follow-up study.

Crop scientists have already widely explored the possibility to use WOFOST in an uncoupled crop and atmosphere setup for operational seasonal crop yield forecasts (e.g. Bussay et al., 2015; de Wit and Van Diepen, 2007), and on the longer term for crop production projections under climate change (e.g. Tao et al., 2016; Peltonen-Sainio et al., 2015). A more interesting perspective for atmospheric scientists and hydrologists though is the possibility to fully couple the WOFOST-opt model with an atmospheric model, like has been attempted by Li et al. (2013). WOFOST-opt seems to be an adequate candidate for such a coupled study because, contrarily to other models from the same line that use the evaporative demand approach (e.g. see GECROS in Combe et al., 2015), its implementation of water stress resembles the simple approach adopted by many land-surface models (Camargo and Kemnani, 2016; Combe et al., 2016). Using a WOFOST-like parameterization of water-stress should yield a realistic evapotranspiration and resulting energy partitioning at the surface under water-limited conditions, like has been demonstrated by Li et al. (2013). The setup would further allow users to investigate crop-atmosphere interactions, to study the interaction of crop production and drought development, and on the longer term to perform coupled carbon-climate simulations to predict crop production under future climate scenarios.

4.6 Conclusion

In this study, we design a crop growth modeling framework in which we assimilate European grain yield data information to constrain a model for cropland net ecosystem exchange. This cropland model is composed of two parts: (1) an agricultural crop growth model and (2) a soil respiration model. The European crop calendars and crop varieties database on which the

model relies is maintained and regularly updated by a leading crop sciences research centre (the JRC in Ispra, Italy) to provide crop yield forecasts to the European community. Our modeling framework is readily operational for the European domain, for its 10 most common crop species, at the 25 km scale. We assess its performance over Europe from 2000 to 2014, from wet to water-limited soil conditions.

We find this modeling framework allows us to generate satisfactory daily to multi-annual hindcasts of cropland GPP, TER and NEE under normal to mild water stress conditions, for various crop species and climates of Europe. We quantify this improvement by computing correlation statistics on the daily CO₂ fluxes, and comparing our framework to observations performed at seven FluxNet sites. Under severe water-stress like for the 2005 Iberian peninsula drought, we find the trade-off between crop growth and soil moisture depletion is largely constrained by our optimization procedure, which we show artificially modifies the shape of the seasonal cycle of NEE, although its inter-annual variability seems reasonable. This alteration of the seasonal cycle could be remedied by providing better estimates of soil moisture at sowing dates and by supplying irrigation information to the model. Further validation of our improved representation of soil moisture could then be done by assessing the FluxNet soil moisture and evapotranspiration measurements in combination to the NEE fluxes, at the dry cropland sites where they are both available.

In the end, our novel framework shows promise as an inexpensive solution to provide realistic cropland CO₂ fluxes to atmospheric models. The cropland fluxes computed with our optimized product will be made available to the scientific community through the ICOS Carbon Portal. In the near future, we plan to use it in a forward modeling study of atmospheric CO₂ to demonstrate the improvement it can bring on modeled atmospheric CO₂ mole fractions. We also plan to use it in an inverse modeling study of atmospheric CO₂, to assess if we can reduce the uncertainty on the terrestrial net carbon sink by adding a more accurate estimation of the crop fingerprint on the atmosphere.

This research was funded by the Netherlands Organization for Scientific Research (NWO) through the VIDI grant number 864.08.012. This research was also supported by a grant for computing time (SH-312-14) from the Netherlands Organization for Scientific Research (NWO). We thank Hendrik Boogaard and the Joint Research Centre (JRC) for granting us access to the European crop and soil input datasets of the European Commission's Crop Growth Monitoring System (CGMS). We also want to thank the FluxNet community for giving free access to their Tier 1 dataset. In particular, we want to acknowledge the help from Cor Jacobs, Wilma Jans, Eddy Moors, Thomas Grünwald, Benjamin Loubet, Nicolas Mascher, Tanguy Manise, Marc Aubinet, Pauline Buysse, Anne Deligne, and Vincenzo Magliulo, who all answered our call and provided their help for understanding the measurements.

5

Discussion and outlook

In this thesis, we question the representation of CO₂ exchange over croplands in land-surface models. We repeat here the major findings from Chapters 2 to 4, organizing them in three overarching topics: (1) the drought response of crops, (2) cropland-atmosphere interactions, and (3) the atmospheric CO₂ budget over croplands. Keeping in mind the relevant processes we presented in the general introduction, we discuss these findings from the daily to the seasonal and multi-annual time scales. Then, we examine their robustness at the European scale. Finally, this leads us to consider possible research directions for the future.

5.1 On the water-stress response of crops

With the current climate change, extreme events such as droughts are expected to become stronger and more frequent (Hartmann et al., 2013; Seneviratne et al., 2012). The most immediate impact of a deficit in soil moisture on the vegetation is the instantaneous reduction of photosynthesis and evapotranspiration. As measured by Tardieu and Simonneau (1998) though, plants respond to soil water stress differently depending on their species, genotype or even geographical location. In this thesis, we focus on the representation of this plant water-stress response in land-surface models, for the mid-latitudes. We first find in Chapter 2 that the evaporative demand approach – used for instance in the GECROS crop growth model – does not allow for a proper representation of the variety of plant water-stress responses, because it downregulates plant fluxes only when soil moisture drops close to wilting point. This leads to unrealistically high photosynthesis and transpiration under mild to strong water-stress conditions. Other models that represent the water-stress response with a downscaling factor that is a function of soil moisture are more flexible, as we illustrate in Chapter 3.

The representation of plant water stress in land-surface models has consequences on the longer timescales predominantly through its coupling with soil moisture, as observed by Teuling et al. (2010) and Miralles et al. (2014). They found that the resulting variation in soil water consumption may have an impact on the development of droughts and heat waves. Our anal-

ysis in Chapter 3 confirms these results and establishes a firm framework to investigate the atmospheric response to the modeled plant water-stress response. With a numerical experiment inspired by the work of van Heerwaarden and Teuling (2014) and Daly et al. (2004) and constrained by observations, we show the type of plant soil moisture management (i.e. “conservative” or “spender”) determines the speed of soil drying and the resulting atmospheric warming during droughts, with the “spender” species delaying the heat wave by two weeks in our simulation. This implies the natural variability of plant water stress responses ought to be represented in weather and climate models to allow for correct drought and heat wave predictions.

At the seasonal scale, and more specifically for croplands, water and other stresses can affect crop growth and ultimately reduce crop yields. As explained by van Ittersum et al. (2003), most crop models represent the potential crop growth (i.e. maximum growth given the climate, soil type, and crop species) and the added effect of soil moisture and/or nutrient stresses, but do not account for other limitations like pests, diseases, weeds, or pollutants. In Chapter 4, we present a novel framework that assimilates European crop yield data to implicitly account for these missing processes and regulate crop productivity down to its actual level. We find that while we can implicitly represent the effect of additional stresses on crop growth at the regional scale, it may modify the development of water stress in the model to an unrealistic extent in the event of an agricultural drought (i.e. when the reported yields were affected by water-stress). Our finding stresses the interactions that exist between crop growth and water consumption (Farré and Faci, 2006). It shows the need for further validation of our soil moisture representation and crop water-stress responses. This validation requires comparison with additional measurements of soil moisture and evapotranspiration fluxes, in conjunction with the carbon fluxes we used in Chapter 4.

Finally, at the seasonal to multi-annual scale, crop management mitigates the impact of water stress on crop yields. For instance, irrigation is widely used over cereals (e.g. maize, wheat, barley) and root crops (e.g. potato, sugar beet) in dry regions such as the Mediterranean (Wriedt et al., 2009a; EUROSTAT 2015), but also other more local practices like replanting after a crop failure, choosing a more drought-resistant crop cultivar, or modifying the crop rotation entirely, are in reality used to alleviate severe water stress effects on crop productivity (Frank et al., 2015). However, the impact of practices like irrigation are rarely integrated in climate models (Rosenzweig et al., 2013). In Chapter 4 we confirm that the misrepresentation of irrigation practices leads to the over prediction of cropland water stress. Since crops occupy a large area in Europe (i.e. 20 % of the European land), we hypothesize that this misrepresentation possibly leads to the overprediction of droughts in Europe in the state-of-the-art climate models mentioned by Rosenzweig et al. (2013).

InfoBox 5.1 – Warming feedback on crop maturation under water-stress

We use a coupled land-atmosphere model (MXL-A-g_s, see Chapters 2 and 3) to show the vegetation control on the ABL temperature and its feedback on crop maturation along the season. For this purpose, we have introduced one additional equation in the model: a diagnostic crop development rate (i.e. the daily rate at which the crop matures, dimensionless variable between 0 and 1). This rate is a function of the 2-meter air temperature, and its formulation was taken from the GECROS crop growth model (see Chapter 2).

We first model a base case that reproduces observations above a grown maize field during a sunny summer day in the Netherlands (see setup in Chapter 2). We then explore other days of the growing season (x-axes) and possible soil moisture contents from the completely dry to wet soil (y-axes of the color figures). As MXL-A-g_s cannot run through nighttime or model carbon pools and phenology, we can only artificially represent the evolution of a growing season on the x-axis. We do so by repeating the base case over and over, changing only 5 initial conditions related to temperature, solar radiation, and crop cover. The values for the initial potential temperature and the maximum incoming solar radiation follow an average seasonal cycle, which we computed with measurements from a nearby meteorological station of the Dutch crop site. And the values for the initial leaf area index, initial vegetation cover fraction, and surface albedo follow observations from the Dutch crop site itself.

With this simple experiment, we find the plant control on the surface exchange starts when LAI becomes high (i.e. after DOY 180, right-half of panel a). In this second half of the growing season, a larger soil moisture deficit (i.e. going from point A to point B in the figure) clearly decreases the stomatal conductance (g_s , contour lines in panel a). This stomatal closure reduces evapotranspiration and increases the amount of sensible heat release (contours in panel b), which stimulates ABL growth (colors in panel b). This results in a warmer ABL at the end of the day (contours in panel c) and it increases the speed of crop maturation (colors in panel c).

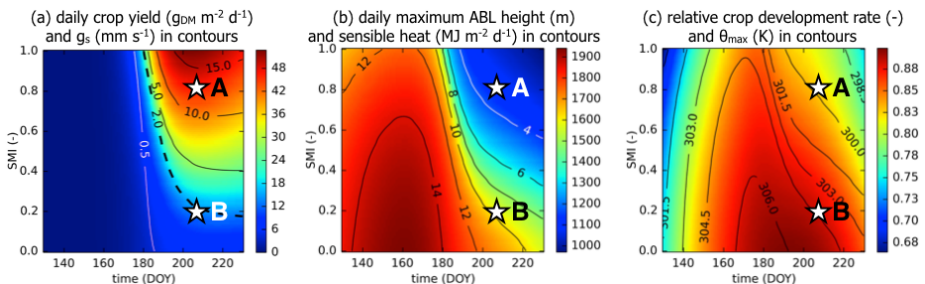


Figure 5.1 – Sensitivity analysis of the land-atmosphere interactions to the soil moisture index (SMI) and to the day of the year (DOY).

5.2 On the coupling of cropland and atmosphere

Over an active vegetated surface (i.e. during the growing season), the diurnal exchange of water and CO₂ occurs through the same exchange point: the stomata (i.e. plant openings at the leaf surface). The size of these openings is dynamically regulated by plants, as a response to various environmental factors such as light, temperature, and vapor pressure deficit. In this thesis, we put emphasis on soil moisture, which is a major controlling factor of stomatal aperture and land-atmosphere interactions under water-limited conditions (Koster et al., 2015; Seneviratne et al., 2010). Under water stress, the plant closes its stomata and decreases photosynthesis and transpiration. This shifts the surface energy balance towards more sensible heat release, which stimulates the boundary-layer growth and the entrainment of air into the atmospheric boundary layer (ABL). As such, a weaker coupling (i.e. high water and carbon exchange) at the surface generates a stronger exchange (i.e. entrainment of moisture and carbon) at top of the ABL, and vice versa. In Chapter 2, but also at the beginning of Chapter 3, we confirm this complementarity of surface exchange vs. upper-atmosphere exchange of carbon and water when soil moisture is limiting.

Over several days up to 2-3 weeks without precipitation, the building soil moisture deficit created by evapotranspiration increase the magnitude of ABL growth and entrainment over time, and exposes plants more and more to warmer and dryer conditions (Miralles et al., 2014). We confirm this in Chapter 3, and demonstrate this exposure creates a positive soil drying feedback. We show an increase in soil moisture deficit leads to a warming of the ABL, which stimulates evapotranspiration and contributes to further soil moisture depletion. Furthermore, we show that the build-up of subsidence that is characteristic of stationary high pressure systems during droughts intensifies ABL warming and increases the speed of soil moisture depletion, indicating a self-enhancing drought mechanism.

The season's precipitation history is key in explaining the development of a heat wave, as it cumulates into soil moisture deficit (Whan et al., 2015; Mueller and Seneviratne, 2012). More specifically for crops, this history and related warming events are particularly important for the speed of crop maturation, since maturation is a function of temperature sums. We illustrate this in a simplified experiment in Box 5.1, where we show that once the crop cover is high, a drastic reduction in available soil moisture (e.g. from SMI 0.7 to 0.2) can lead the surface to warm up the atmosphere by an extra 3K during a day, which leads to a 5% faster crop maturation. Since crops have stable sowing dates, the acceleration of maturation during dry years reduces the length of their growing season, contrarily to natural vegetation where the season could be shifted earlier (Wolf et al., 2016). We confirm this in Chapter 4 for the example of the Iberian peninsula drought of 2005, where we show a shortening of the cereals growing season by 1 to 2 weeks due to a spatially- and yearly-averaged warming of +0.8 K. Our findings all stress the coupling of the carbon and the water cycle, and the

land-atmosphere interactions that determine phenology at the seasonal scale.

5.3 On the atmospheric CO₂ budget over croplands

When interpreting measurements of CO₂ mole fractions, a lot of emphasis is usually being put on the importance of surface exchange. However in this thesis, we aim at emphasizing the significant role of upper-atmospheric conditions in the ABL CO₂ budget, from the diurnal to the synoptic scales. In Chapter 2 we confirm findings from Pino et al. (2012) and McGrath-Spangler and Denning (2010) and show that ABL growth and entrainment contribute to about half of the diurnal CO₂ tendency under mild water stress conditions. Moreover, we demonstrate in Chapter 3 that this contribution increases steeply when soil moisture deficit becomes more severe. While these findings already show the importance of upper-atmosphere conditions for the diurnal CO₂ budget, we in addition find that synoptic changes in upper-atmosphere conditions (i.e. subsidence, free-tropospheric temperature lapse rates, early-morning inversion strength) concur non-linearly to modify CO₂ mole fractions. Our findings stress the need to combine usual measurements at the surface (i.e. soil moisture, surface fluxes of carbon water and heat) to measurements of the ABL height in order to correctly interpret observed diurnal CO₂ concentrations of the ABL.

At the synoptic to seasonal scale, longer-term variations in soil moisture, phenology and large-scale atmospheric transport start playing a predominant role in the CO₂ budget (Williams et al., 2011; Casso-Torralba et al., 2008). During the year, the NEE exchange goes through a seasonal cycle driven by phenology, which is particularly short above croplands (Corbin et al., 2010). In this thesis, we focus on the impact of the net ecosystem exchange (NEE) on the CO₂ concentration at the heart of the crop growing season. As cropland NEE is of high magnitude during the growing season, its imprint can be found on the atmosphere (Tolk et al., 2009), even at remote CO₂ measurement sites (Gray et al., 2014; Zeng et al., 2014). We confirm this in Chapter 3, where we show a complete soil moisture depletion of three weeks can reduce the diurnal CO₂ drawdown by 27 ppm (or 40 %). We also confirm the importance of phenology and soil moisture at the seasonal scale in Box 5.2, where we show the large cropland spring-summer CO₂ uptake we modeled in Chapter 4 creates a widespread and large modeled CO₂ depletion of the ABL. This seasonal CO₂ depletion is larger (i.e. down to -20 ppm) compared to the one that is modeled with a standard terrestrial biosphere model. These findings and the ones from Chapter 4 all stress the importance of crop management. Sowing dates constrain the start of the seasonal CO₂ depletion by croplands, and irrigation can modify the evolution of water stress, thus altering the magnitude of ABL CO₂ depletion along the season.

InfoBox 5.2 – Crop phenology affects CO₂ mole fractions in Europe

We explore the impact of an improved representation of croplands on the atmospheric CO₂ concentration in Europe. For this purpose, we use an atmospheric transport model (WRF-Chem, Skamarock et al., 2012) to transport the 2013 land CO₂ emissions provided by the original SiBCASA terrestrial biosphere model. We then repeat this CO₂ transport experiment, this time replacing the cropland SiBCASA fluxes by our NEE product (see Chapter 4).

We find our improved representation of croplands largely affects the ABL CO₂ concentration during the growing season, with a maximum deviation from the original SiBCASA of 20 ppm. At the heart of the growing season (see Fig. 5.2), in regions where the cropland gross primary production is large (see the July GPP anomaly in map *a*) the ABL is very CO₂-depleted (map *b*). Positive July CO₂ anomalies in Spain relate to the larger cropland respiration (not shown here).

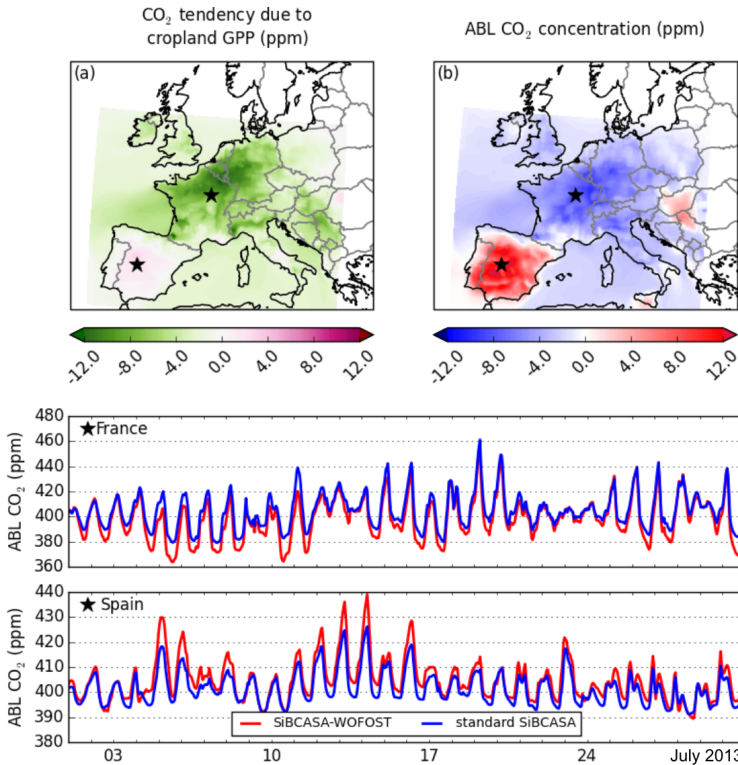


Figure 5.2 – Upper panel: July 2013 anomalies of (a) the ABL CO₂ tendency caused by cropland GPP and (b) the ABL CO₂ concentration. The anomalies are computed for the lowest level of the atmosphere as the monthly average difference of SiBCASA-WOFOST minus the standard SiBCASA. Lower panel: July 2013 time series of the ABL CO₂ concentration at the two locations marked on the maps.

5.4 Scaling our findings up to the European continent

While croplands are by definition a homogeneous land surface at the crop field scale, it is not true at the regional to continental scale on which various crop species are cultivated, each with their own timing and magnitude of seasonal CO₂ exchange. In this thesis, we focus on the impact of cropland NEE on the atmospheric CO₂ mole fractions over Europe. Terrestrial biosphere models (TBM) are commonly used to represent the spatial variability of vegetation behaviours, including croplands. However, most TBM classify plants based on their physiology into plant functional types (PFT), an approach that is known to simplify the spatial variability of vegetation processes such as phenology (Caldararu et al., 2016). In Chapter 4 we showed that there are major phenological differences between crop species or their winter and spring types. For instance, we illustrated that spring varieties of a given species (e.g. spring wheat) have the peak of their growing season much later in the year than their winter varieties (e.g. winter wheat). The approach from TBMs like SiBCASA to use only one cropland PFT to represent all crops is thus very crude, even more so as they approximate the physiology of crops as the one of grassland (see Chapter 4). Instead, we advocate the separate representation of the most grown crop species and their winter and spring type. Such modeling efforts exist, like in the SiBcrop model from (Lokupitiya et al., 2009), ORCHIDEE-STICS from de Noblet-Ducoudré et al. (2004), and LPJmL from (Bondeau et al., 2007). In the same line, in Chapter 4 we use a separate crop growth model to the SiBCASA model Schaefer et al. (2008), in order to provide continental estimates of cropland carbon fluxes. By combining WOFOST with spatially varying input data (i.e. sowing dates, temperature sum requirements) for each of the 10 crop species it can represent, we demonstrate we can very well capture crop phenology for the major species of Europe.

Another vegetation process, which spatial variability is simplified in TBMs, is the instantaneous water-stress response of vegetation (i.e. the reduction in the surface exchange of water and carbon with soil moisture). Powell et al. (2013) showed that a lot of TBMs express a fixed water-stress response across vegetation types. For the reasons outlined in Sect. 5.1, we consider crop (and more widely plant) sensitivity to water-stress to be a key factor of the land-atmosphere coupled system. As stated in research question 3, we ask ourselves the important question of how the instantaneous water-stress response (i.e. the reduction in water and carbon exchange) should be represented in land-surface and crop models. In this thesis, we demonstrate that the flexible response function introduced in Chapter 3 can reproduce the observed natural variability of plant behaviour, and could easily be implemented in a variety of land-surface models that use the same approach (e.g. CTESSEL, CLM, JULES, SiB, see Powell et al., 2013; Boussetta et al., 2013). However, such a simple parameterization of plant water-stress can only be used in global vegetation models if we can classify observed water-stress responses per vegetation type, as is done for crop species in the WOFOST model (see

Chapter 4). For now, it is unclear if that can be achieved at the continental or global scale. For instance, would one water-stress response per C_3/C_4 photosynthetic type be enough? Clearly not, as large intra-species variations can occur (see Verhoef and Egea, 2014; Tardieu and Simonneau, 1998). Then, since many TBMs classify plants in PFTs, is there really a way of assigning one response per PFT? And which one would that be? To answer these open questions, a simple further exploration of the evapotranspiration measurements of the FluxNet dataset could help for vegetation types of the mid-latitudes. Moreover, observations of the intrinsic water-use efficiency (iWUE) at the stand level (with isotopic ^{13}C measurements) or ecosystem level (with eddy-covariance measurements of carbon and water surface fluxes) can also help as water-stress responses seemed linked to iWUE (Keenan et al., 2013; Egea et al., 2011). For the purpose of our study however, where we focus on croplands in the (European) mid-latitudes, the separation of water-stress response per crop species proposed by WOFOST seems to be a reasonable approach, although it is unclear how extensive the experimental support for this classification is.

Logically, as the plant water-stress response in models is a representation of the effect of soil moisture deficit on plant fluxes, it is key to have a robust description of the soil water budget in land-surface models. Flaws in the description of soil moisture does not necessarily imply underperformance in yield prediction models because of compensating errors along the growing season (Van den Berg et al., 2002). However, these flaws are of higher importance for us because we focus on capturing the day-to-day photosynthesis and transpiration fluxes. The 1-layer “bucket” soil models that are widely applied in crop growth models like GECROS or WOFOST are one of the simplest approaches. In Chapter 4, we have pinpointed two limitations of such models in their spatial implementation, which create uncertainty in the spatio-temporal variability of cropland NEE fluxes. First of all, calculations of a crop model do not have a spin-up time, and the soil model is initialized immediately at the provided sowing or emergence date. For the spatial simulations at the continental scale of Chapter 4, we initiated each model run at field capacity. While such an assumption is realistic for the wetter part of Europe, it is probably not for dry regions such as the Mediterranean, especially for spring crops (e.g. maize) that are planted later in the year, and for which we do not account for early soil moisture depletion. Improvement of the setup could entail using better initial soil moisture content values at sowing date for instance from the ERA-Interim soil moisture re-analysis (Dee et al., 2011), or remote sensing soil moisture data, like as been done by de Wit and Van Diepen (2007) with WOFOST. Another important simplification in our soil moisture description is that we assume no irrigation. However, and as demonstrated in Chapter 4, this is not realistic and it alters the shape of the seasonal cycle of cropland NEE and the frequency of modeled water-stress in the dry Mediterranean. Using either irrigation rules within the model (like in ORCHIDEE-STICS, see de Noblet-Ducoudré et al., 2004), or irrigation information (Wriedt et al., 2009b) could remedy this simplification over croplands

and improve the model performance in the dry regions.

Finally, we would like to make a practical remark on how to better account for the sub-grid variability of plant types. TBMs can be run with two different setups: a “mosaic” or a “tiling” setup. With a mosaic setup, each PFT is modeled for all the land grid cells of the spatial domain, and an area-weighted average is then used in each grid cell to compute the final surface fluxes from the mix of PFTs. With a tiling setup on the other hand, only the dominant PFT is represented in each grid cell. In Chapter 4, we use the mosaic setup for the different crop species of WOFOST, as cultivated species can vary below the 25 km resolution of our model. For dry regions like the Mediterranean however, the mosaic approach brings additional challenges in terms of soil moisture description, since crops of a grid cell do not compete with each other. How to disaggregate soil moisture information for the evapotranspiration and irrigation of the different crops is still an open question.

5.5 Outlook

Improved seasonal cropland NEE calculations pave the way for better atmospheric inversions of the terrestrial carbon sink (see Chen et al., 2015). Inversion models basically use measurements of atmospheric CO₂ mole fractions to correct the net terrestrial CO₂ exchange modeled with a TBM, as the latter is very uncertainty. So far in the work of Peters et al. (2010), the SiBCASA model has been used to estimate the terrestrial carbon sink. In Chapter 4 we present a novel observation-driven modeling framework to improve the cropland NEE fluxes of SiBCASA, which we report to be better at simulating the seasonal cycle of daily NEE. Our framework can use grain yield observations to effectively bridge the gap between the modeled and actual level of crop production, and it is a strong alternative to the SiBCASA grassland approximation of croplands. However, before it can be used for this purpose, we must address the remaining issues that exists regarding the description of water-stress in our framework, and which entails better initialization of soil moisture and the added representation of large-scale irrigation. Then, further validation of the water cycle of our framework could be done by using the soil moisture and water surface fluxes of the FluxNet community, as we suggest in Sect. 5.1. Finally, the issue of the interaction between the optimized growth with the development of water stress needs to be re-assessed. For that purpose and similarly to the work of Peng et al. (2015), satellite sun-induced fluorescence measurements could help validate the gross primary production of our framework, which is coupled to the modeled crop transpiration.

The next logical step of our study before the inversions would be to account for the cropland CO₂ budget: the lateral transport of carbon of the crop harvest and its off-site consumption by humans and cattle. West et al. (2011) have shown the lateral transport of the harvest

can strongly modify the spatial patterns of cropland CO₂ exchange. Also, the magnitude of CO₂ respired during the consumption of the harvest in Europe has been estimated to be of similar magnitude to the carbon accumulated in forests, which shows the significance of such carbon flux (Ciais et al., 2008). In order to account for this lateral transport and consumption, we can largely inspire ourselves from the studies of West et al. (2011, 2010, 2009, 2008) over the USA and from Ciais et al. (2008, 2007) over Europe. We could similarly integrate observed import and export data for the harvest (e.g. from EUROSTAT 2015), to account for the transport between regions and in and outside Europe, and then distribute the harvest carbon where the populations are located, and assign it to be respired within a short time-window (e.g. one year). Accounting for that last part of the cropland CO₂ budget will allow us to use WOFOST fluxes in inverse simulations, as a robust and fixed prior for cropland NEE. We expect a large modification of the derived seasonal CO₂ exchange over unmanaged vegetation.

Finally, our work opens up possibilities for the field of weather predictions and coupled carbon-climate modeling. This thesis stresses the importance of cropland-atmosphere interactions that determine the diurnal CO₂ concentrations in the atmosphere. It also emphasizes the importance of the plant water-stress formulation for the interactions that lead to atmospheric heating, drying, and CO₂-depletion during dry spells. Robust coupled land-atmosphere frameworks like the one described in Chapters 2 and 3 are necessary to study and understand these interactions. Our conceptual framework offers possibilities for more research at the diurnal scale, e.g. on the interactions of plants with clouds (Vilà-Guerau de Arellano et al., 2014), of plants with ozone (Super et al., 2015), on the effects of aerosols on ABL warming (Barbaro et al., 2014), and more (see Chapter 2). Larger-scale implementations of its coupled photosynthesis-conductance scheme in a numerical weather prediction model (e.g. see the HTESSSEL model in Boussetta et al., 2013) opens the way for longer-term studies of coupled weather and vegetation, including their interactions on CO₂. The large-scale implementation of a coupled crop-atmosphere model on the other hand (e.g. with WOFOST in Li et al., 2013) opens the way for research on the crop-atmosphere interactions that determine carbon accumulation and yield projections. In the end, we would like to stress that comprehensive sets of observation of the land-atmosphere are necessary to validate such coupled frameworks. These observations need to include soil moisture, surface heat, carbon, and water fluxes, atmospheric temperature, humidity, and CO₂, and especially observations of the boundary layer height. The latter will be key to understand the connections of the surface conditions to the upper-atmosphere.

6

Summary

Croplands are a managed type of vegetation, with a carbon storage that is highly optimized for food production. For instance, their sowing dates are chosen by the farmers, their genetic potential is bred for high grain yields, and their on-field competition with other species is reduced to the minimum. As a result of this human intervention, croplands are a major land cover type (roughly one fifth of the land area over Europe) and they experience a short growing season during which they exchange carbon and water intensively with the atmosphere. Their growth significantly affects the seasonal amplitude of CO₂ mole fractions over the globe, interact with extreme weather events such as droughts and heat waves, and impact surface hydrology due to their water consumption. However and in spite of their relevance, terrestrial biosphere models (TBMs) used in carbon cycle and atmospheric models often assume the phenology of croplands to be similar to the one of grasslands, and they also ignore the impact of crop management. This oversimplification is the motivation for this thesis. We focus on understanding and modeling the key surface and atmospheric processes that shape the cropland water and CO₂ exchange, and the resulting impact on the CO₂ mole fractions of the atmosphere overhead. We study these processes from the daily to the seasonal scale, for croplands of the mid-latitudes.

Since our first motivation is to improve the representation of croplands in TBMs, we logically ask ourselves two fundamental research questions to guide those improvements:

Research question 1: *What are the main surface and atmospheric processes that determine the atmospheric boundary layer CO₂ budget from the hourly to the seasonal scales?*

Research question 2: *What are the advantages and drawbacks of crop growth models compared to terrestrial biosphere models when representing cropland NEE from the diurnal to the seasonal scales?*

To tackle these questions we test different modeling approaches for the cropland surfaces, and

span our analysis from the diurnal, synoptic and seasonal scale across our Chapters. In Chapter 2, we focus on the diurnal scale. There, we investigated the full set of interactions that take place between croplands and the atmosphere. For this we used two land-surface modeling approaches: (1) A-gs, a simple photosynthesis scheme coupled to a stomatal conductance scheme, which is a “physical” approach of the land-surface used in atmospheric sciences, and (2) GECROS, a more complex crop growth model with no coupling to the stomatal conductance, which is a typical “biological” approach used in crop sciences. Both models conserve the same conceptual basis though, where photosynthesis is a function of photosynthetically active radiation, temperature, vapor pressure deficit, atmospheric CO₂ concentration, leaf area index (LAI), and soil moisture. We coupled each land-surface model to the same atmospheric boundary-layer (ABL) scheme, valid in mixed-layer conditions (i.e. for high convective turbulence conditions). These conditions are normally the prototypical ones in the mid-latitudes, in the Spring and Summer periods corresponding to the crop growing season. With our two coupled models (MXL-A-gs and MXL-GECROS), we reproduced a set of comprehensive observations of the soil, crop, and atmosphere, performed over a grown maize field during a sunny summer day in the Netherlands. This analysis allowed us to validate a robust representation for diurnal crop-atmosphere interactions. With this conceptual framework, we studied how land-atmosphere interactions shape the diurnal CO₂ drawdown. Our results showed the importance of ABL growth and entrainment in the ABL CO₂ budget, and the strong contribution of both surface (e.g. soil moisture) and upper-atmosphere conditions (e.g. subsidence) on the diurnal CO₂ drawdown. A shift in these soil moisture and subsidence conditions that is consistent with droughts had competing effects on the ABL height, leading up to an extra 12 ppm drawdown in the mixed layer. Our results stressed the need for complete observations of not only the soil, vegetation and lower atmosphere but also the boundary layer and free troposphere, when analyzing land-atmosphere interactions. Our analysis also shed light on the limits of the GECROS model to represent the downregulation of plant fluxes with water stress as it unrealistically allowed the surface to perform unlimited evapotranspiration. This realization led us to discard this model for the rest of our work.

Chapter 3 expanded our analysis to the synoptic scales. There we focused on the soil moisture control on the surface fluxes, and the importance of the natural variability of plant sensitivity to soil moisture deficit. We changed in the MXL-A-gs model the plant water stress response function that is applied on stomatal conductance to downregulate surface fluxes. This new function has a flexible shape, which curvature can be adapted to represent different plant behaviors. With this conceptual framework, we performed a sensitivity analysis of the coupled land-atmosphere, from completely dry to completely wet soils, and for different prescribed plant sensitivities to soil moisture deficit. Our findings highlighted the complementarity of surface and upper-atmosphere exchange of carbon and water under water limited conditions: when surface exchange is low (i.e. the plants close their stomata) the up-

per atmosphere exchange is large (i.e. the ABL grows higher), and vice versa. But the level of soil drying required to cause stomatal closure and large ABL growth is fundamentally different depending on the assumed plant sensitivity. Notably, insensitive plants respond only little to soil moisture deficit, unless very close to wilting point. These findings had consequences at the large temporal scale when we simulated a dry spell. We hence demonstrated that insensitive plants can delay an atmospheric warming of 6 K and a CO₂ enrichment of 30 ppm by two weeks at the expense of a faster and complete soil moisture depletion. As such, the skill of weather models in simulating droughts and heat waves is tied to the plant water-stress representation. Our analyses emphasized the need to include the natural variability of plant water stress responses in land-surface models. We proceeded to our analysis of the longer time scales, choosing an appropriate method to account for variable crop sensitivities to water stress.

Chapter 4 finally examined the seasonal time scales. At this scale, we abandoned our fully coupled crop-atmosphere setup and focused solely on processes at the cropland surface. Especially, we focused on the seasonal impact of crop growth, crop phenology, sowing dates and crop rotation on the timing and magnitude of the daily rates of CO₂ exchange. These are usually best represented by crop growth models, such as the WOFOST crop growth model. In contrast to GECROS, this model applies a realistic and variable crop response to water stress depending on the species. However, such models usually overestimate crop carbon assimilation because they do not account for additional processes (e.g. pests, diseases) to represent the actual level of crop production. We overcame these limitations of crop growth models by assimilating observations of crop yields, harvests, and cultivated areas into WOFOST, in order to optimize the modeled crop growth. We then combined our optimized net primary production model (WOFOST-opt) with a robust representation of soil respiration to obtain cropland NEE. By validating our new framework against other independent observations of cropland NEE at 7 FluxNet sites in Europe, we demonstrated its satisfactory performance from the wet to mildly water stressed conditions, and showed that improvements are needed for the severe water stress cases. Such improvements would focus on the soil moisture boundary conditions, with better spatial initialization, and the added representation of irrigation in dry regions like the Mediterranean. We find our WOFOST-opt cropland NEE product is a clear improvement to the cropland NEE modeled by the TBM of the CarbonTracker inverse model system (SiBCASA).

Working from the diurnal to the seasonal scales, a third key research question emerged:

Research question 3: *How should we represent plant water-stress in (crop)land-surface models?*

Throughout the thesis, we focussed on empirical representations of water stress, where a

downscaling factor is applied to the stomatal conductance, the photosynthesis flux, or its parameters. In Chapter 2, we directly showed that plant types with an insensitive response to water stress can be unrealistic. Instead in Chapter 3, we indicated there is a natural variability of responses, and models might gain from adopting flexible representations, with room to assign one response per species, ecosystem, or biome. This is the approach of the WOFOST model used in Chapter 4, by assigning one response per species type (e.g. maize, other cereals, tuber crops). We recommend these responses to be fully tested and validated against combined soil moisture, carbon-exchange, and evapotranspiration measurements across vegetation types. Isotopic measurements which have been long used to quantify plant intrinsic water use efficiency could perhaps help further validate these representations.

Finally, and to wrap up our main topic of research, it is interesting to attempt to scale up the impact of croplands on the CO₂ model fractions at the continental and seasonal scale:

Research question 4: *What is the impact of an improved representation of cropland NEE on the modeled CO₂ mole fractions across Europe?*

Chapter 4 presented our best representation of cropland NEE fluxes. In a short experiment introduced in the general discussion, we replaced the standard representation of croplands in the SiBCASA terrestrial biosphere model by our cropland estimates, conserving the NEE from other vegetation types (i.e. forests, grasslands). We use these new boundary CO₂ fluxes over Western Europe, to be transported by a regional atmospheric transport model (WRF-Chem). We find our improved carbon-exchange estimates greatly affect the CO₂ concentrations over a large spatial domain, mainly in the heart of the growing season when the intense NEE of croplands strongly depletes the ABL from CO₂. These results indicate the relevance of our modeling efforts in this thesis, and the potential of the framework presented in Chapter 4 for future studies of CO₂ cropland-atmosphere exchange.

Appendices

Appendix A: GECROS, A-g_s and MXL model settings

Table A.1 – MXL model initial conditions for 4 August 2007.

Variable	Description and unit	Value
latt	latitude [° N]	51.59
long	longitude [° E]	5.38
day	date [DOY]	216
cc	cloud cover [-]	0.225
h_0	initial boundary-layer height [m]	230.0
pressure	atmospheric pressure [hPa]	1022.0
D	large-scale divergence [s^{-1}]	7×10^{-6}
β	entrainment ratio [-]	0.2
θ_0	initial potential temperature [K]	286.0
$\Delta\theta_0$	initial potential temperature jump [K]	5.0
γ_θ	potential temperature lapse rate [$K m^{-1}$]	8×10^{-3}
adv θ	initial heat advection flux [$K s^{-1}$]	3×10^{-4}
adv θ tim	time of heat advection stop [UTC]	10:00
q_0	initial specific humidity [$g kg^{-1}$]	8.5
Δq_0	initial specific humidity jump [$g kg^{-1}$]	-1.0
γ_q	specific humidity lapse rate [$g kg^{-1} m^{-1}$]	-0.0005
adv q	initial humidity advection flux [$g kg^{-1} s^{-1}$]	3.5×10^{-4}
adv q tim	time of humidity advection stop [UTC]	07:30
c_0	initial CO ₂ mole fraction [ppm]	422.0
Δc_0	initial CO ₂ mole fraction jump [ppm]	-50.0
γ_c	CO ₂ mole fraction lapse rate [ppb m^{-1}]	-10.0
u_0	initial mixed-layer u-wind speed [$m s^{-1}$]	5.0
u_g	geostrophic u-wind speed [$m s^{-1}$]	8.0
γ_u	free troposphere u-wind speed lapse rate [s^{-1}]	0.0
$z_{0,m}$	roughness length for momentum [m]	0.15
$z_{0,h}$	roughness length for scalars [m]	0.015

Table A.2 – A-g_s model initial conditions for 4 August 2007.

Variable	Description and unit	Value
albedo	surface albedo [-]	0.198
LAI	leaf area index [$\text{m}^2 \text{m}^{-2}$]	3.5
f_{veg}	vegetation fraction [-]	0.97
$r_{\text{s, min}}$	minimum resistance for transpiration [s m^{-1}]	180.0
$r_{\text{s, soil min}}$	minimum soil resistance [s m^{-1}]	50.0
Λ	thermal diffusivity skin layer [$\text{W m}^{-2} \text{K}^{-1}$]	2.5
g_{D}	VPD correction factor for r_{s} [-]	0.
CG_{sat}	saturated heat soil conductivity [$\text{K m}^{-2} \text{J}^{-1}$]	3.56×10^{-6}
C_{w}	constant water stress correction [-]	0.0016
T_{s}	initial surface temperature [K]	290.0
T_{soil}	temperature of top soil layer [K]	288.0
T_2	temperature of deeper soil layer [K]	289.0
w_{g}	water content top soil layer [$\text{cm}^3 \text{cm}^{-3}$]	0.11
w_2	water content deep soil layer [$\text{cm}^3 \text{cm}^{-3}$]	0.11
w_{sat}	saturation water content [$\text{cm}^3 \text{cm}^{-3}$]	0.36
w_{fc}	field capacity water content [$\text{cm}^3 \text{cm}^{-3}$]	0.15
w_{wilt}	wilting point water content [$\text{cm}^3 \text{cm}^{-3}$]	0.06
$w_{\text{s, max}}$	upper reference value soil water [-]	0.55
$w_{\text{s, min}}$	lower reference value soil water [-]	0.005
$C_{1, \text{sat}}$	coefficient force term moisture [-]	0.132
$C_{2, \text{ref}}$	coefficient restore term moisture [-]	1.8
a	Clapp and Hornberger retention curve parameter a [-]	0.219
b	Clapp and Hornberger retention curve parameter b [-]	4.9
p	Clapp and Hornberger retention curve parameter c [-]	4.
Γ (298 K)	CO_2 compensation concentration at 298 K [mg m^{-3}]	4.3
$Q_{10} \Gamma$	percentage of increase in Γ (298 K) with +10 K [-]	1.5
g_{m} (298 K)	mesophyll conductance at 298 K [mm s^{-1}]	17.5
$Q_{10} g_{\text{m}}$	percentage of increase in g_{m} with +10 K [-]	2.0
$T_{1} g_{\text{m}}$	reference temperature T_1 for g_{m} [K]	286.0
$T_{2} g_{\text{m}}$	reference temperature T_2 for g_{m} [K]	309.0
$A_{\text{m, max}}$ (298 K)	CO_2 maximal primary productivity at 298 K [$\text{mg m}^{-2} \text{s}^{-1}$]	1.7
$Q_{10} A_{\text{m}}$	percentage of increase in $A_{\text{m, max}}$ with +10 K [-]	2.0
$T_1 A_{\text{m}}$	reference temperature T_1 for $A_{\text{m, max}}$ [K]	286.0
$T_2 A_{\text{m}}$	reference temperature T_2 for $A_{\text{m, max}}$ [K]	311.0
f_0	maximum value C_{frac} [-]	0.85
a_{d}	regression coefficient for C_{frac} [kPa^{-1}]	0.15
α_0	initial low light conditions [mg J^{-1}]	0.014
K_{x}	extinction coefficient for PAR [-]	0.7
g_{min}	cuticular minimum conductance [m s^{-1}]	2.5×10^{-4}
R_{10}	respiration at 10 °C [$\text{mg CO}_2 \text{m}^{-2} \text{s}^{-1}$]	0.03
$E_{\text{act}0}$	activation energy [kJ kmol^{-1}]	5.33×10^4

Table A.3 – GECROS model initial conditions for 4 August 2007. See Yin and van Laar (2005) and Sinclair and de Wit (1975) for the rest of the maize average genotype parameters.

Variable	Description and unit	Value
SLP	short day crop	yes
DETER	determinate crop	yes
C3C4	C4 crop	yes
LODGE	lodging allowed	no
LEGUME	legume crop	no
NPL	plant density [plant m ⁻²]	9.1
EG	efficiency of germination [%]	3.6783
HTMX	maximum plant height [m]	2.8
BLD	leaf angle [deg]	50.
SEEDW	seed weight [g]	0.5
MTDV	minimal thermal days for vegetative phase [d]	41.0
MTDR	minimal thermal days for reproductive phase [d]	15.7
PSEN	photoperiod sensitivity of phenological development [h ⁻¹]	0.
TM	development stage when transition from CB to CX is fastest [-]	1.5
CX	factor for initial N concentration of seed fill [-]	1.
CB	factor for final N concentration of seed fill [-]	1.
PNLS	fraction of dead leaf N incorporated into soil litter [-]	1.
CLAY	percentage of clay in the soil [%]	7.
WCMAX	soil water content at maximum holding capacity [m ³ m ⁻³]	0.36
WCFC	soil water content at field capacity [m ³ m ⁻³]	0.15
WCMIN	minimum soil water content [m ³ m ⁻³]	0.06
RPMR0	decomposition rate for resistant plant material [yr ⁻¹]	0.3
DPMR0	decomposition rate for decomposable plant material [yr ⁻¹]	10.
HUMR	decomposition rate for humified organic matter [yr ⁻¹]	0.02
BIOR	decomposition rate for microbial in the soil [yr ⁻¹]	0.66
DRPM	ratio DPM/RPM of added plant material [-]	1.44
RA	residual ammonium-N in the soil [g N m ⁻²]	1.
FBIOC	fraction of initial microbial biomass in the soil in the initial total soil organic carbon (TOC) [-]	0.03
BHC	initial soil microbial biomass + humified soil organic matter [g C m ⁻²]	3500.
TOC	total organic C in the soil [g C m ⁻²]	7193.
RN	residual nitrate-N in the soil [g N m ⁻²]	1.
MULTF	multiplication factor for initial soil water status [-]	1.
TCT	time constant for soil temperature dynamics [d]	4.
RSS	soil resistance for water vapour transfer, equivalent to leaf stomatal resistance [s m ⁻¹]	80.
SD1	thickness of upper evaporative soil layer [cm]	5.
TCP	time constant for some soil dynamic processes [d]	1.
FNA1	ammonium-N added in the 1st fertiliser application [g N m ⁻² d ⁻¹]	10.
FNA1T	day number at which the 1st ammonium-N dose is applied [DOY]	1.

Appendix B: MXL-A-g_s model equations

Equations for the heat and water cycles

This Appendix strictly provides the set of equations necessary to obtain the ABL virtual potential temperature and its jump at the inversion height (see Sect. 3.2.2). More information can be found about the mixed-layer theory in Vilá-Guerau de Arellano et al. (2015).

First, the diurnal evolution of the ABL potential temperature (θ) is described with the following equation:

$$\begin{aligned} \frac{d\theta}{dt} &= \frac{1}{h} \times \left(\underbrace{\overline{w'\theta'_s}}_{\text{Surface turbulent flux of temperature}} - \underbrace{\overline{w'\theta'_e}}_{\text{Entrainment turbulent flux of temperature}} \right) + \underbrace{adv_\theta}_{\text{Horizontal advection of heat}}, \\ &= \frac{1}{h} \times \left(\frac{SH}{\rho_{air} c_p} - w_e \Delta\theta \right) + adv_\theta, \end{aligned} \quad (\text{B.1})$$

with SH the surface sensible heat flux in W m^{-2} , c_p the specific heat of moist air, and $\Delta\theta$ the potential temperature jump at the inversion height. $\Delta\theta$ evolves in time due to the entrainment of free-tropospheric warmer air into the ABL and is expressed as:

$$\frac{d\Delta\theta}{dt} = \gamma_\theta w_e - \frac{d\theta}{dt}, \quad (\text{B.2})$$

with γ_θ the free-troposphere lapse rate of potential temperature. SH is expressed as the temperature gradient between the surface and the ABL times the corresponding surface conductance for heat transfer:

$$SH = \rho_{air} c_p \frac{1}{r_a} (\theta_s - \theta). \quad (\text{B.3})$$

Very similarly to θ , the diurnal evolution of the ABL specific humidity (q) is described with the following equation:

$$\begin{aligned} \frac{dq}{dt} &= \frac{1}{h} \times \left(\underbrace{\overline{w'q'_s}}_{\text{Surface turbulent flux of humidity}} - \underbrace{\overline{w'q'_e}}_{\text{Entrainment turbulent flux of humidity}} \right) + \underbrace{adv_q}_{\text{Horizontal advection of moisture}}, \\ &= \frac{1}{h} \times \left(\frac{LE}{\rho_{air} L_v} + w_e \Delta q \right) + adv_q, \end{aligned} \quad (\text{B.4})$$

with LE the total surface latent heat flux in W m^{-2} and Δq the specific humidity jump at the inversion height. Δq evolves in time due to the entrainment of free-tropospheric dryer air into

the ABL and is expressed as:

$$\frac{d\Delta q}{dt} = \gamma_q w_e - \frac{dq}{dt}, \quad (\text{B.5})$$

with γ_q the free-troposphere lapse rate of specific humidity. LE is expressed as the moisture gradient times the corresponding surface conductance for water transfer:

$$\text{LE} = \rho_{air} L_v \left(\frac{f_{veg}}{r_a + r_s} + \frac{1 - f_{veg}}{r_a + r_{soil}} \right) (q_{sat}(\theta_s) - q), \quad (\text{B.6})$$

with f_{veg} the vegetated fraction of the ground and r_{soil} the bare soil resistance to water transfer. Note that we assume here no evaporation of liquid water (e.g. dew).

Finally, the mixed-layer virtual potential temperature (θ_v) used in the calculation of the entrainment velocity (w_e , see Eq. 3.2 on page 56) is the mixed-layer potential temperature corrected for the variation of density due to the presence of water vapor in the air. For unsaturated air, θ_v and its jump at the inversion height ($\Delta\theta_v$) are calculated as follows:

$$\theta_v = \theta \times (1 + 0.61 q), \quad (\text{B.7})$$

$$\Delta\theta_v = \Delta\theta + 0.61 (q \Delta\theta + \theta \Delta q + \Delta\theta \Delta q). \quad (\text{B.8})$$

Derivation of r_c

As explained in Sect. 3.2.2, the leaf stomatal resistance to CO_2 transfer $r_{l,c}$ can be expressed as:

$$\frac{1}{r_{l,c}} = g_{min,c} + \frac{a_1 A_g^* \beta}{(c - \Gamma) \left(1 + \frac{\text{VPD}}{\text{VPD}_*}\right)}.$$

Then, to upscale $r_{l,c}$ from the leaf to the canopy level (i.e. to obtain r_c), we must integrate this equation over LAI:

$$\begin{aligned} \frac{1}{r_c} &= \int_0^{\text{LAI}} \left[\frac{g_{min,w}}{1.6} + \frac{a_1 A_g^* \beta}{(c - \Gamma) \left(1 + \frac{\text{VPD}}{\text{VPD}_*}\right)} \right] dL, \\ &= \frac{g_{min,w}}{1.6} \text{LAI} + \frac{a_1 \beta \int_0^{\text{LAI}} A_g^* dL}{(c - \Gamma) \left(1 + \frac{\text{VPD}}{\text{VPD}_*}\right)}, \end{aligned} \quad (\text{B.9})$$

with $g_{min,w}$ the cuticular conductance for water transfer, which is related to $g_{min,c}$ by the molecular diffusion constant 1.6. Obtaining r_c then only requires to integrate A_g^* (see Eq. 3.8 on

page 58) over LAI:

$$\begin{aligned} \int_0^{\text{LAI}} A_g^* dL &= \int_0^{\text{LAI}} \left[(A_m + R_{\text{dark}}) \left\{ 1 - \exp\left(-\frac{\text{LUE } K_x \text{ PAR}_t e^{-K_x L}}{(A_m + R_{\text{dark}})}\right)\right\} \right] dL, \\ &= (A_m + R_{\text{dark}}) \left\{ \text{LAI} - \int_0^{\text{LAI}} \exp(-b e^{-K_x L}) dL \right\}, \end{aligned} \quad (\text{B.10})$$

with $b = \text{LUE } K_x \text{ PAR}_t / (A_m + R_{\text{dark}})$. We introduce the transformation $y = b e^{-K_x L}$. Under this transformation, the boundaries of the integral over the leaf area become $L = 0 \Rightarrow y = b$ and $L = \text{LAI} \Rightarrow y = b e^{-K_x \text{LAI}}$. Thus, Eq. B.10 can be rewritten as:

$$\begin{aligned} \int_0^{\text{LAI}} A_g^* dL &= (A_m + R_{\text{dark}}) \left\{ \text{LAI} + \frac{1}{K_x} \int_b^{e^{-K_x \text{LAI}}} \frac{e^{-y}}{y} dy \right\}, \\ &= (A_m + R_{\text{dark}}) \left\{ \text{LAI} + \frac{1}{K_x} \left[E_1(b) - E_1(b e^{-K_x \text{LAI}}) \right] \right\}, \end{aligned} \quad (\text{B.11})$$

with $E_1(x)$ the integral of $\frac{e^{-y}}{y}$ from x to infinity. The final form of Eq. B.10 thus becomes:

$$\begin{aligned} \int_0^{\text{LAI}} A_g^* dL &= (A_m + R_{\text{dark}}) \left\{ \text{LAI} + \frac{1}{K_x} \left[E_1\left(\frac{\text{LUE } K_x \text{ PAR}_t}{(A_m + R_{\text{dark}})}\right) \right. \right. \\ &\quad \left. \left. - E_1\left(\frac{\text{LUE } K_x \text{ PAR}_t}{(A_m + R_{\text{dark}})} e^{-K_x \text{LAI}}\right) \right] \right\}, \end{aligned} \quad (\text{B.12})$$

which can be used in Eq. B.9 to calculate r_c .

Appendix C: Updated MXL-A-g_s model settings (Chapter 3)

Table C.1 – Model constants, boundary and initial conditions of the control case.

Variable	Value	Units	Description
Constants			
C_3/C_4	C_4	–	C_3 or C_4 photosynthesis
Boundary conditions			
lat	51.59	° N	latitude
lon	5.38	° E	longitude
day	216	DOY	date
p	1022.0	hPa	atmospheric pressure
w_s	$7. \times 10^{-6}$	s^{-1}	large-scale divergence
cc	0.225	–	cloud cover
γ_θ	$8. \times 10^{-3}$	$K m^{-1}$	potential temperature lapse rate
γ_q	$-5. \times 10^{-4}$	$g kg^{-1} m^{-1}$	specific humidity lapse rate
γ_c	$-10. \times 10^{-3}$	ppm m^{-1}	CO ₂ mole fraction lapse rate
adv_θ	3.0×10^{-4}	$K s^{-1}$	horizontal advection flux of heat
adv_q	3.5×10^{-4}	$g kg^{-1} s^{-1}$	horizontal advection flux of moisture
α	0.198	–	surface albedo
LAI	3.5	$m^2 m^{-2}$	leaf area index
f_{veg}	0.97	–	Vegetation fraction
Initial conditions			
h_0	230.0	m	initial boundary-layer height
θ_0	286.0	K	initial potential temperature
$\Delta\theta_0$	5.0	K	initial potential temperature jump
q_0	8.5	$g kg^{-1}$	initial specific humidity
Δq_0	-1.0	$g kg^{-1}$	initial specific humidity jump
c_0	422.0	ppm	initial CO ₂ mole fraction
Δc_0	-50.0	ppm	initial CO ₂ mole fraction jump
SMI_0	0.55	–	initial soil moisture index

NB: note that the horizontal advection fluxes are set to zero at 07:30 UTC for moisture and 10:00 UTC for heat.

Appendix D: FluxNet sites information

Table D.1 – Crop rotation and irrigation information for our 7 FluxNet sites, from 2000 to 2014. We exclude here periods with crops we cannot model, such as mustard (BE-Lon, FR-Gri), or managed grass (FI-Jok).

Site ID (Reference)	Crop	Dates		Irrigation
		sowing	harvest	
BE-Lon (Moureaux et al., 2006)	sugar beet	Mar 30 2004	Sep 29 2004	no
	winter wheat	Oct 14 2004	Aug 3 2005	no
	potato	May 1 2006	Sep 15 2006	no
	winter wheat	Oct 13 2006	Aug 5 2007	no
	sugar beet	Apr 22 2008	Nov 4 2008	no
	winter wheat	Nov 13 2008	Aug 7 2009	no
	potato	Apr 25 2010	Sep 5 2010	no
	winter wheat	Nov 14 2010	Aug 16 2011	no
	grain maize	May 14 2012	Oct 13 2012	no
	winter wheat	Oct 25 2012	Aug 12 2013	no
	potato	Apr 7 2014	Aug 22 2014	no
DE-Kli (Prescher et al., 2010)	winter barley	Sep 6 2003	Jul 31 2004	no
	winter rapeseed	Aug 18 2004	Aug 20 2005	no
	winter wheat	Sep 25 2005	Sep 6 2006	no
	fodder maize	Apr 23 2007	Oct 2 2007	no
	spring barley	Apr 25 2008	Aug 27 2008	no
	winter barley	Sep 12 2008	Jul 22 2009	no
	winter rapeseed	Aug 25 2009	Aug 24 2010	no
	winter wheat	Oct 2 2010	Aug 22 2011	no
	fodder maize	Apr 25 2012	Sep 19 2012	no
	spring barley	Apr 17 2013	Aug 24 2013	no
winter barley	Oct 1 2013	July 20 2014	no	
FI-Jok (Lohila et al., 2004)	spring barley	May 25 2001	Sep 21 2001	no
FR-Gri (Loubet et al., 2011)	winter barley	Oct 16 2003	Jul 2 2004	no
	grain maize	May 9 2005	Sep 28 2005	no
	winter wheat	Oct 28 2005	Jul 15 2006	no
	winter barley	Oct 4 2006	Jun 29 2007	no
	grain maize	Apr 4 2008	Sep 10 2008	no
	winter wheat	Oct 17 2008	Jul 31 2009	no
	winter triticale	Oct 14 2009	Jul 18 2010	no
	fodder maize	Apr 21 2011	Sep 6 2011	no
	winter wheat	Oct 20 2011	Aug 3 2012	no
	winter rapeseed	Aug 31 2012	Aug 15 2013	no
IT-BCi (Vitale et al., 2007)	grain maize	May 9 2004	Aug 26 2004	yes
	grain maize	May 17 2005	Aug 24 2005	yes
	grain maize	Apr 27 2006	?	yes
	grain maize	May 9 2007	?	yes
	fodder maize	Apr 30 2008	Aug 22 2008	yes
	fodder maize	Jun 11 2009	Sep 8 2009	yes
NL-Dij (Jans et al., 2010)	fodder maize	May 5 2007	Oct 9 2007	no
NL-Lan (Moors et al., 2010)	grain maize	May 18 2005	Oct 19 2005	no

Appendix E: WOFOST-opt model statistics

Table E.1 – Statistics of the GPP models: (a) SiBCASA (SIB), (b) original WOFOST (WOF), and (c) optimized WOFOST (OPT). The measurements from 2000-2011 of Table D.1 are used to compute these statistics.

	Number of years	Climates	RMSE on GPP ($\text{gC m}^{-2} \text{d}^{-1}$)			R ² of GPP model (-)			min - max f_{gap} range
			SIB	WOF	OPT	SIB	WOF	OPT	
<i>Winter wheat</i>									
FR-Gri	3	Cfb	3.72	2.79	2.84	0.50	0.87	0.88	0.69 - 1.00
DE-Kli	2	Cfb	2.98	7.13	2.68	0.69	0.45	0.81	
BE-Lon	5	Cfb	4.70	3.02	2.36	0.44	0.90	0.88	
<i>Grain maize</i>									
IT-BCi	6	Cfa	8.50	14.37	14.37	0.20	0.15	0.15	0.70 - 1.00
FR-Gri	0	Cfb	4.39	8.06	5.82	0.42	0.03	0.63	
NL-Lan	1	Cfb	4.09	6.44	5.06	0.49	0.67	0.68	
<i>Fodder Maize</i>									
IT-BCi	0	Cfa	8.60	15.13	15.13	0.43	0.29	0.29	1.00 - 1.00
FR-Gri	3	Cfb	4.51	7.21	5.34	0.59	0.05	0.67	
DE-Kli	2	Cfb	3.68	8.00	7.07	0.44	0.00	0.87	
NL-Dij	0	Cfb	6.22	5.50	5.50	0.48	0.86	0.86	
<i>Winter barley</i>									
FR-Gri	2	Cfb	4.19	10.75	2.43	0.23	0.00	0.90	0.69 - 0.73
DE-Kli	3	Cfb	4.03	5.58	2.39	0.37	0.74	0.86	
<i>Spring barley</i>									
DE-Kli	0	Cfb	4.37	9.85	2.47	0.67	0.61	0.87	0.69 - 0.70
FI-Jok	1	Dfb	3.29	1.96	0.64	0.61	0.93	0.93	
<i>Winter rapeseed</i>									
DE-Kli	2	Cfb	3.18	9.96	3.42	0.58	0.04	0.79	0.92 - 0.98
<i>Potato</i>									
BE-Lon	3	Cfb	3.75	3.19	3.19	0.42	0.53	0.53	0.69 - 1.00
<i>Sugar beet</i>									
BE-Lon	2	Cfb	4.22	3.27	2.68	0.50	0.87	0.80	0.84 - 0.86

Table E.2 – Statistics of the TER models: (a) SiBCASA (SIB), (b) original WOFOST (WOF), and (c) optimized WOFOST (OPT). The measurements from 2000-2011 of Table D.1 are used to compute these statistics.

	Number of years	Climates	RMSE on TER ($\text{gC m}^{-2} \text{d}^{-1}$)			R ² of TER model (-)			min - max f_{gap} range
			SIB	WOF	OPT	SIB	WOF	OPT	
<i>Winter wheat</i>									
FR-Gri	3	Cfb	1.69	1.21	1.28	0.63	0.81	0.83	0.69 - 1.00
DE-Kli	2	Cfb	2.08	1.84	1.28	0.60	0.67	0.76	
BE-Lon	5	Cfb	1.99	1.13	1.04	0.53	0.81	0.81	
<i>Grain maize</i>									
IT-BCi	6	Cfa	3.37	4.29	4.29	0.00	0.09	0.09	0.70 - 1.00
FR-Gri	0	Cfb	2.11	2.73	2.46	0.41	0.15	0.43	
NL-Lan	1	Cfb	2.38	2.27	2.27	0.68	0.67	0.69	
<i>Fodder Maize</i>									
IT-BCi	0	Cfa	3.08	4.05	4.05	0.21	0.11	0.11	1.00 - 1.00
FR-Gri	3	Cfb	2.30	2.38	2.46	0.34	0.18	0.47	
DE-Kli	2	Cfb	1.93	1.93	1.95	0.76	0.39	0.77	
NL-Dij	0	Cfb	1.83	1.76	1.76	0.79	0.72	0.72	
<i>Winter barley</i>									
FR-Gri	2	Cfb	1.70	2.75	0.97	0.61	0.19	0.63	0.69 - 0.73
DE-Kli	3	Cfb	1.71	1.25	1.15	0.72	0.77	0.87	
<i>Spring barley</i>									
DE-Kli	0	Cfb	3.48	2.98	1.02	0.76	0.82	0.94	0.69 - 0.70
FI-Jok	1	Dfb	2.24	0.75	0.61	0.80	0.91	0.92	
<i>Winter rapeseed</i>									
DE-Kli	2	Cfb	1.78	2.25	1.37	0.74	0.57	0.78	0.92 - 0.98
<i>Potato</i>									
BE-Lon	3	Cfb	2.71	1.02	1.02	0.52	0.81	0.81	0.69 - 1.00
<i>Sugar beet</i>									
BE-Lon	2	Cfb	2.44	1.36	1.00	0.60	0.82	0.81	0.84 - 0.86

References

- Ahmadov, R., Gerbig, C., Kretschmer, R., Koerner, S., Neining, B., Dolman, A. J., and Sarrat, C.: Mesoscale covariance of transport and CO₂ fluxes: Evidence from observations and simulations using the WRF–VPRM coupled atmosphere–biosphere model, *J. Geophys. Res.*, 112, D22 107, doi:10.1029/2007JD008552, 2007.
- Albergel, C., Calvet, J. C., Mahfouf, J. F., Rüdiger, C., Barbu, A. L., Lafont, S., Roujean, J. L., Walker, J. P., Crapeau, M., and Wigneron, J. P.: Monitoring of water and carbon fluxes using a land data assimilation system: A case study for southwestern France, *Hydrology and Earth System Sciences*, 14, 1109–1124, doi:10.5194/hess-14-1109-2010, 2010.
- Alden, C. B., Miller, J. B., Gatti, L. V., Gloor, M. M., Guan, K., Michalak, A. M., van der Laan-Luijkx, I. T., Touma, D., Andrews, A., Basso, L. S., Correia, C. S. C., Domingues, L. G., Joiner, J., Krol, M. C., Lyapustin, A. I., Peters, W., Shiga, Y. P., Thoning, K., van der Velde, I. R., van Leeuwen, T. T., Yadav, V., and Diffenbaugh, N. S.: Regional atmospheric CO₂ inversion reveals seasonal and geographic differences in Amazon net biome exchange, *Global Change Biology*, doi:10.1111/gcb.13305, 2016.
- Arora, V. K., Boer, G. J., Friedlingstein, P., Eby, M., Jones, C. D., Christian, J. R., Bonan, G., Bopp, L., Brovkin, V., Cadule, P., Hajima, T., Ilyina, T., Lindsay, K., Tjiputra, J. F., and Wu, T.: Carbon–Concentration and Carbon–Climate Feedbacks in CMIP5 Earth System Models, *J. Clim.*, 26, 5289–5314, doi:10.1175/JCLI-D-12-00494.1, 2013.
- Aubinet, M., Vesala, T., and Papale, D., eds.: *Eddy Covariance: A Practical Guide to Measurement and Data Analysis*, Springer, Dordrecht, The Netherlands, 2012.
- Baker, I. T., Prihodko, L., Denning, A. S., Goulden, M., Miller, S., and da Rocha, H. R.: Seasonal drought stress in the Amazon: Reconciling models and observations, *J. Geophys. Res.–Biogeo.*, 113, G00B01, doi:10.1029/2007JG000644, 2008.
- Baldocchi, D., Falge, E., Gu, L., and Olson, R.: FluxNet: a new tool to study the temporal and spatial variability of ecosystem-scale carbon dioxide, water vapor, and energy flux densities, *Bulletin of the American Meteorological Society*, 82, 2415–2434, doi:10.1175/1520-0477(2001)082<2415:fantts>2.3.co;2, 2001.
- Baldocchi, D. D.: Assessing the eddy covariance technique for evaluating carbon dioxide exchange rates of ecosystems: past, present and future, *Global Change Biology*, 9, 479–492, doi:10.1046/j.1365-2486.2003.00629.x, 2003.
- Ball, J. T.: An analysis of stomatal conductance, Ph.D. thesis, Stanford University, Stanford, CA, 1988.
- Ball, J. T., Woodrow, I. E., and Berry, J. A.: A model predicting stomatal conductance and its contribution to the control of photosynthesis under different environmental conditions, in: *Progress in photosynthesis research*, edited by Biggins, J., pp. 221–224, 1987.

REFERENCES

- Barbaro, E., Vilà-Guerau De Arellano, J., Ouwersloot, H. G., Schröter, J., Donovan, D. P., and Krol, M. C.: Aerosols in the convective boundary layer: Shortwave radiation effects on the coupled land-atmosphere system, *J. Geophys. Res.–Atmos.*, 119, 5845–5863, doi:10.1002/2013JD021237, 2014.
- Barbu, A. L., Calvet, J. C., Mahfouf, J. F., Albergel, C., and Lafont, S.: Assimilation of Soil Wetness Index and Leaf Area Index into the ISBA-A-gs land surface model: Grassland case study, *Biogeosciences*, 8, 1971–1986, doi:10.5194/bg-8-1971-2011, 2011.
- Beer, C., Reichstein, M., Tomelleri, E., Ciais, P., Jung, M., Carvalhais, N., Rödenbeck, C., Arain, M. A., Baldocchi, D., Bonan, G. B., Bondeau, A., Cescatti, A., Lasslop, G., Lindroth, A., Lomas, M., Luysaert, S., Margolis, H., Oleson, K. W., Rouspard, O., Veenendaal, E., Viovy, N., Williams, C., Woodward, F. I., and Papale, D.: Terrestrial Gross Carbon Dioxide Uptake: Global Distribution and Covariation with Climate, *Science*, 329, 834–838, doi:10.1126/science.1184984, 2010.
- Beljaars, A. and Bosveld, F. C.: Cabauw data for the validation of land surface parameterization schemes, *Journal of Climate*, 10, 1172–1193, 1997.
- Berry, J. A., Beerling, D. J., and Franks, P. J.: Stomata: key players in the earth system, past and present, *Curr. Opin. Plant Biol.*, 13, 232–239, doi:10.1016/j.pbi.2010.04.013, 2010.
- Bert, F. E., Laciana, C. E., Podestá, G. P., Satorre, E. H., and Menéndez, A. N.: Sensitivity of CERES-Maize simulated yields to uncertainty in soil properties and daily solar radiation, *Agricultural Systems*, 94, 141–150, doi:10.1016/j.agsy.2006.08.003, 2007.
- Best, M. J., Pryor, M., Clark, D. B., Rooney, G. G., Essery, R. L. H., Menard, C. B., Edwards, J. M., Hendry, M. A., Porson, A., Gedney, N., Mercado, L. M., Sitch, S., Blyth, E., Boucher, O., Cox, P. M., Grimmond, C. S. B., and Harding, R. J.: The Joint UK Land Environment Simulator (JULES), model description - Part 1: Energy and water fluxes, *Geosci. Model Dev.*, 4, 677–699, doi:10.5194/gmd-4-677-2011, 2011.
- Betts, A. K.: Non-precipitating cumulus convection and its parameterization, *Quart. J. Roy. Meteorol. Soc.*, 99, 178–196, doi:10.1002/qj.49709941915, 1973.
- Betts, A. K.: Understanding hydrometeorology using global models, *Bulletin of the American Meteorological Society*, 85, 1673–1688, 2004.
- Betts, R. A.: Integrated approaches to climate-crop modelling: needs and challenges., *Philos. Trans. R. Soc. London, Ser. B*, 360, 2049–2065, 2005.
- Bonan, G. B.: Forests and climate change: forcings, feedbacks, and the climate benefits of forests., *Science*, 320, 1444–1449, 2008.
- Bondeau, A., Smith, P. C., Zaehle, S., Schaphoff, S., Lucht, W., Cramer, W., Gerten, D., Lotze-Campen, H., Müller, C., Reichstein, M., and Smith, B.: Modelling the role of agriculture for the 20th century global terrestrial carbon balance, *Global Change Biology*, 13, 679–706, doi:10.1111/j.1365-2486.2006.01305.x, 2007.
- Boogaard, H., Wolf, J., Supit, I., Niemeier, S., and van Ittersum, M.: A regional implementation of WOFOST for calculating yield gaps of autumn-sown wheat across the European Union, *Field Crops Research*, 143, 130–142, 2013.

- Booth, B. B. B., Jones, C. D., Collins, M., Totterdell, I. J., Cox, P. M., Sitch, S., Huntingford, C., Betts, R. A., Harris, G. R., and Lloyd, J.: High sensitivity of future global warming to land carbon cycle processes, *Environ. Res. Lett.*, 7, 024002, doi:10.1088/1748-9326/7/2/024002, 2012.
- Boussetta, S., Balsamo, G., Beljaars, A., Panareda, A. A., Calvet, J. C., Jacobs, C., Van Den Hurk, B., Viterbo, P., Lafont, S., Dutra, E., Jarlan, L., Balzarolo, M., Papale, D., and Van Der Werf, G.: Natural land carbon dioxide exchanges in the ECMWF integrated forecasting system: Implementation and offline validation, *J. Geophys. Res.–Atmos.*, 118, 5923–5946, 2013.
- Bregaglio, S., Frasso, N., Pagani, V., Stella, T., Francone, C., Cappelli, G., Acutis, M., Balaghi, R., Ouabbou, H., Palerri, L., and Confalonieri, R.: New multi-model approach gives good estimations of wheat yield under semi-arid climate in Morocco, *Agronomy for Sustainable Development*, 35, 157–167, doi:10.1007/s13593-014-0225-6, 2014.
- Brienen, R., Wanek, W., and Hietz, P.: Stable carbon isotopes in tree rings indicate improved water use efficiency and drought responses of a tropical dry forest tree species, *Trees*, 25, 103–113, doi:10.1007/s00468-010-0474-1, 2011.
- Buckley, T. N. and Schymanski, S. J.: Stomatal optimisation in relation to atmospheric CO₂, *The New phytologist*, 201, 372–377, doi:10.1111/nph.12552, 2014.
- Bussay, A., van der Velde, M., Fumagalli, D., and Seguini, L.: Improving operational maize yield forecasting in Hungary, *Agricultural Systems*, 141, 94–106, doi:10.1016/j.agry.2015.10.001, 2015.
- Caldararu, S., Purves, D. W., and Smith, M. J.: The effect of using the plant functional type paradigm on a data-constrained global phenology model, *Biogeosciences*, 13, 925–941, doi:10.5194/bg-13-925-2016, 2016.
- Calvet, J.-C., Noilhan, J., Roujean, J.-L., Bessemoulin, P., Cabelguenne, M., Olioso, A., and Wigneron, J.-P.: An interactive vegetation SVAT model tested against data from six contrasting sites, *Agric. For. Meteorol.*, 92, 73–95, doi:10.1016/S0168-1923(98)00091-4, 1998.
- Calvet, J.-C., Rivalland, V., Picon-Cochard, C., and Guehl, J.-M.: Modelling forest transpiration and CO₂ fluxes–response to soil moisture stress, *Agric. For. Meteorol.*, 124, 143–156, doi:10.1016/j.agrformet.2004.01.007, 2004.
- Camargo, G. G. T. and Kemanian, A. R.: Six crop models differ in their simulation of water uptake, *Agricultural and Forest Meteorology*, 220, 116–129, doi:10.1016/j.agrformet.2016.01.013, 2016.
- Canut, G., Couvreur, F., Lothon, M., Pino, D., and Saïd, F.: Observations and Large-Eddy Simulations of Entrainment in the Sheared Sahelian Boundary Layer, *Bound.-Lay. Meteorol.*, 142, 79–101, 2012.
- Carmo-Silva, A. E., Soares, A. S., Marques da Silva, J., Bernardes da Silva, A., Keys, A. J., and Arrabaça, M. C.: Photosynthetic responses of three C4 grasses of different metabolic subtypes to water deficit, *Funct. Plant Biol.*, 34, 204, doi:10.1071/FP06278, 2007.
- Carson, D. J.: The development of a dry inversion-capped convectively unstable boundary layer, *Quart. J. Roy. Meteorol. Soc.*, 99, 450–467, doi:10.1002/qj.49709942105, 1973.
- Casso-Torralba, P., Vilà-Guerau de Arellano, J., Bosveld, F., Soler, M. R., Vermeulen, A., Werner, C., and Moors, E.: Diurnal and vertical variability of the sensible heat and carbon dioxide budgets in the atmospheric surface layer, *J. Geophys. Res.*, 113, D12 119, doi:10.1029/2007JD009583, 2008.

REFERENCES

- Challinor, A. J., Ewert, F., Arnold, S., Simelton, E., and Fraser, E.: Crops and climate change: progress, trends, and challenges in simulating impacts and informing adaptation., *J. Exp. Bot.*, 60, 2775–2789, 2009.
- Chen, F. and Xie, Z.: Effects of crop growth and development on regional climate: a case study over East Asian monsoon area, *Climate Dynamics*, 38, 2291–2305, 2011.
- Chen, J. M., Fung, J. W., Mo, G., Deng, F., and West, T. O.: Atmospheric inversion of surface carbon flux with consideration of the spatial distribution of US crop production and consumption, *Biogeosciences*, 12, 323–343, 2015.
- Ciais, P., Bousquet, P., Freibauer, A., and Naegler, T.: Horizontal displacement of carbon associated with agriculture and its impacts on atmospheric CO₂, *Global Biogeochemical Cycles*, 21, GB2014, doi:10.1029/2006GB002741, 2007.
- Ciais, P., Borges, A. V., ABRIL, G., Meybeck, M., Folberth, G., Hauglustaine, D., and Janssens, I. A.: The impact of lateral carbon fluxes on the European carbon balance, *Biogeosciences*, 5, 1259–1271, 2008.
- Ciais, P., Wattenbach, M., Vuichard, N., Smith, P., Piao, S. L., Don, A., Luysaert, S., Janssens, I. A., Bondeau, A., Dechow, R., Leip, A., Smith, P. C., Beer, C., van der Werf, G., Gervois, S., van Oost, K., Tomelleri, E., Freibauer, A., and Schulze, E. D.: The European carbon balance. Part 2: Croplands, *Global Change Biol.*, 16, 1409–1428, 2010.
- Ciais, P., Sabine, C., Bala, G., Bopp, L., Brovkin, V., Canadell, J., Chhabra, A., DeFries, R., Galloway, J., Heimann, M., Jones, C., Le Quéré, C., Myneni, R. B., Piao, S., and Thornton, P.: Carbon and Other Biogeochemical Cycles, in: *Climate Change: The Physical Science Basis*, edited by Stocker, T. F., Qin, D., Plattner, G. K., Tignor, M., Allen, S. K., Boschung, J., Nauels, A., Xia, Y., Bex, V., and Midgley, P. M., pp. 465–570, Cambridge University Press, Cambridge, United Kingdoms and New York, NY, USA, 2013.
- Clapp, R. B. and Hornberger, G. M.: Empirical equations for some soil hydraulic properties, *Water Resour. Res.*, 14, doi:10.1029/WR014i004p00601, 1978.
- Collatz, G. J., Ball, J. T., Grivet, C., and Berry, J. A.: Physiological and environmental regulation of stomatal conductance, photosynthesis and transpiration: a model that includes a laminar boundary layer, *Agric. For. Meteorol.*, 54, 107–136, doi:10.1016/0168-1923(91)90002-8, 1991.
- Combe, M., Vilà-Guerau de Arellano, J., Ouwersloot, H. G., Jacobs, C. M. J., and Peters, W.: Two perspectives on the coupled carbon, water, and energy exchange in the planetary boundary layer, *Biogeosciences*, 12, 103–123, doi:10.5194/bg-12-103-2015, 2015.
- Combe, M., Vilà-Guerau de Arellano, J., Ouwersloot, H. G., and Peters, W.: Plant water-stress parameterization determines the strength of land–atmosphere coupling, *Agricultural and Forest Meteorology*, 217, 61–73, doi:10.1016/j.agrformet.2015.11.006, 2016.
- Corbin, K. D., Denning, A. S., Lokupitiya, E. Y., Schuh, A. E., Miles, N. L., Davis, K. J., Richardson, S., and Baker, I. T.: Assessing the impact of crops on regional CO₂ fluxes and atmospheric concentrations, *Tellus Ser. B*, 62, 521–532, doi:10.1111/j.1600-0889.2010.00485.x, 2010.
- Cowan, I. R.: Stomatal behaviour and environment, *Advances in botanical research*, 4, 117–228, 1978.

- Cox, P. M., Pearson, D., Booth, B. B., Friedlingstein, P., Huntingford, C., Jones, C. D., and Luke, C. M.: Sensitivity of tropical carbon to climate change constrained by carbon dioxide variability, *Nature*, 494, 341–344, doi:10.1038/nature11882, 2013.
- Daly, E., Porporato, A., and Rodriguez-Iturbe, I.: Coupled dynamics of photosynthesis, transpiration, and soil water balance. Part II: Stochastic analysis and ecohydrological significance, *J. Hydrometeorol.*, 5, 559–566, doi:10.1175/1525-7541(2004)005<0559:CDOPTA>2.0.CO;2, 2004.
- Davidson, E. A. and Janssens, I. A.: Temperature sensitivity of soil carbon decomposition and feedbacks to climate change., *Nature*, 440, 165–173, doi:10.1038/nature04514, 2006.
- de Bruin, H. A. R. and Holtslag, A. A. M.: A Simple Parameterization of the Surface Fluxes of Sensible and Latent-Heat During Daytime Compared with the Penman-Monteith Concept, *J. Appl. Meteorol.*, 21, 1610–1621, 1982.
- De Kauwe, M. G., Medlyn, B. E., Zaehle, S., Walker, A. P., Dietze, M. C., Hickler, T., Jain, A. K., Luo, Y., Parton, W. J., Prentice, I. C., Smith, B., Thornton, P. E., Wang, S., Wang, Y.-P., Wårlind, D., Weng, E., Crous, K. Y., Ellsworth, D. S., Hanson, P. J., Seok Kim, H., Warren, J. M., Oren, R., and Norby, R. J.: Forest water use and water use efficiency at elevated CO₂: a model-data inter-comparison at two contrasting temperate forest FACE sites, *Global Change Biology*, 19, 1759–1779, doi:10.1111/gcb.12164, 2013.
- de Noblet-Ducoudré, N., Gervois, S., Ciais, P., Viovy, N., Brisson, N., Seguin, B., and Perrier, A.: Coupling the Soil-Vegetation-Atmosphere-Transfer Scheme ORCHIDEE to the agronomy model STICS to study the influence of croplands on the European carbon and water budgets, *Agronomie*, 24, 397–407, 2004.
- De Pury, D. G. G. and Farquhar, G. D.: Simple scaling of photosynthesis from leaves to canopies without the errors of big-leaf models, *Plant Cell Environ.*, 20, 537–557, 1997.
- de Wit, A., Baruth, B., Boogaard, H., van Diepen, K., van Kraalingen, D., Micale, F., te Roller, J., Supit, I., and van den Wijngaart, R.: Using ERA-Interim for regional crop yield forecasting in Europe, *Climate Research*, 44, 41–53, doi:10.3354/cr00872, 2010.
- de Wit, A. J. W. and Van Diepen, C. A.: Crop model data assimilation with the Ensemble Kalman filter for improving regional crop yield forecasts, *Agric. For. Meteorol.*, 146, 38–56, 2007.
- de Wit, C. T.: Simulation of Assimilation, Respiration and Transpiration of Crops, Pudoc, Wageningen, the Netherlands, 1978.
- Dee, D. P., Uppala, S. M., Simmons, A. J., Berrisford, P., Poli, P., Kobayashi, S., Andrae, U., Balsameda, M. A., Balsamo, G., Bauer, P., Bechtold, P., Beljaars, A. C. M., van de Berg, L., Bidlot, J., Bormann, N., Delsol, C., Dragani, R., Fuentes, M., Geer, A. J., Haimberger, L., Healy, S. B., Hersbach, H., Hólm, E. V., Isaksen, L., Kållberg, P., Kohler, M., Matricardi, M., McNally, A. P., Monge Sanz, B. M., Morcrette, J. J., Park, B. K., Peubey, C., de Rosnay, P., Tavolato, C., Thépaut, J. N., and Vitart, F.: The ERA-Interim reanalysis: configuration and performance of the data assimilation system, *Quarterly Journal of the Royal Meteorological Society*, 137, 553–597, doi:10.1002/qj.828, 2011.
- Dekker, S. C., Groenendijk, M., Booth, B. B., Huntingford, C., and Cox, P. M.: Spatial and temporal variations in plant water-use efficiency inferred from tree-ring, eddy covariance and atmospheric observations, *Earth System Dynamics*, 7, 525–533, doi:10.5194/esd-7-525-2016, 2016.

REFERENCES

- Dirmeyer, P. A., Koster, R. D., and Guo, Z.: Do Global Models Properly Represent the Feedback between Land and Atmosphere?, *J. Hydrometeorol.*, 7, 1177–1198, 2006.
- Dua, V. K., Singh, B. P., Govindakrishnan, P. M., Kumar, S., and Lal, S. S.: Impact of climate change on potato productivity in Punjab – a simulation study, *Current Science*, 105, 787–794, 2013.
- Duykerke, P. G.: Radiation fog: a comparison of model simulation with detailed observations, *Mon. Weather Rev.*, 119, 324–341, doi:10.1175/1520-0493(1991)119<0324:RFACOM>2.0.CO;2, 1991.
- Egea, G., Verhoef, A., and Vidale, P. L.: Towards an improved and more flexible representation of water stress in coupled photosynthesis–stomatal conductance models, *Agric. For. Meteorol.*, 151, 1370–1384, doi:10.1016/j.agrformet.2011.05.019, 2011.
- Eitzinger, J., Formayer, H., Thaler, S., Trnka, M., Zdenek, Z., and Alexandrov, V.: Aspects on results and uncertainties of climate change impact simulation studies for agricultural crop production in Europe, *Bodenkultur*, 59, 131–147, 2008.
- Eitzinger, J., Thaler, S., Schmid, E., Strauss, F., Ferrise, R., Moriondo, M., Bindi, M., Palosuo, T., Rötter, R., Kersebaum, K. C., Olesen, J. E., Patil, R. H., Şaylan, L., Çaldağ, B., and Çaylak, O.: Sensitivities of crop models to extreme weather conditions during flowering period demonstrated for maize and winter wheat in Austria, *Journal of Agricultural Science*, 151, 813–835, 2013.
- Ek, M. B. and Holtslag, A. A. M.: Influence of soil moisture on boundary layer cloud development, *J. Hydrometeorol.*, 5, 86–99, doi:10.1175/1525-7541(2004)005<0086:IOSMOB>2.0.CO;2, 2004.
- EUROSTAT 2015: European regional statistics on agriculture, land use, and demography, Online database of the Statistical Office of the European Union, URL <http://ec.europa.eu/eurostat/web/regions/data/database>, Last accessed on February 18, 2016.
- FAOSTAT 2011 land-use statistics: The land-use resources sub-domain covers land area, temporary crops area and permanent crops area, FAOSTAT online database, URL <http://faostat3.fao.org/faostat-gateway/go/to/download/R/RL/E>, Last accessed on March 3, 2014.
- Farquhar, G. D., von Caemmerer, S., and Berry, J. A.: A biochemical model of photosynthetic CO₂ assimilation in leaves of C3 species, *Planta*, 149, 78–90, doi:10.1007/BF00386231, 1980.
- Farquhar, G. D., O’Leary, M. H., and Berry, J. A.: On the Relationship Between Carbon Isotope Discrimination and the Intercellular Carbon Dioxide Concentration in Leaves, *Australian Journal of Plant Physiology*, 9, 121–137, 1982.
- Farré, I. and Faci, J. M.: Comparative response of maize (*Zea mays* L.) and sorghum (*Sorghum bicolor* L. Moench) to deficit irrigation in a Mediterranean environment, *Agricultural Water Management*, 83, 135–143, doi:10.1016/j.agwat.2005.11.001, 2006.
- Fischer, E. M. and Knutti, R.: Detection of spatially aggregated changes in temperature and precipitation extremes, *Geophysical Research Letters*, 41, 547–554, doi:10.1002/2013GL058499, 2014.
- Foken, T.: The energy balance closure problem: An overview, *Ecological Applications*, 18, 1351–1367, 2008.
- Foken, T., Mauder, M., Liebethal, C., Wimmer, F., Beyrich, F., Leps, J. P., Raasch, S., DeBruin, H. A. R., Meijninger, W. M. L., and Bange, J.: Energy balance closure for the LITFASS-2003 experiment, *Theoretical and Applied Climatology*, 101, 149–160, 2010.

- Foltescu, V. L.: Prediction of crop yield in Sweden based on mesoscale meteorological analysis, *Meteorological Applications*, 7, 313–321, doi:10.1017/S1350482700001687, 2000.
- Frank, D., Reichstein, M., Bahn, M., Thonicke, K., Frank, D., Mahecha, M. D., Smith, P., van der Velde, M., Vicca, S., Babst, F., Beer, C., Buchmann, N., Canadell, J. G., Ciais, P., Cramer, W., Ibrom, A., Miglietta, F., Poulter, B., Rammig, A., Seneviratne, S. I., Walz, A., Wattenbach, M., Zavala, M. A., and Zscheischler, J.: Effects of climate extremes on the terrestrial carbon cycle: concepts, processes and potential future impacts, *Global Change Biology*, 21, 2861–2880, doi:10.1111/gcb.12916, 2015.
- Franks, P. J., Adams, M. A., Amthor, J. S., Barbour, M. M., Berry, J. A., Ellsworth, D. S., Farquhar, G. D., Ghannoum, O., Lloyd, J., McDowell, N., Norby, R. J., Tissue, D. T., and von Caemmerer, S.: Sensitivity of plants to changing atmospheric CO₂ concentration: from the geological past to the next century, *New Phytologist*, 197, 1077–1094, doi:10.1111/nph.12104, 2013.
- Friedlingstein, P., Cox, P., Betts, R., Bopp, L., Von Bloh, W., Brovkin, V., Cadule, P., Doney, S., Eby, M., Fung, I., Bala, G., John, J., Jones, C., Joos, F., Kato, T., Kawamiya, M., Knorr, W., Lindsay, K., Matthews, H. D., Raddatz, T., Rayner, P., Reick, C., Roeckner, E., Schnitzler, K. G., Schnur, R., Strassmann, K., Weaver, A. J., Yoshikawa, C., and Zeng, N.: Climate–Carbon Cycle Feedback Analysis: Results from the C⁴MIP Model Intercomparison, *J. Clim.*, 19, 3337–3353, doi:10.1175/JCLI3800.1, 2006.
- Gervois, S., De Noblet-Ducoudré, N., Viovy, N., Ciais, P., Brisson, N., Seguin, B., and Perrier, A.: Including croplands in a global biosphere model: methodology and evaluation at specific sites, *Earth Interactions*, 8, 1–25, 2004.
- Gervois, S., Ciais, P., de Noblet-Ducoudré, N., Brisson, N., Vuichard, N., and Viovy, N.: Carbon and water balance of European croplands throughout the 20th century, *Global Biogeochem. Cycles*, 22, GB2022, doi:10.1029/2007GB003018, 2008.
- Goudriaan, J.: *Crop micrometeorology: a simulation study*, Pudoc, Wageningen, the Netherlands, 1977.
- Grassi, G. and Magnani, F.: Stomatal, mesophyll conductance and biochemical limitations to photosynthesis as affected by drought and leaf ontogeny in ash and oak trees, *Plant Cell Environ.*, 28, 834–849, 2005.
- Gray, J. M., Frohling, S., Kort, E. A., Ray, D. K., Kucharik, C. J., Ramankutty, N., and Friedl, M. A.: Direct human influence on atmospheric CO₂ seasonality from increased cropland productivity, *Nature*, 515, 398–401, doi:10.1038/nature13957, 2014.
- Harman, I. N. and Finnigan, J. J.: A simple unified theory for flow in the canopy and roughness sublayer, *Bound.-Lay. Meteorol.*, 123, 339–363, doi:10.1007/s10546-006-9145-6, 2007.
- Hartmann, D. L., Klein Tank, A. M. G., Rusticucci, M., Alexander, L. V., Brönniman, S., Charabi, Y., Dentener, F. J., Dlugokenchy, E. J., Easterling, D. R., Kaplan, A., Soden, B. J., Thorne, P. W., Wild, M., and Zhai, P. M.: Observations: Atmosphere and Surface, in: *Climate Change: The Physical Science Basis*, edited by Stocker, T. F., Qin, D., Plattner, G. K., Tignor, M., Allen, S. K., Boschung, J., Nauels, A., Xia, Y., Bex, V., and Midgley, P. M., pp. 159–254, Cambridge University Press, Cambridge, United Kingdoms and New York, NY, USA, 2013.
- Hashimoto, S., Carvalhais, N., Ito, A., Migliavacca, M., Nishina, K., and Reichstein, M.: Global spatiotemporal distribution of soil respiration modeled using a global database, *Biogeosciences*, 12, 4121–4132, doi:10.5194/bg-12-4121-2015, 2015.

REFERENCES

- Hong, S., Lakshmi, V., Small, E. E., Chen, F., Tewari, M., and Manning, K. W.: Effects of vegetation and soil moisture on the simulated land surface processes from the coupled WRF/Noah model, *J. Geophys. Res.–Atmos.*, 114, D18 118, doi:10.1029/2008JD011249, 2009.
- Hope, C. and Schaefer, K.: Economic impacts of carbon dioxide and methane released from thawing permafrost, *Nature Climate Change*, 6, 56–59, doi:10.1038/nclimate2807, 2015.
- Huang, Y., Zhu, Y., Li, W. L., Cao, W. X., and Tian, Y. C.: Assimilating remotely sensed information with the wheatgrow model based on the ensemble square root filter for improving regional wheat yield forecasts, *Plant Production Science*, 16, 352–364, 2013.
- Ines, A. V. M., Das, N. N., Hansen, J. W., and Njoku, E. G.: Assimilation of remotely sensed soil moisture and vegetation with a crop simulation model for maize yield prediction, *Remote Sensing of Environment*, 138, 149–164, 2013.
- Jacobs, A. F. G., Heusinkveld, B. G., and Holtslag, A. A. M.: Seasonal and interannual variability of carbon dioxide and water balances of a grassland, *Climatic Change*, 82, 163–177, doi:10.1007/s10584-006-9182-7, 2007a.
- Jacobs, C., Jacobs, A., Bosveld, F. C., Hendriks, D., Hensen, A., Kroon, P. S., Moors, E. J., Nol, L., Schrier-Uijl, A., and Veenendaal, E. M.: Variability of annual CO₂ exchange from Dutch grasslands, *Biogeosciences*, 4, 803–816, doi:10.5194/bg-4-803-2007, 2007b.
- Jacobs, C. M. J.: Direct impact of atmospheric CO₂ enrichment on regional transpiration, Ph.D. thesis, Wageningen University, 1994.
- Jacobs, C. M. J., van den Hurk, B. M. M., and de Bruin, H. A. R.: Stomatal behaviour and photosynthetic rate of unstressed grapevines in semi-arid conditions, *Agric. For. Meteorol.*, 80, 111–134, doi:10.1016/0168-1923(95)02295-3, 1996.
- Jans, W. W. P., Jacobs, C. M. J., Kruijt, B., Elbers, J. A., Barendse, S., and Moors, E. J.: Carbon exchange of a maize (*Zea mays* L.) crop: Influence of phenology, *Agric. Ecosyst. Environ.*, 139, 316–324, doi:10.1016/j.agee.2010.06.008, 2010.
- Jarvis, P. G.: The Interpretation of the Variations in Leaf Water Potential and Stomatal Conductance Found in Canopies in the Field, *Philos. Trans. R. Soc. London, Ser. B*, 273, 593–610, doi:10.1098/rstb.1976.0035, 1976.
- Jégo, G., Pattey, E., and Liu, J.: Using Leaf Area Index, retrieved from optical imagery, in the STICS crop model for predicting yield and biomass of field crops, *Field Crops Research*, 131, 63–74, 2012.
- Joetzjer, E., Delire, C., Douville, H., Ciais, P., Decharme, B., Fisher, R., Christoffersen, B., Calvet, J. C., da Costa, A. C. L., Ferreira, L. V., and Meir, P.: Predicting the response of the Amazon rainforest to persistent drought conditions under current and future climates: a major challenge for global land surface models, *Geosci. Model Dev.*, 7, 2933–2950, doi:10.5194/gmd-7-2933-2014, 2014.
- Jongen, M., Pereira, J. S., Aires, L. M. I., and Pio, C. A.: The effects of drought and timing of precipitation on the inter-annual variation in ecosystem-atmosphere exchange in a Mediterranean grassland, *Agric. For. Meteorol.*, 151, 595–606, doi:10.1016/j.agrformet.2011.01.008, 2011.

- Karhu, K., Auffret, M. D., Dungait, J. A., Hopkins, D. W., Prosser, J. I., Singh, B. K., Subke, J. A., Wookey, P. A., Agren, G. I., Sebastià, M. T., Gouriveau, F., Bergkvist, G., Meir, P., Nottingham, A. T., Salinas, N., and Hartley, I. P.: Temperature sensitivity of soil respiration rates enhanced by microbial community response., *Nature*, 513, 81–84, doi:10.1038/nature13604, 2014.
- Kassie, B. T., Van Ittersum, M. K., Hengsdijk, H., Asseng, S., Wolf, J., and Rötter, R. P.: Climate-induced yield variability and yield gaps of maize (*Zea mays* L.) in the Central Rift Valley of Ethiopia, *Field Crops Research*, 160, 41–53, doi:10.1016/j.fcr.2014.02.010, 2014.
- Katul, G., Manzoni, S., Palmroth, S., and Oren, R.: A stomatal optimization theory to describe the effects of atmospheric CO₂ on leaf photosynthesis and transpiration, *Annals of Botany*, 105, 431–442, doi:10.1093/aob/mcp292, 2010.
- Keenan, T., Sabate, S., and Gracia, C.: Soil water stress and coupled photosynthesis–conductance models: Bridging the gap between conflicting reports on the relative roles of stomatal, mesophyll conductance and biochemical limitations to photosynthesis, *Agric. For. Meteorol.*, 150, 443–453, doi:10.1016/j.agrformet.2010.01.008, 2010a.
- Keenan, T., Sabate, S., and Gracia, C.: The importance of mesophyll conductance in regulating forest ecosystem productivity during drought periods, *Global Change Biol.*, 16, 1019–1034, doi:10.1111/j.1365-2486.2009.02017.x, 2010b.
- Keenan, T. F., Hollinger, D. Y., Bohrer, G., Dragoni, D., Munger, J. W., Schmid, H. P., and Richardson, A. D.: Increase in forest water-use efficiency as atmospheric carbon dioxide concentrations rise., *Nature*, 499, 324–327, 2013.
- Kogan, F., Kussul, N., Adamenko, T., Skakun, S., Kravchenko, O., Kryvobok, O., Shelestov, A., Kolotii, A., Kussul, O., and Lavrenyuk, A.: Winter wheat yield forecasting in Ukraine based on Earth observation, meteorological data and biophysical models, *International Journal of Applied Earth Observations and Geoinformation*, 23, 192–203, doi:10.1016/j.jag.2013.01.002, 2013.
- Kohler, M., Kalthoff, N., and Kottmeier, C.: The impact of soil moisture modifications on CBL characteristics in West Africa: A case–study from the AMMA campaign, *Quart. J. Roy. Meteorol. Soc.*, 136, 442–455, 2010.
- Koster, R. D.: Regions of Strong Coupling Between Soil Moisture and Precipitation, *Science*, 305, 1138–1140, doi:10.1126/science.1100217, 2004.
- Koster, R. D., Salvucci, G. D., Rigden, A. J., Jung, M., Collatz, G. J., and Schubert, S. D.: The pattern across the continental United States of evapotranspiration variability associated with water availability, *Frontiers in Earth Science*, 3, 1–10, doi:10.3389/feart.2015.00035, 2015.
- Krinner, G., Viovy, N., De Noblet-Ducoudré, N., Ogée, J., Polcher, J., Friedlingstein, P., Ciais, P., Sitch, S., and Prentice, I. C.: A dynamic global vegetation model for studies of the coupled atmosphere–biosphere system, *Global Biogeochem. Cycles*, 19, 1–33, doi:10.1029/2003GB002199, 2005.
- Kutsch, W. L., Aubinet, M., Buchmann, N., Smith, P., Osborne, B., Eugster, W., Wattenbach, M., Schrupf, M., Schulze, E. D., Tomelleri, E., Ceschia, E., Bernhofer, C., Béziat, P., Carrara, A., Di Tommasi, P., Grünwald, T., Jones, M., Magliulo, V., Marloie, O., Moureaux, C., Olioso, A., Sanz, M. J., Saunders, M., Sjøgaard, H., and Ziegler, W.: The net biome production of full crop rotations in Europe, "Agriculture, Ecosystems and Environment", 139, 336–345, 2010.

REFERENCES

- Lal, R.: Soil Carbon Sequestration Impacts on Global Climate Change and Food Security, *Science*, 304, 1623–1627, 2004.
- Lawlor, D. W.: Genetic engineering to improve plant performance under drought: physiological evaluation of achievements, limitations, and possibilities, *Journal of Experimental Botany*, 64, 83–108, doi:10.1093/jxb/ers326, 2013.
- Le Quéré, C., Moriarty, R., Andrew, R. M., Canadell, J. G., Sitch, S., Korsbakken, J. I., Friedlingstein, P., Peters, G. P., Andres, R. J., Boden, T. A., Houghton, R. A., House, J. I., Keeling, R. F., Tans, P., Arneeth, A., Bakker, D. C. E., Barbero, L., Bopp, L., Chang, J., Chevallier, F., Chini, L. P., Ciais, P., Fader, M., Feely, R. A., Gkritzalis, T., Harris, I., Hauck, J., Ilyina, T., Jain, A. K., Kato, E., Kitidis, V., Klein Goldewijk, K., Koven, C., Landschützer, P., Lauvset, S. K., Lefèvre, N., Lenton, A., Lima, I. D., Metz, N., Millero, F., Munro, D. R., Murata, A., Nabel, J. E. M. S., Nakaoka, S., Nojiri, Y., O'Brien, K., Olsen, A., Ono, T., Pérez, F. F., Pfeil, B., Pierrot, D., Poulter, B., Rehder, G., Rödenbeck, C., Saito, S., Schuster, U., Schwinger, J., Séférian, R., Steinhoff, T., Stocker, B. D., Sutton, A. J., Takahashi, T., Tilbrook, B., van der Laan-Luijkx, I. T., van der WERF, G. R., van Heuven, S., Vandemark, D., Viovy, N., Wiltshire, A., Zaehle, S., and Zeng, N.: Global Carbon Budget 2015, *Earth System Science Data*, 7, 349–396, doi:10.5194/essd-7-349-2015, 2015.
- Lehuger, S., Gabrielle, B., Cellier, P., Loubet, B., Roche, R., Béziat, P., Ceschia, E., and Wattenbach, M.: Predicting the net carbon exchanges of crop rotations in Europe with an agro-ecosystem model, *Agric. Ecosyst. Environ.*, 139, 384–395, 2010.
- Leuning, R., Kelliher, F. M., Pury, D. G. G., and Schulze, E. D.: Leaf nitrogen, photosynthesis, conductance and transpiration: scaling from leaves to canopies, *Plant Cell Environ.*, 18, 1183–1200, doi:10.1111/j.1365-3040.1995.tb00628.x, 1995.
- Li, Y., Zhou, J., Kinzelbach, W., Cheng, G., Li, X., and Zhao, W.: Coupling a SVAT heat and water flow model, a stomatal-photosynthesis model and a crop growth model to simulate energy, water and carbon fluxes in an irrigated maize ecosystem, *Agricultural and Forest Meteorology*, 176, 10–24, doi:10.1016/j.agrformet.2013.03.004, 2013.
- Lilly, D. K.: Models of cloud-topped mixed layers under a strong inversion, *Quart. J. Roy. Meteorol. Soc.*, 94, 292–309, doi:10.1002/qj.49709440106, 1968.
- Lloyd, J. and Taylor, J. A.: On the temperature dependence of soil respiration, *Functional ecology*, 8, 315–323, doi:10.2307/2389824, 1994.
- Lobell, D. B., Schlenker, W., and Costa-Roberts, J.: Climate Trends and Global Crop Production Since 1980, *Science*, 333, 616–620, 2011.
- Lohila, A., Aurela, M., Tuovinen, J.-P., and Laurila, T.: Annual CO₂ exchange of a peat field growing spring barley or perennial forage grass, *Journal of Geophysical Research*, 109, D18 116, doi:10.1029/2004JD004715, 2004.
- Lokupitiya, E., Denning, S., Paustian, K., Baker, I., Schaefer, K., Verma, S., Meyers, T., Bernacchi, C. J., Suyker, A., and Fischer, M.: Incorporation of crop phenology in Simple Biosphere Model (SiBcrop) to improve land-atmosphere carbon exchanges from croplands, *Biogeosciences*, 6, 969–986, 2009.

- Loubet, B., Laville, P., Lehuger, S., Larmanou, E., Fléchar, C., Mascher, N., Genermont, S., Roche, R., Ferrara, R. M., Stella, P., Personne, E., Durand, B., Decuq, C., Flura, D., Masson, S., Fanucci, O., Rampon, J.-N., Siemens, J., Kindler, R., Gabrielle, B., Schrupf, M., and Cellier, P.: Carbon, nitrogen and Greenhouse gases budgets over a four years crop rotation in northern France, *Plant and Soil*, 343, 109–137, doi:10.1007/s11104-011-0751-9, 2011.
- Maseyk, K., Hemming, D., Angert, A., Leavitt, S. W., and Yakir, D.: Increase in water-use efficiency and underlying processes in pine forests across a precipitation gradient in the dry Mediterranean region over the past 30 years, *Oecologia*, 167, 573–585, doi:10.1007/s00442-011-2010-4, 2011.
- McDowell, N. G., Fisher, R. A., Xu, C., Domec, J. C., Hölttä, T., Mackay, D. S., Sperry, J. S., Boutz, A., Dickman, L., Gehres, N., Limousin, J. M., Macalady, A., Martínez-Vilalta, J., Mencuccini, M., Plaut, J. A., Ogee, J., Pangle, R. E., Rasse, D. P., Ryan, M. G., Sevanto, S., Waring, R. H., Williams, A. P., Yezpe, E. A., and Pockman, W. T.: Evaluating theories of drought-induced vegetation mortality using a multimodel-experiment framework., *New Phytol.*, 200, 304–321, doi:10.1111/nph.12465, 2013.
- McGrath-Spangler, E. L. and Denning, A. S.: Impact of entrainment from overshooting thermals on land-atmosphere interactions during summer 1999, *Tellus Ser. B*, 62, 441–454, doi:10.1111/j.1600-0889.2010.00482.x, 2010.
- Medlyn, B. E., Duursma, R. A., Eamus, D., Ellsworth, D. S., Prentice, I. C., Barton, C. V. M., Crous, K. Y., de Angelis, P., Freeman, M., and Wingate, L.: Reconciling the optimal and empirical approaches to modelling stomatal conductance, *Global Change Biology*, 17, 2134–2144, doi:10.1111/j.1365-2486.2010.02375.x, 2011.
- Meir, P., Cox, P., and Grace, J.: The influence of terrestrial ecosystems on climate, *Trends in Ecology & Evolution*, 21, 254–260, 2006.
- Meyers, T. P. and Hollinger, S. E.: An assessment of storage terms in the surface energy balance of maize and soybean, *Agric. For. Meteorol.*, 125, 105–115, 2004.
- Miralles, D. G., Teuling, A. J., van Heerwaarden, C. C., and Vilà-Guerau de Arellano, J.: Mega-heatwave temperatures due to combined soil desiccation and atmospheric heat accumulation, *Nat. Geosci.*, 7, 345–349, doi:10.1038/ngeo2141, 2014.
- Moors, E. J., Jacobs, C., Jans, W., Supit, I., Kutsch, W. L., Bernhofer, C., Béziat, P., Buchmann, N., Carrara, A., Ceschia, E., Elbers, J., Eugster, W., Kruijt, B., Loubet, B., Magliulo, E., Moureaux, C., Olioso, A., Saunders, M., and Soegaard, H.: Variability in carbon exchange of European croplands, *Agriculture, Ecosystems and Environment*, 139, 325–335, doi:10.1016/j.agee.2010.04.013, 2010.
- Moreira, D. S., Freitas, S. R., Bonatti, J. P., Mercado, L. M., Rosário, N. M. É., Longo, K. M., Miller, J. B., Gloor, M., and Gatti, L. V.: Coupling between the JULES land-surface scheme and the CCATT-BRAMS atmospheric chemistry model (JULES-CCATT-BRAMS1.0): applications to numerical weather forecasting and the CO₂ budget in South America, *Geosci. Model Dev.*, 6, 1243–1259, 2013.
- Moureaux, C., Debacq, A., Bodson, B., Heinesch, B., and Aubinet, M.: Annual net ecosystem carbon exchange by a sugar beet crop, *Agricultural and Forest Meteorology*, 139, 25–39, 2006.
- Mueller, B. and Seneviratne, S. I.: Hot days induced by precipitation deficits at the global scale, *Proceedings of the National Academy of Sciences*, 109, 12 398–12 403, doi:10.1073/pnas.1204330109, 2012.

REFERENCES

- Myhre, G., Shindell, D., Bréon, F.-M., Collins, W., Fuglestedt, J., Huang, J., Koch, D., Lamarque, J.-F., Lee, D., Mendoza, B., Nakajima, T., Robock, A., Stephens, G., Takemura, T., and Zhang, H.: Anthropogenic and Natural Radiative Forcing, in: *Climate Change The Physical Science Basis*, edited by Stocker, T. F., Qin, D., Plattner, G. K., Tignor, M., Allen, S. K., Boschung, J., Nauels, A., Xia, Y., Bex, V., and Midgley, P. M., pp. 659–740, Cambridge University Press, Cambridge, doi:10.1017/cbo9781107415324.018, 2013.
- Niu, S., Luo, Y., Li, D., Cao, S., Xia, J., Li, J., and Smith, M. D.: Plant growth and mortality under climatic extremes: An overview, *Environmental and Experimental Botany*, 98, 13–19, doi:10.1016/j.envexpbot.2013.10.004, 2014.
- Noilhan, J. and Planton, S.: A simple parameterization of land surface processes for meteorological models, *Mon. Weather Rev.*, 117, 536–549, doi:10.1175/1520-0493(1989)117<0536:ASPOLS>2.0.CO;2, 1989.
- Ouwersloot, H. G., Vilà-Guerau De Arellano, J., Nölscher, A. C., Krol, M. C., Ganzeveld, L. N., Breitenberger, C., Mammarella, I., Williams, J., and Lelieveld, J.: Characterization of a boreal convective boundary layer and its impact on atmospheric chemistry during HUMPPA-COPEC-2010, *Atmos. Chem. Phys.*, 12, 9335–9353, doi:10.5194/acp-12-9335-2012, 2012.
- Pan, Y., Birdsey, R. A., Fang, J., and Houghton, R.: A large and persistent carbon sink in the world's forests, *Science*, 333, 988–993, doi:10.1126/science.1201609, 2011.
- Peel, M. C., Finlayson, B. L., and McMahon, T. A.: Updated world map of the Köppen-Geiger climate classification, *Hydrology and Earth System Sciences*, 11, 1633–1644, doi:10.5194/hess-11-1633-2007, 2007.
- Peltonen-Sainio, P., Jauhainen, L., Palosuo, T., Hakala, K., and Ruosteenoja, K.: Rainfed crop production challenges under European high-latitude conditions, *Regional Environmental Change*, 16, 1521–1533, doi:10.1007/s10113-015-0875-1, 2015.
- Peng, S., Ciais, P., Chevallier, F., Peylin, P., Cadule, P., Sitch, S., Piao, S., Ahlström, A., Huntingford, C., Levy, P., Li, X., Liu, Y., Lomas, M., Poulter, B., Viovy, N., Wang, T., Wang, X., Zaehle, S., Zeng, N., Zhao, F., and Zhao, H.: Benchmarking the seasonal cycle of CO₂ fluxes simulated by terrestrial ecosystem models, *Global Biogeochemical Cycles*, 29, 46–64, doi:10.1002/2014gb004931, 2015.
- Penning De Vries, F. W. T., Brunsting, A. H. M., and Van Laar, H. H.: Products, requirements and efficiency of biosynthesis a quantitative approach, *Journal of Theoretical Biology*, 45, 339–377, doi:10.1016/0022-5193(74)90119-2, 1974.
- Peñuelas, J., Rutishauser, T., and Filella, I.: Phenology Feedbacks on Climate Change, *Science*, 324, 887–888, doi:10.1126/science.1173004, 2009.
- Peters, W., Krol, M. C., van der Werf, G. R., Houweling, S., Jones, C. D., Hughes, J., Schaefer, K., Masarie, K. A., Jacobson, A. R., Miller, J. B., Cho, C. H., Ramonet, M., Schmidt, M., Ciattaglia, L., Apadula, F., Heltai, D., Meinhardt, F., di Sarra, A. G., Piacentino, S., Sferlazzo, D., Aalto, T., Hatakka, J., Ström, J., Haszpra, L., Meijer, H. A. J., van der Laan, S., Neubert, R. E. M., Jordan, A., Rodó, X., Morguí, J. A., Vermeulen, A. T., Popa, E., Rozanski, K., Zimnoch, M., Manning, A. C., Leuenberger, M., Uglietti, C., Dolman, A. J., Ciais, P., Heimann, M., and Tans, P. P.: Seven years of recent European net terrestrial carbon dioxide exchange constrained by atmospheric observations, *Global Change Biol.*, 16, 1317–1337, 2010.

- Pietersen, H. P., Vilà-Guerau De Arellano, J., Augustin, P., van de Boer, A., de Coster, O., Delbarre, H., Durand, P., Fourmentin, M., Gioli, B., Hartogensis, O., Lohou, F., Lothon, M., Ouwensloot, H. G., Pino, D., and Reuder, J.: Study of a prototypical convective boundary layer observed during BLLAST: contributions by large-scale forcings, *Atmos. Chem. Phys.*, 15, 4241–4257, doi:10.5194/acp-15-4241-2015, 2015.
- Pingali, P. L.: Green Revolution: Impacts, limits, and the path ahead, *Proceedings of the National Academy of Sciences*, 109, 12 302–12 308, doi:10.1073/pnas.0912953109, 2012.
- Pino, D., de Arellano, J. V. G., and Kim, S. W.: Representing sheared convective boundary layer by zeroth- and first-order-jump mixed-layer models: Large-eddy simulation verification, *J. Appl. Meteorol. Clim.*, 45, 1224–1243, 2006.
- Pino, D., Vilà-Guerau de Arellano, J., Peters, W., Schröter, J., Heerwaarden, C. C. v., and Krol, M. C.: A conceptual framework to quantify the influence of convective boundary layer development on carbon dioxide mixing ratios, *Atmos. Chem. Phys.*, 12, 2969–2985, doi:10.5194/acp-12-2969-2012, 2012.
- Powell, T. L., Galbraith, D. R., Christoffersen, B. O., Harper, A., Imbuzeiro, H. M. A., Rowland, L., Almeida, S., Brando, P. M., da Costa, A. C. L., Costa, M. H., Levine, N. M., Malhi, Y., Saleska, S. R., Sotta, E., Williams, M., Meir, P., and Moorcroft, P. R.: Confronting model predictions of carbon fluxes with measurements of Amazon forests subjected to experimental drought, *New Phytol.*, 200, 350–365, doi:10.1111/nph.12390, 2013.
- Prescher, A.-K., Grünwald, T., and Bernhofer, C.: Land use regulates carbon budgets in eastern Germany: From NEE to NBP, *Agricultural and Forest Meteorology*, 150, 1016–1025, doi:10.1016/j.agrformet.2010.03.008, 2010.
- Ramankutty, N., Foley, J. A., and Olejniczak, N. J.: People on the land: Changes in global population and croplands during the 20th century, *AMBIO: A Journal of the Human ...*, 31, 251, doi:10.1639/0044-7447(2002)031[0251:potlci]2.0.co;2, 2002.
- Reichstein, M., Falge, E., Baldocchi, D., Papale, D., Aubinet, M., Berbigier, P., Bernhofer, C., Buchmann, N., Gilmanov, T., Granier, A., Grünwald, T., Havránková, K., Ilvesniemi, H., Janous, D., Knohl, A., Laurila, T., Lohila, A., Loustau, D., Matteucci, G., Meyers, T., Miglietta, F., Ourcival, J.-M., Pumpanen, J., Rambal, S., Rotenberg, E., Sanz, M., Tenhunen, J., Seufert, G., Vaccari, F., Vesala, T., Yakir, D., and Valentini, R.: On the separation of net ecosystem exchange into assimilation and ecosystem respiration: review and improved algorithm, *Global Change Biology*, 11, 1424–1439, doi:10.1111/j.1365-2486.2005.001002.x, 2005.
- Richardson, A. D., Anderson, R. S., Arain, M. A., Barr, A. G., Bohrer, G., Chen, G., Chen, J. M., Ciais, P., Davis, K. J., Desai, A. R., Dietze, M. C., Dragoni, D., Garrity, S. R., Gough, C. M., Grant, R., Hollinger, D. Y., Margolis, H. A., McCaughey, H., Migliavacca, M., Monson, R. K., Munger, J. W., Poulter, B., Raczka, B. M., Ricciuto, D. M., Sahoo, A. K., Schaefer, K., Tian, H., Vargas, R., Verbeeck, H., Xiao, J., and Xue, Y.: Terrestrial biosphere models need better representation of vegetation phenology: results from the North American Carbon Program Site Synthesis, *Global Change Biology*, 18, 566–584, doi:10.1111/j.1365-2486.2011.02562.x, 2011.
- Richardson, A. D., Keenan, T. F., Migliavacca, M., Ryu, Y., Sonnentag, O., and Toomey, M.: Climate change, phenology, and phenological control of vegetation feedbacks to the climate system, *Agric. For. Meteorol.*, 169, 156–173, doi:10.1016/j.agrformet.2012.09.012, 2013.

REFERENCES

- Roberts, L.: 9 Billion?, *Science*, 333, 540–543, doi:10.1126/science.333.6042.540, 2011.
- Ronda, R. J., De Bruin, H. A. R., and Holtslag, A. A. M.: Representation of the canopy conductance in modeling the surface energy budget for low vegetation, *J. Appl. Meteorol.*, 40, 1431–1444, doi:10.1175/1520-0450(2001)040<1431:ROTCCI>2.0.CO;2, 2001.
- Rosenzweig, C., Jones, J. W., Hatfield, J. L., Ruane, A. C., Boote, K. J., Thorburn, P., Antle, J. M., Nelson, G. C., Porter, C., Janssen, S., Asseng, S., Basso, B., Ewert, F., Wallach, D., Baigorria, G., and Winter, J. M.: The Agricultural Model Intercomparison and Improvement Project (AgMIP): Protocols and pilot studies, *Agricultural and Forest Meteorology*, 170, 166–182, doi:10.1016/j.agrformet.2012.09.011, 2013.
- Sabater, J. M., Rüdiger, C., Calvet, J. C., Fritz, N., Jarlan, L., and Kerr, Y.: Joint assimilation of surface soil moisture and LAI observations into a land surface model, *Agric. For. Meteorol.*, 148, 1362–1373, 2008.
- Sánchez, B., Rasmussen, A., and Porter, J. R.: Temperatures and the growth and development of maize and rice: A review, *Global Change Biol.*, 20, 408–417, 2014.
- Santanello, Jr, J. A., Peters-Lidard, C. D., Kumar, S. V., Alonge, C., and Tao, W. K.: A modeling and observational framework for diagnosing local land-atmosphere coupling on diurnal time scales, *J. Hydrometeorol.*, 10, 577–599, 2009.
- Santanello, Jr, J. A., Peters-Lidard, C. D., Kennedy, A., and Kumar, S. V.: Diagnosing the Nature of Land–Atmosphere Coupling: A Case Study of Dry/Wet Extremes in the U.S. Southern Great Plains, *J. Hydrometeorol.*, 14, 3–24, doi:10.1175/JHM-D-12-023.1, 2013.
- Sargordi, F., Bansouleh, B. F., Sharifi, M. A., and Van Keulen, H.: Spatio-temporal variation of wheat and silage maize water requirement using CGMS model, *International Journal of . . .*, 7, 207–224, 2013.
- Schaefer, K., Collatz, G. J., Tans, P., Denning, A. S., Baker, I., Berry, J., Prihodko, L., Suits, N., and Philpott, A.: Combined Simple Biosphere/Carnegie-Ames-Stanford Approach terrestrial carbon cycle model, *J. Geophys. Res.*, 113, G03 034, 2008.
- Scheid, F.: Gaussian integration, in: *Theory and problems of numerical analysis*, McGraw-Hill Book Company, New York, USA, 1968.
- Schuh, A. E., Denning, A. S., and Corbin, K. D.: A regional high-resolution carbon flux inversion of North America for 2004, *Biogeosciences*, 7, 1625–1644, doi:10.5194/bg-7-1625-2010, 2010.
- Seneviratne, S. I., Corti, T., Davin, E. L., Hirschi, M., Jaeger, E. B., Lehner, I., Orlowsky, B., and Teuling, A. J.: Investigating soil moisture-climate interactions in a changing climate: A review, *Earth Sci. Rev.*, 99, 125–161, doi:10.1016/j.earscirev.2010.02.004, 2010.
- Seneviratne, S. I., Nicholls, M., Easterling, D. R., Goodess, C. M., Kanae, S., Kossin, J., Luo, Y., Marengo, J., McInnes, K., Rahimi, M., Reichstein, M., Sorteberg, A., Vera, C., and Zhang, X.: Changes in Climate Extremes and their Impacts on the Natural Physical Environment, in: *Managing the Risks of Extreme Events and Disasters to Advance Climate Change Adaptation*, edited by Field, C. B., Barros, V., Stocker, T. F., Qin, D., Dokken, D. J., Ebi, K. L., Mastrandrea, M. D., Mach, K. J., Plattner, G. K., Allen, S. K., Tignor, M., and Midgley, P. M., pp. 109–230, Cambridge, UK, and New York, NY, USA, 2012.

- Shi, Y., Matsunaga, T., Saito, M., Yamaguchi, Y., and Chen, X.: Comparison of global inventories of CO₂ emissions from biomass burning during 2002-2011 derived from multiple satellite products, *Environmental Pollution*, 206, 479–487, doi:10.1016/j.envpol.2015.08.009, 2015.
- Silva, L. C. R. and Horwath, W. R.: Explaining Global Increases in Water Use Efficiency: Why Have We Overestimated Responses to Rising Atmospheric CO₂ in Natural Forest Ecosystems?, *PLoS ONE*, 8, e53 089, doi:10.1371/journal.pone.0053089, 2013.
- Sinclair, T. S. and de Wit, C. T.: Photosynthate and nitrogen requirements for seed production by various crops, *Science*, 189, 565–567, 1975.
- Sitch, S., Smith, B., Prentice, I. C., Arneth, A., Bondeau, A., Cramer, W., Kaplan, J. O., Levis, S., Lucht, W., and Sykes, M. T.: Evaluation of ecosystem dynamics, plant geography and terrestrial carbon cycling in the LPJ dynamic global vegetation model, *Global Change Biol.*, 9, 161–185, doi:10.1046/j.1365-2486.2003.00569.x, 2003.
- Sitch, S., Huntingford, C., Gedney, N., Levy, P. E., Lomas, M., Piao, S. L., Betts, R., Ciais, P., Cox, P., Friedlingstein, P., Jones, C. D., Prentice, I. C., and Woodward, F. I.: Evaluation of the terrestrial carbon cycle, future plant geography and climate–carbon cycle feedbacks using five Dynamic Global Vegetation Models (DGVMs), *Global Change Biol.*, 14, 2015–2039, doi:10.1111/j.1365-2486.2008.01626.x, 2008.
- Skamarock, W. C., Klemp, J. B., Dudhia, J., Gill, D. O., Barker, D. M., Duda, M. G., Huang, X. Y., Wang, W., and Powers, J. G.: A Description of the Advanced Research WRF Version 3, Tech. Rep. NCAR Technical Note NCAR/TN-475+STR, NCAR, Boulder, Colorado, USA, 2012.
- Smallman, T. L., Moncrieff, J. B., and Williams, M.: WRFv3.2-SPAv2: development and validation of a coupled ecosystem–atmosphere model, scaling from surface fluxes of CO₂ and energy to atmospheric profiles, *Geosci. Model Dev.*, 6, 1079–1093, 2013.
- Smith, P., Bustamante, M., Ahammad, H., Clark, H., Dong, H., Elsiddig, E. A., Haberl, H., Harper, R., House, J., Jafari, M., Masera, O., Mbow, C., Ravindranath, N. H., Rice, C. W., Robledo Abad, C., Romanovskaya, A., Sperling, F., and Tubiello, F.: Agriculture, Forestry and Other Land Use (AFOLU), in: *Climate Change 2014: Mitigation of Climate Change*, edited by Edenhofer, O., Pichs-Madruga, R., Sokona, Y., Farahani, E., Kadner, S., Seyboth, K., Adler, A., Baum, I., Brunner, S., Eickemeier, P., Kriemann, B., Savolainen, J., Schlömer, S., von Stechow, C., Zwickel, T., and Minx, J. C., pp. 811–922, Cambridge University Press, Cambridge, United Kingdoms and New York, NY, USA, 2014.
- Smith, P. C., De Noblet-Ducoudré, N., Ciais, P., Peylin, P., Viovy, N., Meurdesoif, Y., and Bondeau, A.: European-wide simulations of croplands using an improved terrestrial biosphere model: Phenology and productivity, *J. Geophys. Res.*, 115, G01 014, 2010.
- Spinoni, J., Naumann, G., Vogt, J. V., and Barbosa, P.: The biggest drought events in Europe from 1950 to 2012, *Journal of Hydrology: Regional Studies*, 3, 509–524, doi:10.1016/j.ejrh.2015.01.001, 2015.
- Stull, R. B.: Boundary Conditions and Surface Forcings, in: *An Introduction to Boundary Layer Meteorology*, edited by Stull, R. B., pp. 251–294, Springer Netherlands, doi:10.1007/978-94-009-3027-8_7, 1988.

REFERENCES

- Super, I., Vilà-Guerau de Arellano, J., and Krol, M. C.: Cumulative ozone effect on canopy stomatal resistance and the impact on boundary layer dynamics and CO₂ assimilation at the diurnal scale: A case study for grassland in the Netherlands, *Journal of Geophysical Research: Biogeosciences*, 120, 1348–1365, doi:10.1002/2015JG002996, 2015.
- Supit, I., Hooijer, A. A., and Van Diepen, C. A., eds.: System description of the WOFOST 6.0 crop simulation model implemented in the CGMS Vol. 1: Theory and algorithms, European Commission, Brussels, Luxembourg, 1994.
- Sus, O., Williams, M., Bernhofer, C., Béziat, P., Buchmann, N., Ceschia, E., Doherty, R., Eugster, W., Grünwald, T., Kutsch, W., Smith, P., and Wattenbach, M.: A linked carbon cycle and crop developmental model: Description and evaluation against measurements of carbon fluxes and carbon stocks at several European agricultural sites, *Agric. Ecosyst. Environ.*, 139, 402–418, 2010.
- Tao, S., Shen, S., Li, Y., Wang, Q., Gao, P., and Mugume, I.: Projected Crop Production under Regional Climate Change Using Scenario Data and Modeling: Sensitivity to Chosen Sowing Date and Cultivar, *Sustainability*, 8, 214–23, doi:10.3390/su8030214, 2016.
- Tao, Z., Santanello, J. A., Chin, M., Zhou, S., Tan, Q., Kemp, E. M., and Peters-Lidard, C. D.: Effect of land cover on atmospheric processes and air quality over the continental United States – a NASA Unified WRF (NU-WRF) model study, *Atmos. Chem. Phys.*, 13, 6207–6226, doi:10.5194/acp-13-6207-2013, 2013.
- Tardieu, F. and Simonneau, T.: Variability among species of stomatal control under fluctuating soil water status and evaporative demand: Modelling isohydric and anisohydric behaviours, *J. Exp. Bot.*, 49, 419–432, doi:10.1093/jxb/49.Special_Issue.419, 1998.
- Tennekes, H.: A model for the dynamics of the inversion above a convective boundary layer, *J. Atmos. Sci.*, 30, 558–567, doi:10.1175/1520-0469(1973)030<0558:AMFTDO>2.0.CO;2, 1973.
- Teuling, A. J., Seneviratne, S. I., Stöckli, R., Reichstein, M., Moors, E., Ciais, P., Luyssaert, S., van den Hurk, B., Ammann, C., Bernhofer, C., Dellwik, E., Gianelle, D., Gielen, B., Grünwald, T., Klumpp, K., Montagnani, L., Moureaux, C., Sottocornola, M., and Wohlfhart, G.: Contrasting response of European forest and grassland energy exchange to heatwaves, *Nat. Geosci.*, 3, 722–727, doi:10.1038/ngeo950, 2010.
- Tolk, L. F., Peters, W., Meesters, A. G. C. A., Groenendijk, M., Vermeulen, A. T., Steeneveld, G. J., and Dolman, A. J.: Modelling regional scale surface fluxes, meteorology and CO₂ mixing ratios for the Cabauw tower in the Netherlands, *Biogeosciences*, 6, 2265–2280, 2009.
- Twine, T. E., Kustas, W. P., Norman, J. M., Cook, D. R., Houser, P. R., Meyers, T. P., Prueger, J. H., Starks, P. J., and Wesely, M. L.: Correcting eddy-covariance flux underestimates over a grassland, *Agric. For. Meteorol.*, 103, 279–300, 2000.
- Van den Berg, M., Driessen, P. M., and Rabbinge, R.: Water uptake in crop growth models for land use systems analysis: II. Comparison of three simple approaches, *Ecological Modelling*, 148, 233–250, doi:10.1016/s0304-3800(01)00436-7, 2002.
- van der Molen, M. K., Dolman, A. J., Ciais, P., Eglin, T., Gobron, N., Law, B. E., Meir, P., Peters, W., Phillips, O. L., Reichstein, M., Chen, T., Dekker, S. C., Doubková, M., Friedl, M. A., Jung, M., van den Hurk, B. J. J. M., de Jeu, R. A. M., Kruijt, B., Ohta, T., Rebel, K. T., Plummer, S.,

- Seneviratne, S. I., Sitch, S., Teuling, A. J., van der Werf, G., and Wang, G.: Drought and ecosystem carbon cycling, *Agric. For. Meteorol.*, 151, 765–773, doi:10.1016/j.agrformet.2011.01.018, 2011.
- van der Velde, I. R., MILLER, J. B., SCHAEFER, K., van der WERF, G. R., Krol, M. C., and Peters, W.: Terrestrial cycling of ^{13}C by photosynthesis, respiration, and biomass burning in SiBCASA, *Biogeosciences*, 11, 6553–6571, doi:10.5194/bg-11-6553-2014, 2014.
- van Heerwaarden, C. C. and Teuling, A. J.: Disentangling the response of forest and grassland energy exchange to heatwaves under idealized land–atmosphere coupling, *Biogeosciences*, 11, 6159–6171, doi:10.5194/bg-11-6159-2014, 2014.
- van Heerwaarden, C. C., Vilà-Guerau de Arellano, J., Moene, A. F., and Holtslag, A. A. M.: Interactions between dry-air entrainment, surface evaporation and convective boundary-layer development, *Quart. J. Roy. Meteorol. Soc.*, 135, 1277–1291, doi:10.1002/qj.431, 2009.
- van Heerwaarden, C. C., Vilà-Guerau de Arellano, J., Gounou, A., Guichard, F., and Couvreux, F.: Understanding the Daily Cycle of Evapotranspiration: A Method to Quantify the Influence of Forcings and Feedbacks, *J. Hydrometeorol.*, 11, 1405–1422, doi:10.1175/2010JHM1272.1, 2010.
- van Ittersum, M. K., Leffelaar, P. A., Van Keulen, H., Kropff, M. J., Bastiaans, L., and Goudriaan, J.: On approaches and applications of the Wageningen crop models, *Eur. J. Agron.*, 18, 201–234, 2003.
- van Keulen, H.: Simulation of water use and herbage growth in arid regions, Pudoc, Wageningen, the Netherlands, 1975.
- van Stratum, B. J. H., Vilà-Guerau de Arellano, J., van Heerwaarden, C. C., and Ouwersloot, H. G.: Subcloud-Layer Feedbacks Driven by the Mass Flux of Shallow Cumulus Convection over Land, *J. Atmos. Sci.*, 71, 881–895, doi:10.1175/JAS-D-13-0192.1, 2014.
- Verhoef, A. and Egea, G.: Modeling plant transpiration under limited soil water: Comparison of different plant and soil hydraulic parameterizations and preliminary implications for their use in land surface models, *Agric. For. Meteorol.*, doi:10.1016/j.agrformet.2014.02.009, 2014.
- Vilà-Guerau De Arellano, J., Gioli, B., Miglietta, F., Jonker, H. J. J., Baltink, H. K., Hutjes, R. W. A., and Holtslag, A. A. M.: Entrainment process of carbon dioxide in the atmospheric boundary layer, *J. Geophys. Res.–Atmos.*, 109, D18 110, doi:10.1029/2004JD004725, 2004.
- Vilà-Guerau de Arellano, J., van den Dries, K., and Pino, D.: On inferring isoprene emission surface flux from atmospheric boundary layer concentration measurements, *Atmos. Chem. Phys.*, 9, 3629–3640, 2009.
- Vilà-Guerau de Arellano, J., van Heerwaarden, C. C., and Lelieveld, J.: Modelled suppression of boundary-layer clouds by plants in a CO_2 -rich atmosphere, *Nat. Geosci.*, 5, 1–4, doi:10.1038/ngeo1554, 2012.
- Vilà-Guerau de Arellano, J., Ouwersloot, H. G., Baldocchi, D., and Jacobs, C. M. J.: Shallow cumulus rooted in photosynthesis, *Geophys. Res. Lett.*, 41, 1796–1802, doi:10.1002/2014GL059279, 2014.
- Vilà-Guerau de Arellano, J., van Heerwaarden, C. C., van Stratum, B. J. H., and van den Dries, K.: Atmospheric boundary layer: integrating atmospheric chemistry and land interactions, Cambridge University Press, Cambridge, UK, 2015.

REFERENCES

- Vitale, L., Di Tommasi, P., Arena, C., Fierro, A., Virzo De Santo, A., and Magliulo, V.: Effects of water stress on gas exchange of field grown *Zea mays* L. in Southern Italy: an analysis at canopy and leaf level, *Acta Physiologiae Plantarum*, 29, 317–326, doi:10.1007/s11738-007-0041-6, 2007.
- Wang, T., Lu, C., and Yu, B.: Production potential and yield gaps of summer maize in the Beijing-Tianjin-Hebei Region, *Journal of Geographical Sciences*, 21, 677–688, doi:10.1007/s11442-011-0872-3, 2011.
- West, T. O., Brandt, C. C., Wilson, B. S., Hellwinckel, C. M., Tyler, D. D., Marland, G., De La Torre Ugarte, D. G., Larson, J. A., and Nelson, R. G.: Estimating Regional Changes in Soil Carbon with High Spatial Resolution, *Soil Science Society of America Journal*, 72, 285, 2008.
- West, T. O., Marland, G., Singh, N., Bhaduri, B. L., and Roddy, A. B.: The human carbon budget: an estimate of the spatial distribution of metabolic carbon consumption and release in the United States, *Biogeochemistry*, 94, 29–41, doi:10.1007/s10533-009-9306-z, 2009.
- West, T. O., Brandt, C. C., Baskaran, L. M., Hellwinckel, C. M., Mueller, R., Bernacchi, C. J., Bandaru, V., Yang, B., Wilson, B. S., and Marland, G.: Cropland carbon fluxes in the United States: increasing geospatial resolution of inventory-based carbon accounting, *Ecological Applications*, 20, 1074–1086, 2010.
- West, T. O., Bandaru, V., Brandt, C. C., Schuh, A. E., and Ogle, S. M.: Regional uptake and release of crop carbon in the United States, *Biogeosciences*, 8, 2037–2046, 2011.
- Whan, K., Zscheischler, J., Orth, R., Shongwe, M., Rahimi, M., Asare, E. O., and Seneviratne, S. I.: Impact of soil moisture on extreme maximum temperatures in Europe, *Weather and Climate Extremes*, 9, 57–67, doi:10.1016/j.wace.2015.05.001, 2015.
- Williams, I. N., Riley, W. J., Torn, M. S., Berry, J. A., and Biraud, S. C.: Using boundary layer equilibrium to reduce uncertainties in transport models and CO₂ flux inversions, *Atmos. Chem. Phys.*, 11, 9631–9641, doi:10.5194/acp-11-9631-2011, 2011.
- Wolf, J., Ouattara, K., and Supit, I.: Sowing rules for estimating rainfed yield potential of sorghum and maize in Burkina Faso, *Agricultural and Forest Meteorology*, 214–215, 208–218, doi:10.1016/j.agrformet.2015.08.262, 2015.
- Wolf, S., Eugster, W., Ammann, C., Häni, M., Zielis, S., Hiller, R., Stieger, J., Imer, D., Merbold, L., and Buchmann, N.: Contrasting response of grassland versus forest carbon and water fluxes to spring drought in Switzerland, *Environ. Res. Lett.*, 8, doi:10.1088/1748-9326/8/3/035007, 2013.
- Wolf, S., Keenan, T. F., Fisher, J. B., Baldocchi, D. D., Desai, A. R., Richardson, A. D., Scott, R. L., Law, B. E., Litvak, M. E., Brunsell, N. A., Peters, W., and van der Laan-Luijkx, I. T.: Warm spring reduced carbon cycle impact of the 2012 US summer drought, *Proceedings of the National Academy of Sciences*, 113, 5880–5885, doi:10.1073/pnas.1519620113, 2016.
- Wriedt, G., van der Velde, M., Aloe, A., and Bouraoui, F.: Estimating irrigation water requirements in Europe, *Journal of Hydrology*, 373, 527–544, doi:10.1016/j.jhydrol.2009.05.018, 2009a.
- Wriedt, G., van der Velde, M., Aloe, A., and Bouraoui, F.: A European irrigation map for spatially distributed agricultural modelling, *Agricultural Water Management*, 96, 771–789, doi:10.1016/j.agwat.2008.10.012, 2009b.

-
- Yin, X. and van Laar, H. H.: Crop systems dynamics : an ecophysiological simulation model for genotype-by-environment interactions, Wageningen Academic Publishers, Wageningen, The Netherlands, 2005.
- Zeng, N., Zhao, F., Collatz, G. J., Kalnay, E., Salawitch, R. J., West, T. O., and Guanter, L.: Agricultural Green Revolution as a driver of increasing atmospheric CO₂ seasonal amplitude, *Nature*, 515, 394–397, doi:10.1038/nature13893, 2014.
- Zhao, W. and Qualls, R. J.: Modeling of long-wave and net radiation energy distribution within a homogeneous plant canopy via multiple scattering processes, *Water Resour. Res.*, 42, W08 436, doi:10.1029/2005WR004581, 2006.
- Zhao, Y., Chen, S., and Shen, S.: Assimilating remote sensing information with crop model using Ensemble Kalman Filter for improving LAI monitoring and yield estimation, *Ecological Modelling*, 270, 30–42, 2013.
- Zhou, S., Duursma, R. A., Medlyn, B. E., Kelly, J. W. G., and Prentice, I. C.: How should we model plant responses to drought? An analysis of stomatal and non-stomatal responses to water stress, *Agric. For. Meteorol.*, 182, 204–214, doi:10.1016/j.agrformet.2013.05.009, 2013.

REFERENCES

Acknowledgments

Throughout my journey as a PhD, I have benefited from the help and support from my family, close friends, and colleagues. I want to give them my heartfelt thanks for their unconditional love and support, and for believing in me until the end. I couldn't have made it without them.

I would like to start by thanking my first promotor, Wouter Peters. Wouter, I am grateful that you decided to take a chance on a crop scientist. You thought I could be a good PhD candidate within a group of physicists and mathematicians. You taught me all I know about the global carbon cycle and programming in Python. How to write an engaging scientific piece of text, how to respond – positively – to reviewers, and also how not to alienate an editor (!!). How to break a problem into smaller ones, and then down again into achievable tasks. With your Dutch-American style, you basically tried to give me the structure that carried you so far in your carrier. There is no doubt you made me a much better scientist than I was 5 years ago – with lots of room for improvement still, for instance with planning! Wouter, hartelijk bedankt! I deeply appreciate your efforts, and for not giving up on me. I am happy and proud to be the first PhD student that you promote at Wageningen University.

Then, I would like to thank my co-promotor and second daily supervisor: Jordi Vilà. Jordi, you thought me everything I know about atmospheric boundary layers. I fled from your course during my MSc in 2008, but finally passed it at the beginning of my PhD in 2012. It seems I couldn't escape physics in a meteorology department after all! Thanks for being such a good and passionate teacher. You tried to stimulate my critical thinking, and pushed me to give my best. I will always remember your positive attitude, your friendliness, and how that carried me in the really bad moments. I deeply appreciate that I had two daily supervisors with such different views and opinions. It perhaps made my progress slower, but it did teach me a lot in the end. Jordi, mille fois merci!

Then to Maarten Krol, my second promotor. Maarten I collaborated less with you on a daily basis, but I will never thank you enough for your help during the last stretch of my PhD. When I was struggling with the general discussion, you took time to listen to me, ask me the right questions and stimulate my imagination. Not only that, you've always behaved like a friend to me. I've really enjoyed getting to know you on a personal level, around a beer or a singing choir. And I look forward to your next performance!

I would like to continue by thanking all my colleagues at MAQ, for the laughs, scientific

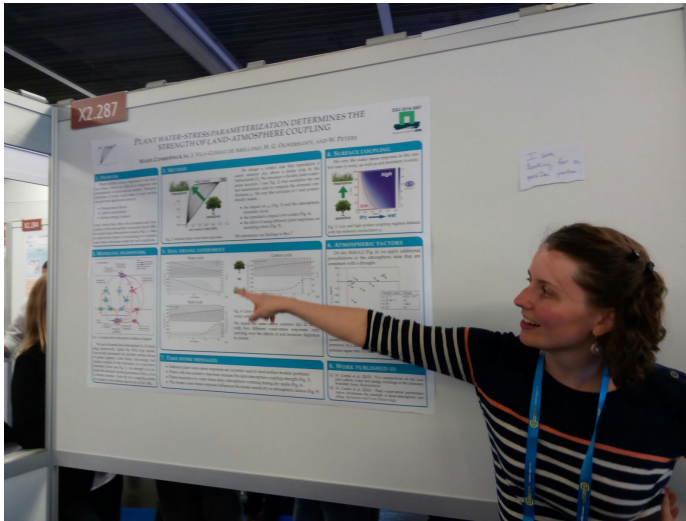
ACKNOWLEDGEMENTS

discussions, arguments, beers, and reconciliations (note the order). Thanks to you all, I have felt at home in a foreign territory – both geographically and scientifically. I have to give special thanks to some of my older PhD brothers and sisters: Denica for being my sister in struggle and fun, and to Huug for being such a good and upbeat friend. You guys saved me from my mid-PhD personal crisis. I want to give special thanks also to Michal and Marina for their kindness, to Eduardo and Danielle for the music sessions, to Natalie and Henk for the beers and good times, to Ivar and to Magdalena for the movie nights. Then, I want to thank all my little PhD brothers and sisters: Alba, Anna-Lena (chicas, you're just awesome), Xabi, Martin, Folmer, Ingrid S, Peter, Gerbrand, Imme, Arjan, Thomas. Thank you for the warmth of your friendship and for the triple Karmeliets! To Ingrid vdL, Folkert, and Michiel, my Air Quality buddies, thank you for the advice and great laughs! To Kees and Caroline, thanks for the top-notch support! And finally to my extended Meteorology family: Cor, Meto, Ruud, Chiel, Gert-Jan, Bart, Oscar, Leo, Arnold, the 3 Berts, Reinder, Jisk, Wilco, thanks for the cakes, beers and good times!

Then I would like to thank my friends from outside Wageningen: Célia, Narcisa, Vali, Elena, Magdalena, Sony, Anshu, Tjolina, Joseph, Lydia, who all belong to the extended IMAU family. I enjoyed singing, partying, and just having fun with you guys!! Don't worry, I will be back in Utrecht! To Jieying and Ana: I look forward to the future road trips we'll go on together!! Carlos, Mariano, Jon-An, thanks for bringing Madrid to Wageningen! I will return the favor one day and come to the Complutense! David FB, thanks for the good vibes and friendly push! Clara, merci à toi d'avoir apporté un peu de soleil, d'énergie et de bonne humeur à Wageningen! Nikos and Ioanna, thanks for the crazy laughter sessions and awesome dinners!!! Pohema, thanks for the companionship during my last week in Wageningen!! À Marisette et Andy, un gros merci du fond du coeur pour votre amitié sincère, et la confiance que vous m'accordez! J'espère continuer être à la hauteur! À Aurélie, Stéphane, Fabien et Blandine, merci pour les bons moments passés ensemble! Ça compte! Et pour le club des cinq: merci les filles de continuer à me soutenir, je sais que je peux compter sur vous, même avec la distance! Je vous embrasse toutes et tous!

And last but not least, I would like to thank my close family members. Sophie, un grand merci à toi d'avoir créé la couverture de ma thèse, que j'adore!! À toi et à Manu, merci pour votre soutien inaltérable et pour les grosses barres de rires infantiles! Jokérini! Manu et Aude, merci à vous d'avoir agrandi la famille, je vais bosser sur mes cours de danse classique pour Martin! Et enfin à papa et maman, mais aussi à Sylvie et Jean-Louis, un grand MERCI!! C'est grâce à vous si j'ai pu devenir la personne que je suis aujourd'hui, faire les études de mon choix et que j'aime. C'est un grand luxe, j'en suis bien consciente! C'est pour ça que je voudrais dédier mon travail à mes deux mamies et mon papy: Arlette Rivier, Marie-Louise Rosset et René Combe. Je suis très fière d'être Docteure, et je suis sûre que vous l'êtes aussi pour moi, où que vous soyez! Je vous embrasse tous très fort!

About the author



The author presenting her work at the EGU General Assembly in Vienna (April 21, 2016).

Marie Combe is an Earth System Science researcher currently working as a postdoc at the Computational and Applied Vegetation Ecology group of Ghent University, Belgium. After finishing a Bachelor level in Agricultural Sciences at the Institut Supérieur d'Agriculture Rhône-Alpes Lyon (France) in 2008, Marie completed a double Master degree in 2011, effectively earning the French title of "Ingénieur en Agriculture" and the Dutch MSc diploma of "Climate Studies". She ended her studies with a 9-month internship at the Laboratoire des Sciences du Climat et de l'Environnement in France, where she assessed the impact of future climate change on European crop yields. Later that year, she decided to go back to the Netherlands to start a Ph.D. at the crossroads of crop and atmospheric sciences, at the Meteorology and Air Quality department of Wageningen University. After almost 5 years, she completed her dissertation and immediately started as a postdoc in Belgium. She finally got to defend her thesis on December 2, 2016. Marie's current areas of interest are land-atmosphere interactions, carbon cycling, and vegetation modeling.

List of journal publications

1. Bozhinova, D., **Combe, M.**, Palstra, S. W. L. , Meijer, H. A. J., Krol, M. C., and Peters, W. (2013): The importance of crop growth modeling to interpret the $\Delta^{14}\text{CO}_2$ signature of annual plants, *Global Biogeochem. Cycles*, 27, 792-803, doi:10.1002/gbc.20065.
2. **Combe, M.**, Vilà-Guerau de Arellano, J., Ouwensloot, H. G., Jacobs, C. M. J., and Peters, W. (2015): Two perspectives on the coupled carbon, water, and energy exchange in the planetary boundary layer, *Biogeosciences*, 12, 103-123, doi:10.5194/bg-12-103-2015.
3. **Combe, M.**, Vilà-Guerau de Arellano, J., Ouwensloot, H. G., and Peters, W. (2016): Plant water-stress parameterization determines the strength of land-atmosphere coupling, *Agr. Forest Meteorol.*, 217C, 61-73, doi:10.1016/j.agrformet.
4. **Combe, M.**, de Wit, A., Vilà-Guerau de Arellano, J., and Peters, W.: Grain yield observations constrain cropland CO_2 fluxes over Europe: method and validation, *in preparation*.
5. Minda, T. T., Vilà-Guerau de Arellano, J., van der Molen, M. K., Struik, P. C., **Combe, M.**, Jiménez, P. A., and Khan, M. S.: Modelling potato productivity in complex terrain: a 10-year study based on a high-spatial resolution weather-crop model, *in preparation*.



*Netherlands Research School for the
Socio-Economic and Natural Sciences of the Environment*

D I P L O M A

For specialised PhD training

The Netherlands Research School for the
Socio-Economic and Natural Sciences of the Environment
(SENSE) declares that

Marie Combe

born on 21 May 1986 in Lyon 3e, France

has successfully fulfilled all requirements of the
Educational Programme of SENSE.

Wageningen, 2 December 2016

the Chairman of the SENSE board

Prof. dr. Huub Rijnaarts

the SENSE Director of Education

Dr. Ad van Dommelen

The SENSE Research School has been accredited by the Royal Netherlands Academy of Arts and Sciences (KNAW)



K O N I N K L I J K E N E D E R L A N D S E
A K A D E M I E V A N W E T E N S C H A P P E N



The SENSE Research School declares that **Ms Marie Combe** has successfully fulfilled all requirements of the Educational PhD Programme of SENSE with a work load of 54.9 EC, including the following activities:

SENSE PhD Courses

- o Basic statistics (2012)
- o Environmental research in context (2012)
- o Research in context activity: Co-organising a symposium on 'Climate-Carbon Interactions: From Science To Policy', Wageningen University (2015)

Other PhD and Advanced MSc Courses

- o Boundary-layer processes, Wageningen University (2012)
- o Photosynthesis, climate and change, Wageningen University (2013)
- o Project and time management, Wageningen University (2014)
- o Introduction to computer science and programming using Python, Massachusetts Institute of Technology (MIT) online course (2015)
- o Employability outside academia, PostDoc Career Development Initiative (PCDI), Utrecht (2015)

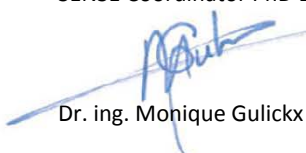
Management and Didactic Skills Training

- o Assisting in correcting the reader for the MSc course 'Boundary-layer processes' (2011)
- o Teaching assistant in the MSc course 'Earth system modelling' (2012-2015)
- o External reviewer for the 'Journal of Geophysical Research: Biogeosciences' (2016)

Selection of Oral Presentations

- o *First steps towards an improved carbon balance of European croplands.* Buys-Ballot Research School for Fundamental Processes in the Climate System (BBOS) autumn symposium, 24-26 October 2012, Nijmegen, The Netherlands
- o *Sensitivity of the carbon cycle to surface and atmospheric processes.* BBOS autumn symposium, 29-31 October 2014, 't Horntje (Texel), The Netherlands
- o *Plant water-stress determines the strength of the land-atmosphere coupling.* Seminar at the Centre for Research of Ecological and Forestry Applications (CREAF), 23 October 2015, Barcelona, Spain
- o *Modeling the carbon balance of European croplands.* Seminar at the Laboratoire des Sciences du Climat et de l'Environnement, 3 November 2015, Gif-sur-Yvette, France

SENSE Coordinator PhD Education



Dr. ing. Monique Gulickx

This project was financially supported by the Netherlands Organization for Scientific Research (NWO, project 864.08.012).

Financial support from Wageningen University for printing this thesis is gratefully acknowledged.

Front and back cover © Sophie Combe, 2016

Printed by Digiforce